

TALLINN UNIVERSITY OF TECHNOLOGY
DOCTORAL THESIS
54/2020

Numerical Analysis of Nonlinear Wave Propagation

MART RATAS



TALLINN UNIVERSITY OF TECHNOLOGY
School of Science
Department of Cybernetics

**The dissertation was accepted for the defence of the degree of Doctor of Philosophy
(Physical Sciences) on 20 November 2020**

Supervisor: Prof. Andrus Salupere,
Department of Cybernetics, School of Science
Tallinn University of Technology
Tallinn, Estonia

Co-supervisor: Prof. Jüri Majak,
Department of Mechanical and Industrial Engineering, School of Engineering
Tallinn University of Technology
Tallinn, Estonia

Opponents: Professor Carlo Cattani,
University of Tuscia
Viterbo, Italy

Dr. Helle Hein,
University of Tartu
Tartu, Estonia

Defence of the thesis: 17 December 2020, Tallinn

Declaration:

Hereby I declare that this doctoral thesis, my original investigation and achievement, submitted for the doctoral degree at Tallinn University of Technology, has not been submitted for any academic degree elsewhere.

Mart Ratas

signature

Copyright: Mart Ratas, 2020
ISSN 2585-6898 (publication)
ISBN 978-9949-83-637-6 (publication)
ISSN 2585-6901 (PDF)
ISBN 978-9949-83-638-3 (PDF)
Printed by Auratrükk

TALLINNA TEHNIKAÜLIKOOL
DOKTORITÖÖ
54/2020

Mittelineaarse lainelevi numbriline analüüs

MART RATAS



Contents

List of Publications	7
Author's Contributions to the Publications	8
Abbreviations.....	10
1 Introduction	11
1.1 Numerical analysis of nonlinear problems	11
1.2 Descriptions of treated equations	12
2 Numerical methods and statement of the problem.....	15
2.1 The pseudospectral method	15
2.2 2D spectral analysis	16
2.3 The Haar wavelet methods	17
2.4 Evaluation criteria	23
2.5 Statement of the problem	24
3 Case studies	25
3.1 The Kadomtsev–Petviashvili equation.....	25
3.2 The Burgers' equation	26
3.3 The 2D Burgers' equation	27
3.4 The Korteweg–de Vries equation.....	28
3.5 The modified Korteweg–de Vries equation	29
3.6 The Sine–Gordon equation	29
4 Numerical results	31
4.1 2D Spectral analysis	31
4.2 The Haar wavelet method	34
5 Conclusions	43
List of Figures	44
List of Tables	45
References	46
Acknowledgements	57
Abstract.....	58
Kokkuvõte	59
Appendix 1.....	61
Appendix 2	71
Appendix 3	91
Appendix 4	117

Appendix 5	125
Curriculum Vitae	131
Elulookirjeldus.....	134

List of Publications

The present PhD thesis is based on the following publications that are referred to in the text by Roman numbers.

- I A. Salupere and M. Ratas. On the application of 2D discrete spectral analysis in case of the KP equation. *Mech. Res. Comm.*, 93:141–147, 2018
- II M. Ratas and A. Salupere. Application of higher order Haar wavelet method for solving nonlinear evolution equations. *Math. Model. Anal.*, 25(2):271–288, 2020
- III M. Ratas, A. Salupere, and J. Majak. Solving nonlinear PDEs using the higher order Haar wavelet method on nonuniform and adaptive grids. *Math. Model. Anal.*, [accepted]
- IV M. Ratas. Application of Haar wavelet method for solving nonlinear evolution equations. *AIP Conference Proceedings*, 2116(1):330004, 2019
- V M. Ratas, S. K. Jena, and S. Chakraverty. Application of Haar wavelet based methods for solving wave propagation problems. *AIP Conference Proceedings*, 2293(1):230002, 2020

Author's Contributions to the Publications

- In I, I was the secondary author, wrote the simulation program, carried out the simulations and the analysis of the results, prepared the figures, and helped write the manuscript.
- In II- V, I was the main author, wrote the simulation program, analysed the results, prepared the figures, and wrote the manuscript.

Approbation

I presented the results of the thesis at the following conferences:

1. **M. Ratas.** 'Application of Haar wavelet method for solving nonlinear evolution equations', 16th International Conference of Numerical Analysis and Applied Mathematics 2018: 8–12 September 2018, Rhodes, Greece
2. **M. Ratas.** 'Numerical solution of PDE-s using Haar wavelet based methods', Mathematical Modelling and Analysis: 28–31 May 2019, Tallinn
3. **M. Ratas, S. K. Jena, S. Chakraverty.** 'Application of Haar Wavelet based methods for solving wave propagation problems', 17th International Conference of Numerical Analysis and Applied Mathematics 2019: 23–28 September 2019, Rhodes, Greece
4. **M. Ratas.** 'Application of the Adaptive Higher Order Haar Wavelet based methods for solving the sine–Gordon equation', 18th International Conference of Numerical Analysis and Applied Mathematics 2020: 17–23 September 2020, Rhodes, Greece (virtual presentation)

Abbreviations

ODE	Ordinary Differential Equation
PDE	Partial Differential Equation
PsM	Pseudospectral Method
HWM	Haar Wavelet Method
HOHWM	Higher Order Haar Wavelet Method
KP	Kadomtsev–Petviashvili (equation)
KdV	Korteweg–de Vries (equation)
mKdV	modified Korteweg–de Vries (equation)

1 Introduction

Numerical analysis has been defined as the study of methods and procedures used to obtain approximate solutions to mathematical problems. It allows providing approximate solutions to problems for which there is no reasonable hope of obtaining the exact solution [117]. While effective approximate numerical solutions to mathematical problems were available centuries ago [53, 145, 149], it was the 20th century when numerical analysis formed its own separate discipline and saw a surge in activity [29, 64].

The development of numerical methods for use in numerical analysis is a vast and growing field of study [7, 40, 74, 124]. Many of the numerical methods find use in numerically solving equations of mathematical physics known as PDEs [8, 60, 77]. Other numerical methods focus on analysis of numerical results. One such tool is discrete spectral analysis [133, 135].

Within this thesis, the discrete spectral analysis is extended to the 2D case and the Haar wavelet based Haar Wavelet Method (HWM) is improved by not only employing a improved approach called the Higher Order Haar Wavelet Method (HOHWM) but also using it in nonuniform and even adaptive grid settings. While the majority of the case studies included within the thesis revolve around PDEs describing nonlinear wave propagation, there are two exceptions where nonlinear ODEs are solved using the HOHWM.

1.1 Numerical analysis of nonlinear problems

Virtually all physical systems are nonlinear in their nature. Linear systems are often simplified linearized models of the underlying nonlinear system. These linear systems frequently only describe the underlying system accurately under a certain set of operating conditions. Thus, in order to gain a more accurate understanding of physical phenomenon, the underlying nonlinear systems must be used [143].

However, nonlinear PDEs pose a number of problems. For instance, the existence and uniqueness of their solutions are not guaranteed. Furthermore, if solutions do exist, they do not adhere to the superposition principle nor the homogeneity principle which are taken as granted in linear systems [75, 104].

Zabusky and Kruskal were among the first to use computer simulations to gain insights into nonlinear PDEs. In doing so, they discovered solitary waves which they named solitons [157]. This led to the development of the inverse scattering transform [4, 5, 61, 62].

In the decades since then, many different numerical methods have been employed for solving linear as well as nonlinear PDEs. Most local methods are based on the finite difference approach [141]. Methods based on finite elements are also popular [43, 142, 159]. Another important set of methods are the spectral methods [33, 118]. The Pseudospectral Method (PsM) [57, 56, 119] deserves a mention here. While the PsM is often used alongside the Fourier basis and transform, any orthogonal set of base functions are suited for this method. Wavelet based numerical methods have been used for more than two decades by now [21, 22]. Haar wavelets are the simplest of all wavelet families. They are made up of piece-wise constant functions and were originally proposed by Alfred Haar in [65].

This thesis mainly focuses on the PsM and the Haar wavelet based Haar Wavelet Method (HWM). The former is used alongside 2D discrete spectral analysis (Paper I). The latter was originally developed by Chen and Hsiao [41]. However, a higher order expansion called the Higher Order Haar Wavelet Method (HOHWM) has also been developed [108]. The methods are described in detail in Section 2.

1.2 Descriptions of treated equations

The model equations are described roughly in the order in which they were handled during the course of the research. In other situations some other order might be more appropriate.

1.2.1 The Kadomtsev–Petviashvili equation

The Kadomtsev–Petviashvili (KP) equation

$$(u_t + 6uu_x + u_{xxx})_x + 3\sigma^2 u_{yy} = 0 \quad (1)$$

is considered the two dimensional generalization of the Korteweg–de Vries equation. It was first introduced by Kadomtsev and Petviashvili in 1960 and thus bears their name [24, 83]. The value of the parameter σ defines two separate versions of the KP equation. The case $\sigma^2 = -1$ is called the KPI equation and the case $\sigma^2 = 1$ is called the KPII equation. The latter can be used to model water waves with small surface tension and the former describes waves in thin films with high surface tension as well as rogue waves [2, 24, 50].

Within the context of this thesis, a more general form of the equation is used. The KPI equation is used in the form of

$$(u_t + \alpha_1 u u_x + \alpha_2 u_{xxx})_x - \alpha_3 u_{yy} = 0, \quad (2)$$

where α_1 is the nonlinear coefficient, α_2 is the dispersion coefficient and α_3 is the transverse perturbation coefficient. Within the contents of the thesis, only cases where $\alpha_1 = \alpha_3 = 1$ are used, whereas different values for α_2 are introduced. The KP equation has been widely studied analytically as well as numerically, e.g [3, 39, 55, 84, 88, 114].

It is clear that if $\alpha_3 = 0$ the KP equation (2) becomes the Korteweg–de Vries (KdV) equation (9). That means the solutions of the KdV equation will also satisfy the KP equation since they do not introduce any transverse perturbation. Given that the KdV has been studied extensively at harmonic initial conditions (e.g [134, 136, 137]) the initial condition used for the KP equation was the curved sinusoid in 3D space,

$$u(x, y, 0) = \sin(a_x x + \beta \cos(a_y y)), \quad (3)$$

where a_x and a_y define the number of space periods per 2π and β is an arbitrary parameter.

1.2.2 The Burgers' equation

The equation of the form

$$u_t + uu_x = \nu u_{xx} \quad (4)$$

is called the Burgers' equation. It was originally introduced by Bateman in [19] and later studied by Burgers after whom the equation was named [31, 32]. The Burgers' equation has been used to model turbulence [31] and traffic flow [116] as well nonlinear acoustics [66] and non-stationary shock waves in fluids [93]. The equation has been numerically studied by numerous methods using the HWM [82, 98, 106, 121] as well as many other methods (e.g [71, 91, 92]).

The analytical solution of the Burgers' equation has been shown to be [6, 16, 90]

$$u_e(x, t) = \frac{2\nu\pi}{L} \frac{\sum_{n=1}^{\infty} \exp(-E_n t) n I_n(R^l) \sin(n\pi x/L)}{I_0(R^l) + 2 \sum_{n=1}^{\infty} \exp(-E_n t) I_n(R^l) \cos(n\pi x/L)}, \quad (5)$$

where $R' = R_0/(2\pi)$ and $R_0 = u_0L/\nu$ is the Reynolds number, $E_n = \nu n^2 \pi^2/L^2$, I_n represents the modified Bessel functions of first kind, u_0 is the amplitude of the initial wave, ν is the viscosity and $L = B - A$ is the x domain range [20, 44]. It is this analytical solution that is used to validate the numerical experiments. It can also be shown that at $t = 0$ the exact solution (5) gives

$$u(x, 0) = u_0 \sin \frac{\pi x}{L}, \quad (6)$$

which will be used at the initial condition.

1.2.3 The 2D Burgers' equation

The Burgers' equation (4) can be generalized in two dimensions and the resulting equation

$$u_t + uu_x + \nu u_y = \frac{1}{R} (u_{xx} + u_{yy}), \quad v_t + uv_x + \nu v_y = \frac{1}{R} (v_{xx} + v_{yy}). \quad (7)$$

is called the 2D Burgers' equation of the form [15, 23, 42, 76, 158]. Similarly to its one-dimensional cousin it has been used to model fluid dynamics, the phenomena of turbulence, and flow through a shock wave traveling in a viscous fluid and traffic flow [9, 15, 18, 148].

The exact solution to the 2D Burgers equation (7) has been discovered in the form [54]

$$\begin{aligned} u_e(x, y, t) &= \frac{3}{4} - \frac{1}{4 \{1 + \exp [(-4x + 4y - t)R/32]\}}, \\ v_e(x, y, t) &= \frac{3}{4} + \frac{1}{4 \{1 + \exp [(-4x + 4y - t)R/32]\}}. \end{aligned} \quad (8)$$

The initial conditions used in this thesis are obtained from this exact solution and the numerical results are evaluated against it.

1.2.4 The Korteweg-de Vries equation

The Korteweg-de Vries (KdV) equation was first introduced by Boussinesq in 1877 [26, 47], however it was later rediscovered by Diederik Korteweg and Gustav de Vries [89]. The equation has many forms, but in the current thesis it is used in the form

$$u_t + \alpha u u_x + \beta u_{xxx} = 0, \quad (9)$$

where α is the nonlinear parameter and β is the dispersion parameter. The equation was first derived as a model to describe the movement of long unidirectional shallow water waves in a rectangular channel but has been found to model different nonlinear phenomena nowadays [49, 130].

There exists a number of different exact solutions for the KdV equation. The one-soliton solution

$$u_e(x, t) = \frac{3c}{\alpha} \operatorname{sech}^2 \left[\frac{1}{2} \sqrt{\frac{c}{\beta}} (x - ct - x_0) \right], \quad (10)$$

where c is the phase speed for the travelling wave and x_0 is the initial phase is used within the thesis. Additionally, the two-soliton solution [1, 94, 136, 155] is used in the form

$$u(x, t) = \frac{3(c_B - c_S)}{|\alpha|} \frac{(c_B \operatorname{csch}^2(\xi_B) + c_S \operatorname{sech}^2(\xi_S))}{(\sqrt{c_B} \coth(\xi_B) - \sqrt{c_S} \tanh(\xi_S))^2}, \quad (11)$$

where

$$\begin{aligned} \xi_B &= \frac{1}{2} \sqrt{c_B/\beta} (x - c_B t - x_{0B}), \\ \xi_S &= \frac{1}{2} \sqrt{c_S/\beta} (x - c_S t - x_{0S}), \end{aligned} \quad (12)$$

and c_B and x_{0B} are the phase speed and initial phase of the bigger soliton, respectively and c_S and x_{0S} are the phase speed and initial phases of the smaller soliton, respectively. Using the exact solution (11)-(12) soliton interactions can be observed.

1.2.5 The modified Korteweg-de Vries equation

The modified Korteweg-de Vries (mKdV) equation can be written in the form

$$u_t - 6\alpha u^2 u_x + \beta u_{xxx} = 0, \quad (13)$$

where α is the nonlinear coefficient and β is the dispersion coefficient. It is used in modelling of behaviour of anharmonic lattices [70, 156]. Equation (13) closely resembles the KdV equation (9) and only differs by the power in the nonlinear term.

There exists an exact solution for the mKdV equation in the form of

$$u_e(x, t) = \sqrt{-\frac{c}{\alpha\beta}} \operatorname{sech} \left[\sqrt{\frac{c}{\beta}} (x - ct - x_0) \right], \quad (14)$$

where x_0 is the initial phase and c is the phase speed of the travelling wave [5, 70, 123, 146].

1.2.6 The sine-Gordon equation

The sine-Gordon equation was originally developed to model surfaces with constant mean curvature [25]. It has also been used in one-dimensional crystal dislocation theory [58, 59] and many other fields of research [27, 85, 112, 113, 132, 139]. The equation can be written in the form

$$u_{tt} - u_{xx} + \sin u = 0. \quad (15)$$

Its analytical travelling wave solution has been found in the form [94, 123]

$$u_e(x, t) = 4 \arctan \left[\exp \left(\frac{x - ct - x_0}{\sqrt{1 - c^2}} \right) \right], \quad (16)$$

where c is the phase speed of the travelling wave and x_0 is the initial phase. Whereas the travelling wave solutions of KdV and mKdV equations are bell-shaped, the exact solution (16) produces a sort of traveling step.

2 Numerical methods and statement of the problem

This section will describe the numerical methods used within this thesis in more detail. The equation specific implementations will be presented in Section 3.

2.1 The pseudospectral method

In order to solve PDEs both spatial as well as temporal derivatives need to be approximated. The idea of the pseudospectral method (PsM) is that a function can be approximated using a set of basis functions. Frequently, trigonometric functions are used for those basis functions. This is because the fast Fourier transform (FFT) [28, 30, 45, 67] is an efficient algorithm for the discrete Fourier transform. It allows converting from the physical space to the Fourier space [56, 57, 133]. By approximating a function using trigonometric functions, the derivatives of said approximations can be calculated analytically. This allows effective approximations of the spatial derivatives when the function itself is known.

The discrete Fourier transform (DFT) on the interval $0 \leq x < 2\pi$ on a space grid of N points with a space step of $\Delta x = 2\pi/N$ transforms the function $u(x, t)$ into

$$U(k, t) = Fu = \sum_{j=0}^{N-1} u(j\Delta x, t) \exp\left(-2\frac{\pi i j k}{N}\right). \quad (17)$$

The inverse DFT (IDFT) performs the same action in reverse as

$$u(j\Delta x, t) = F^{-1}U = \frac{1}{N} \sum_k U(k, t) \exp\left(-2\frac{\pi i j k}{N}\right). \quad (18)$$

In (17) F denotes the DFT and in (18) F^{-1} denotes the IDFT, i is the imaginary unit and k denotes the wave numbers as

$$k = 0, \pm 1, \pm 2, \pm(N/2 - 1), -N/2. \quad (19)$$

In practice, the FFT algorithm introduced in [45] is often used. It requires that the number of grid points N be a power of two [45, 67].

The DFT allows the n th spatial derivatives of a function $u(x, t)$ in the domain $0 \leq x < 2m\pi$ to be approximated as

$$\frac{\partial^n u(x, t)}{\partial x^n} = F^{-1} \left[\left(\frac{ik}{m}\right)^n Fu(x, t) \right] \quad (20)$$

and the integral of the same function can be approximated as

$$\int u(x, t) dx = F^{-1} \left[\frac{Fu(x, t)}{ik/m} \right] + C, \quad (21)$$

where C is the integration constant.

When presented with a PDE in the form of

$$u_t = \Phi\left(u, u_x, u_{xx}, \dots, u_y, u_{yy}, \dots, u_{xy}, u_{xyy}, \dots, u_{xxy}, u_{xxyy}, \dots, \int u dx\right) \quad (22)$$

one can use the formulae (20)-(21) to convert (22) to the form

$$u_t = \Psi(u). \quad (23)$$

In this form, the equation can be solved with solvers meant for ODEs. In this thesis, the *Isoda* solver from ODEPACK [69] provided by *SciPy* [144] was used. It automatically switches between Adams and BDF [17, 46, 63] solvers according to [122].

It must be noted that because of the use of the DFT within PsM, periodic boundary conditions are assumed for the function and its derivatives.

In case of PDEs with two spatial dimensions, the above formulation needs to be applied for either axis separately. In such a case, one obtains

$$\begin{aligned}\frac{\partial^n u(x, y, t)}{\partial x^n} &= F_x^{-1} \left[\left(\frac{ik}{m} \right)^n F_y u(x, y, t) \right] \\ \frac{\partial^n u(x, y, t)}{\partial y^n} &= F_y^{-1} \left[\left(\frac{ik}{m} \right)^n F_x u(x, y, t) \right] \\ \int u(x, t, t) dx &= F_x^{-1} \left[\frac{F_x u(x, y, t)}{ik/m} \right] + C(y),\end{aligned}\tag{24}$$

where the indices x and y of F and F^{-1} indicate that the operator transforms the function with respect to x and y , respectively; and the integration constant $C(y)$ now depends on y . The above formulation assumes that the same domain $[0, 2m\pi]$ as well as number of grid points are used for both spatial axes. While this is not strictly necessary, it is the case used within this thesis.

2.2 2D spectral analysis

Discrete spectral analysis (DSA) is the process where DFT related spectral characteristics (amplitude spectrum and phase spectrum) are used to analyse the space-time behaviour of wave-structures.

Any complex number z can be represented in the form

$$z = |z| (\cos \phi + i \sin \phi) = |z| \exp i\phi,\tag{25}$$

where $|z|$ is the magnitude and ϕ is the argument of the complex number z . An arbitrary function $u(x, t)$ produces complex values for the Fourier' coefficients $U(k, t)$ in (17). Thus, given DFT of the form (17), the function $u(x, t)$ can be approximated as a Fourier' series

$$u(x, t) \approx \sum_{k=0}^N a_k \cos [kx + \phi_k(t)] = a_0(t) + \sum_{k=1}^N a_k \cos [kx + \phi_k(t)]\tag{26}$$

where the coefficients are defined as

$$\begin{aligned}a_k(t) &= \frac{|U(k, t)|}{N}, \quad k = 0, \frac{N}{2}, \\ a_k(t) &= \frac{2|U(k, t)|}{N}, \quad k = 1, 2, \dots, \frac{N}{2} - 1, \\ \phi_k(t) &= \arg [U(k, t)]\end{aligned}\tag{27}$$

The coefficients $a_k(t)$ are referred to as the spectral amplitudes or the amplitude spectrum and $\phi_k(t)$ are referred to as the phase spectrum.

In case of a two dimensional PDE, however, the above formulation needs to be adopted for the 2D case. In that case, spectral amplitudes can be defines as

$$\begin{aligned}a_k(y, t) &= \frac{|U(k, y, t)|}{N}, \quad k = 0, \\ a_k(y, t) &= \frac{2|U(k, y, t)|}{N}, \quad k = 1, 2, \dots, \frac{N}{2} - 1\end{aligned}\tag{28}$$

and the phase spectrum can be defined as

$$\phi_k(y, t) = \arg(U[k, y, t]). \quad (29)$$

When applying DSA to 1D waves the spectral amplitudes can be shown within a single 2D plot where different lines refer to different spectral amplitudes $a_k(t)$. However, in the two dimensional case, such a simple approach is not possible. Thus, a new way of looking at spectral analysis was developed, where a pseudocolor plot is formed for each spectral amplitude $a_k(y, t)$ and phase $\phi_k(y, t)$ ($k = 1, \dots, N/2$). In most cases, only the first few spectral amplitudes are of interest since the values of the higher spectral amplitudes tend to be smaller. This approach results in one image for each spectral amplitude or phase in consideration.

2.3 The Haar wavelet methods

In subsequent subsections, firstly, the Haar wavelet family is introduced. Then the Haar wavelet method (HWM) is described in some detail. And finally, the higher order Haar wavelet method (HOHWM) is introduced.

2.3.1 The Haar wavelet family

The Haar wavelet family is now defined. The notation introduced by Lepik [99] and Oruç in [120] is used. The Haar wavelet family will be defined for the nonuniform grid. While not all the case studies were conducted using nonuniform grid, the uniform grid formulation can easily be extracted from the nonuniform formulation and the simplifications it implies will be noted.

Given the domain $[A, B]$, one can divide it into $2M$ sub-intervals at maximal resolution J . The number of sub-intervals and resolution are related as $M = 2^J$. This shows that the number of such sub-intervals will always be a power of 2. The base Haar wavelet family can be described as

$$h_i(x) = \begin{cases} 1 & \text{for } x \in [\xi_1(i), \xi_2(i)], \\ -c_i & \text{for } x \in [\xi_2(i), \xi_3(i)], \\ 0 & \text{elsewhere,} \end{cases} \quad i = 1, \dots, 2M, \quad (30)$$

where

$$\begin{aligned} \xi_1(i) &= x^s(2k\mu), & \xi_2(i) &= x^s((2k+1)\mu), \\ \xi_3(i) &= x^s(2(k+1)\mu), & \mu &= M/m. \end{aligned} \quad (31)$$

The coefficients c_i are calculated from

$$\int_A^B h_i(x) dx = 0, \quad (32)$$

which gives

$$c_i = \frac{\xi_2(i) - \xi_1(i)}{\xi_3(i) - \xi_2(i)}. \quad (33)$$

It can be noted that for a uniform grid, $\xi_2(i) - \xi_1(i) = \xi_3(i) - \xi_2(i)$, which means that $c_i = 1$ in such a case.

In (30)-(33), $k = 0, 1, \dots, m-1$ is the translation parameter; the parameter $m = 2^j$ describes the maximum number of square waves that can be sequentially deployed in

the interval $[A, B]$ for the given dilation parameter $j = 0, 1, \dots, J$; the index i is calculated from $i = m + k + 1$. While the scaling function $h_1(x) = 1$ is constant, the rest of the Haar functions contain a single rectangular (or square in case of a uniform grid) wave. Since the scaling function $h_1(x)$ does not include a wave, in its case $m = 0, \xi_1 = A, \xi_2 = B, \xi_3 = B$. A general example of the Haar wavelets for $J = 2$ on a nonuniform grid is shown in Fig. 1. Locations at which vertical lines cross the horizontal axis as well as the boundaries determine the grid points.

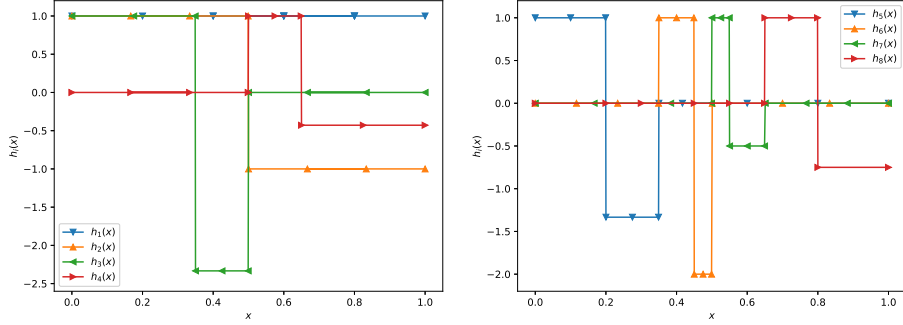


Figure 1 - Haar wavelets on a nonuniform grid for $J = 2$ as described by (31)–(33)

The Haar functions form an orthogonal transform basis

$$\int_A^B h_i(x)h_l(x)dx = \begin{cases} 2^{-j} & i = l, \\ 0 & i \neq l. \end{cases} \quad (34)$$

Therefore, one is able to expand any square integrable function $f(x)$ into Haar wavelets as

$$f(x) = \sum_{i=1}^{\infty} a_i h_i(x), \quad (35)$$

where a_i denote the Haar coefficients. When a finite number ($2M$) of Haar wavelets is used the approximation

$$f(x) \approx \sum_{i=1}^{2M} a_i h_i(x) \quad (36)$$

is obtained.

The n th order integral of the Haar functions (30) has been shown to be analytically found as [102]

$$p_{n,i}(x) = \begin{cases} 0 & \text{for } x \in [A, \xi_1(i)), \\ \frac{[x - \xi_1(i)]^n}{n!} & \text{for } x \in [\xi_1(i), \xi_2(i)), \\ \frac{[x - \xi_1(i)]^n - (1 + c_i)[x - \xi_2(i)]^n}{n!} & \text{for } x \in [\xi_2(i), \xi_3(i)), \\ \frac{[x - \xi_1(i)]^n - (1 + c_i)[x - \xi_2(i)]^n + c_i[x - \xi_3(i)]^n}{n!} & \text{for } x \in [\xi_3(i), B). \end{cases} \quad (37)$$

Within the thesis, the matrix form of the above formulation is used. The elements of the $(2M) \times (2M)$ matrix \mathbf{H} , are given as values of the Haar functions in collocation points

$x_l = (l - 1/2)\Delta x$ as

$$H_{il} = h_i(x_l). \quad (38)$$

The elements of the $(2M) \times (2M)$ matrix \mathbf{P}_n are found as

$$(\mathbf{P}_n)_{il} = p_{n,i}(x_l). \quad (39)$$

\mathbf{P}_n denotes the n th integral of the Haar wavelet matrix for a given resolution J . Given (38) and (39) and considering the Haar wavelet coefficient vector \mathbf{a} one obtains

$$f(x) = \mathbf{a} \cdot \mathbf{H} \quad (40)$$

instead of (35) and

$$\underbrace{\int \cdots \int}_n \underbrace{\int_A^x}_n \mathbf{H} d\xi \dots d\xi = \mathbf{P}_n. \quad (41)$$

It is important to note that the matrices \mathbf{H} and \mathbf{P}_n depend on the coordinate x .

One can see from (37) that in boundary points A and B the following holds

$$\begin{aligned} (\mathbf{P}_n(A))_i &= 0 \quad \forall n > 0, \quad \forall i \\ (\mathbf{P}_n(B))_i &= p_{n,i}(B) = \frac{(B - \xi_1(i))^n - (1 - c_i)(B - \xi_2(i))^n + c_i(B - \xi_3(i))^n}{n!}. \end{aligned} \quad (42)$$

This often simplifies the boundary conditions for particular problems.

2.3.2 The Haar wavelet method

The Haar Wavelet Method (HWM) was first introduced by Chen and Haar in 1997 in their article [41]. It was used in order to solve various differential equations [41, 72, 73, 100]. It has also been extended for solving a different integro-differential and integral equations [10, 11, 12, 14, 36, 52, 97, 101, 151]. According to the HWM, the highest order derivative included in the differential equations is expanded into the Haar series. Lepik developed the integration techniques for the HWM in [95, 96, 97, 98, 101, 102]. A comprehensive overview of the HWM and its applications can be found in [103]. The HWM has also been adopted for the weak formulation in [106]. The method has been applied in solid mechanics [97, 98, 102], analysis and modelling of composite structures [37, 38, 68, 131], as well as free vibration analysis [81, 105, 150, 152, 153, 154], among others. However, engineering is not the only area of research where the Haar wavelets have found application in. They have been used in various research areas from informatics to medicine [34, 35, 147].

Within the present thesis, in cases where only the spatial derivatives are expanded into the Haar wavelet series temporal integration is done with the aid of either *SciPy*'s [144] ODEPACK [69] or *MATLAB*'s *ode45* [140] based on Runge-Kutta (4,5) formula [48]. Thus, the spatial derivatives are expanded at a fixed time moment t_j in such cases.

When dealing with a PDE of the form

$$u_{mt}(x, t) = f(u(x, t), u_x(x, t), \dots, u_{nx}(x, t)), \quad (43)$$

the HWM proposes that the highest order derivative within the equation is expanded into the Haar series. Therefore,

$$u_{nx}(x, t_j) = \mathbf{a} \cdot \mathbf{H} \quad (44)$$

is obtained. After integrating (44) n times, one obtains

$$u(x, t_j) = \mathbf{a} \cdot \mathbf{P}_n + \sum_{i=0}^{n-1} d_i \frac{\mathbf{x}^i}{i!}, \quad (45)$$

where \mathbf{a} is the Haar wavelet coefficient vector and d_i are integrating constants. It must be noted that \mathbf{x}^i in (44) means element-wise power here as well as in upcoming formulae. The n boundary conditions can thus be used with (44) (or its derivatives) to determine the coefficients d_i . After inserting the coefficients into (44) one obtains the function

$$u(x, t_j) = \mathbf{a} \cdot \mathbf{R}_n + \mathbf{S}_n, \quad (46)$$

where \mathbf{R}_n and \mathbf{S}_n are matrices which do not change in time. They only depend on the boundary conditions and the grid as well as (in case of variable boundary conditions) t . Thus, in case of constant boundary conditions, the values of these matrices can be calculated when the grid has been specified.

At each fixed time moment t_j the Haar coefficients are obtained from the known $u(x, t_j)$ using (46). After that all the spatial derivatives in the equation are approximated using (46) and substituted into (43). This results in the equation taking the form

$$u_{mt}(x, t) = F[u(x, t)], \quad (47)$$

which can be treated as an ODE and thus one of the aforementioned ODE solving algorithms can be used.

Given a PDE with two spatial dimensions in the form

$$u_{mt} = \Phi(u, u_x, u_{xx}, \dots, u_y, u_{yy}, \dots, u_{xy}, u_{xxy}, \dots, u_{xxy}, u_{xxy}, \dots), \quad (48)$$

the function needs to be expanded into the Haar series with respect to the two spatial coordinates separately. This can be done as

$$\begin{aligned} u_{n_x x}(x, y, t_j) &= \mathbf{a}_x \cdot \mathbf{H}_x, \\ u_{n_y y}(x, y, t_j) &= \mathbf{H}_y^T \cdot \mathbf{a}_y, \end{aligned} \quad (49)$$

where n_x and n_y denote the maximal x and y derivative, respectively; and the indices of \mathbf{a} and \mathbf{H} denote which coordinate the Haar coefficients and matrix involve. In case of equal resolution on either axis, $\mathbf{H}_x = \mathbf{H}_y$ and they are simply used in their transposed form in the formula. However, the two axes are not required to have the same resolution.

After integrating (49) n_x and n_y times, respectively, one obtains

$$\begin{aligned} u(x, y, t_j) &= \mathbf{a}_x \cdot \mathbf{P}_{xn_x} + \sum_{i=0}^{n_x-1} d_i \frac{\mathbf{x}^i}{i!}, \\ u(x, y, t_j) &= \mathbf{P}_{yn_y}^T \cdot \mathbf{a}_y + \sum_{j=0}^{n_y-1} \frac{\mathbf{y}^j}{j!} e_j, \end{aligned} \quad (50)$$

where d_i and e_j are integration constants for x and y axis, respectively; \mathbf{P}_{xn_x} and $\mathbf{P}_{yn_y}^T$ denote the n_x th integral with respect to x and n_y th integral with respect to the y axis, respectively.

Given that the two formulae in (50) need to be equal, one obtains

$$\mathbf{a}_x \cdot \mathbf{P}_{xn_x} + \sum_{i=0}^{n_x-1} d_i \frac{\mathbf{x}^i}{i!} = \mathbf{P}_{yn_y}^T \cdot \mathbf{a}_y + \sum_{j=0}^{n_y-1} \frac{\mathbf{y}^j}{j!} e_j. \quad (51)$$

This matrix equation gives the relationship between \mathbf{a}_x and \mathbf{a}_y . This can be substituted into one of (50) and thus all the spatial derivatives in the PDE (48) can be approximated using one set of Haar coefficient matrices (either \mathbf{a}_x or \mathbf{a}_y).

It must be noted that a 2D PDE can directly expanded into Haar series with respect to both spatial coordinates as

$$u(x, y, t) = \mathbf{P}_{yn_y}^T \cdot \mathbf{C} \cdot \mathbf{P}_{xn_x} + \sum_{i=0}^{n_x-1} d_i \frac{\mathbf{x}^i}{i!} + \sum_{j=0}^{n_y-1} \frac{\mathbf{y}^j}{j!} e_i. \quad (52)$$

This approach can be shown to be equivalent to the above since

$$\begin{aligned} \mathbf{C} &= \left(\mathbf{P}_{yn_y}^T \right)^{-1} \cdot \mathbf{a}_x - \left(\mathbf{P}_{yn_y}^T \right)^{-1} \cdot \left(\sum_{j=0}^{n_y-1} \frac{\mathbf{y}^j}{j!} e_i \right) \cdot \left(\mathbf{P}_{xn_x} \right)^{-1}, \\ \mathbf{C} &= \mathbf{a}_y \cdot \left(\mathbf{P}_{xn_x} \right)^{-1} - \left(\mathbf{P}_{yn_y}^T \right)^{-1} \cdot \left(\sum_{i=0}^{n_x-1} d_i \frac{\mathbf{x}^i}{i!} \right) \cdot \left(\mathbf{P}_{xn_x} \right)^{-1}. \end{aligned} \quad (53)$$

However, the above mentioned approach results in simpler formulae which are easier to manage.

2.3.3 The higher order Haar wavelet method

The higher order Haar wavelet method (HOHWM) was developed relatively recently in [108]. It was proposed as an improvement to the HWM. The HOHWM has been shown to increase accuracy as well to have a higher convergence rate than the regular HWM [78, 79, 86, 87, 107, 108]. The HOHWM proposes that a derivative of $2s$ higher order (than is present within the equation) is expanded into the Haar series. This introduces additional $2s$ integration coefficients. In [108] two algorithms for determining these $2s$ coefficients are proposed. The first algorithm is based on employing selected uniform grid points. The second algorithm is based on employing selected Chebyshev–Gauss–Lobatto grid points. In case of $s = 1$, according to both algorithms the governing equation can be evaluated at its boundaries in order to solve for those two extra coefficients.

In case of the HOHWM one expands into Haar series

$$u_{(n+2s)x}(x, t_j) = \mathbf{a} \cdot \mathbf{H}. \quad (54)$$

The function u is obtained by integrating (54) $n + 2s$ times

$$u(x, t_j) = \mathbf{a} \cdot \mathbf{P}_{n+2s} + \sum_{i=0}^{n+2s-1} d_i \frac{\mathbf{x}^i}{i!}, \quad (55)$$

where d_i are unknown coefficients. The n th order equation has n spatial derivatives, which provide n boundary conditions that can be evaluated in order to solve for the unknown coefficients d_i . However, the additional $2s$ coefficients introduced by the HOHWM (in comparison to the HWM) must be obtained using supplementary information as described in the previous paragraph.

In the present thesis, only $s = 1$ is used. This gives

$$u_{(n+2)x}(x, t_j) = \mathbf{a} \cdot \mathbf{H}. \quad (56)$$

After integrating $n + 2$ times one obtains

$$u(x, t_j) = \mathbf{a} \cdot \mathbf{P}_{n+2} + \sum_{i=0}^{n+1} d_i \frac{\mathbf{x}^i}{i!}. \quad (57)$$

Using the n boundary conditions and by evaluating the differential equation at its boundaries (A and B) one obtains the $n + 2$ equations that are used to solve for the $n + 2$ unknown coefficients d_i . These coefficients can depend on the Haar wavelet coefficients vector \mathbf{a} . After finding the unknown coefficients and inserting them into (57) one obtains

$$u(x, t_j) = \mathbf{a} \cdot \mathbf{R}_{n+2} + \mathbf{S}_{n+2}, \quad (58)$$

where the matrices \mathbf{R}_{n+2} and \mathbf{S}_{n+2} are similar to (46) in the case of the HWM.

2.3.4 Nonuniform grid

The collocation method is used alongside both the HWM as well as the HOHWM. As such, the collocation points lie in the middle of an adjacent pair of grid points. Therefore, given the domain $x \in [A, B]$, the $2M + 1$ grid points can be described as

$$x^g(l), \quad l = 0, 1, \dots, 2M, \quad x^g(l+1) > x^g(l) \forall l, \quad x^g(0) = A, \quad x^g(2M) = B \quad (59)$$

and the $2M$ collocation points can be obtained as

$$x(l) = \frac{x^g(l) + x^g(l+1)}{2}, \quad l = 0, 1, \dots, 2M-1. \quad (60)$$

Two different nonuniform grid approaches were used. The first type of nonuniform grid within the domain $x \in [0, 1]$ follows the formula

$$x^g(l) = \frac{q^l - 1}{q^{2M} - 1}, \quad l = 0, 1, \dots, 2M, \quad (61)$$

where q is an arbitrary constant. For $q < 1$ the nonuniform grid (61) leads to a concentration of grid points around the right hand boundary 1 and in the case of $q > 1$ the grid points are concentrated around the boundary 0. When $q \rightarrow 1$ the uniform grid is described. This type of grid is most applicable in cases where abrupt changes to the solution are expected near a boundary. This type of nonuniform grid has previously been used in [120].

For the second time of nonuniform grid, more grid points are gathered near the center of the domain. It follows the formula

$$x^g(l) = \begin{cases} 0, & l = 0 \\ \frac{(l-1)(1-2\gamma)}{2M-2} + \gamma, & 0 < l < 2M, \\ 1, & l = 2M \end{cases} \quad (62)$$

where the gap parameter γ describes how far from either boundary the coarse grid starts and ends. Such a grid can be used when the characteristic behaviour of a solution is expected to stay in the middle of the domain.

2.3.5 Adaptive grid

When the characteristic behaviour of a solution of is expected to change position in time, an adaptive grid method can be considered. Such a method was developed by the author of the thesis. The adaptive grid described here is based on the constrained least-squares statement [51]. When changing the grid, the grid points of the new grid s can be found as

$$s_{k+1} - s_k = \frac{1}{\sum_{i=1}^{N-1} \frac{w_{k+1/2}}{w_{i+1/2}}} (s_{max} - s_{min}), \quad k = 1, \dots, N-1, \quad (63)$$

where s_{min} and s_{max} are the minimal and maximal boundary points, respectively and w is the weight function. It must be noted, that the weight function is used in the middle of two grid points ($w_{i+1/2}$). However, since the collocation points lie in the middle of two subsequent grid points according to (60), thus the values of the weight function at the collocation points can be used directly. The absolute value of the function itself or its first derivative is scaled to the power of d and a constant e is added (to ensure the weights never reach 0). The result is used as the weight function in the form of

$$w = |u|^d + e, \quad (64)$$

where d is the scaling factor and e is the offset. Similarly, when using the derivative instead of the function, one obtains

$$w = |u_x|^d + e. \quad (65)$$

The algorithm (63) is carried out iteratively until the grid points converge. During each iteration, the weight function is estimated at the new collocation points by interpolating.

A new grid is only calculated only if the characteristic point in the numerical result (i.e the maximal point of the function or its derivative) has moved by δ . This ensures the grid is not recalculated too often which helps to save on computational time.

It must be noted that implementing the adaptive grid (63) for the HOHWM does not significantly affect computational complexity. The standard Haar matrices determined for uniform grid cannot be employed, the Haar functions are evaluated in adaptive collocation points instead.

2.4 Evaluation criteria

When evaluating the performance of the HOHWM, various different evaluation criteria were used. These will be described here.

In case of ODEs, the convergence of the solution with respect to itself as well as the exact solution were used. The order of convergence with respect to the exact solution at resolution k_J^e at resolution J and the convergence with respect to the numerical solutions k_J can be found as [108, 109, 110]

$$k_J^e = \log_2 \left(\frac{F_{J-1} - F_e}{F_J - F_e} \right), k_J = \log_2 \left(\frac{F_{J-2} - F_{J-1}}{F_{J-1} - F_J} \right), \quad (66)$$

where F_J and F_e stand for the numerical solution at resolution J and exact solution, respectively. The numerical solution at the midpoint of the domain ($\frac{A+B}{2}$) is to evaluate convergence. Since (66) shows that the solution at the current as well as previous resolution (as well as the exact solution) are need in order to calculate k_J^e , it cannot be calculated for the lowest resolution and is therefore omitted. Similarly, since k_J depends on the solution at the current resolution as well as two lower resolutions, it cannot be calculated for the two lowest resolutions and is thus omitted in those cases.

The maximum deviation from exact solution $\Delta u = \max_{x,t} |u(x,t) - u_e(x,t)|$ is used for all the cases where the exact solution exists. This allows showing the improvements to accuracy.

In certain situations, the maximal time at which the specified accuracy could not be maintained needs to be used. Given the final time the calculation was carried out for t_F , the time moment $t_f = \max(t_F, t_c)$ was determined by obtaining the value of critical time moment t_c which is the maximal time t for which $\max_{x,t < t_c} |u(x,t) - u_e(x,t)| < 10^{-3}$.

2.5 Statement of the problem

There exist many different numerical methods for solving PDEs in literature. Some of these methods have been described within the introduction to this thesis. However, the main focus of this paper will be on the HWM as well as its higher order cousin, the HOHWM. The motivation in developing the HOHWM was to improve the accuracy. Similar motivation is used here by exploring the performance of both the HWM as well as HOHWM and employing nonuniform as well as adaptive grids alongside the HOHWM in order to further improve its accuracy. To the best knowledge of the author, this is the first time that the HOHWM has been used on nonuniform as well as adaptive grids.

The main goals of the thesis can be summarised as

- to show the capabilities of the PsM and 2D DSA in case of the KP equation;
- to introduce ways of increasing the accuracy of the HWM and the HOHWM;
- to demonstrate the improvements of the accuracy of the HOHWM when compared to the HWM on a number of model equations;
- to develop algorithms for applying nonuniform and adaptive grids with the HOHWM.

3 Case studies

Numerical experiments were carried out on several different nonlinear differential equations throughout the years leading up to this thesis. While the underlying methods were the same, the implementation is slightly different for each model equation. This section will outline the equation parameters values, initial and boundary conditions as well as describe the specific implementation(s) of the method(s) used for each model equation. The KP equation (2) was integrated using the 2D PSM. The HWM was used to numerically solve the 2D Burgers' equation (7). Both the HWM and the HOHWM were used to numerically solve the Burgers' equation (4), the KdV equation (9), the mKdV equation (13) and the sine-Gordon equation (15).

3.1 The Kadomtsev-Petviashvili equation

The PsM was used to solve the KP equation (2). Periodic boundary conditions

$$\begin{aligned} u(x, y, t) &= u(x + 2m\pi, y, t), & u_x(x, y, t) &= u_x(x + 2m\pi, y, t), \\ u_{xx}(x, y, t) &= u_{xx}(x + 2m\pi, y, t), & u_{xxx}(x, y, t) &= u_{xxx}(x + 2m\pi, y, t), \\ u_{4x}(x, y, t) &= u_{4x}(x + 2m\pi, y, t), & u_{yy}(x, y, t) &= u_{yy}(x, y + 2m\pi, t), \end{aligned} \quad (67)$$

were used due to the nature of the PsM. In order to use solvers meant for solving ODEs, the KP equation needs to assume the form

$$u_t = \Psi(u). \quad (68)$$

Therefore, the KP equation needs to be transformed. At first, a new variable

$$\varphi = u_x \quad (69)$$

is introduced. Using it, the KP equation assumes the form

$$\varphi_t = -\alpha_1 (\varphi^2 - u\varphi_x) - \alpha_2 \varphi_{xxx} + \alpha_3 u_y, \quad (70)$$

where

$$\begin{aligned} \varphi_x &= F_x^{-1} \left[\frac{ik}{m} F_x \varphi \right], & \varphi_{xxx} &= F_1^{-1} \left[-\frac{ik^3}{m^3} F_x \varphi \right], \\ u &= F_x^{-1} \left[\frac{F_x \varphi}{ik/m} \right] + C(y), & u_{yy} &= F_y^{-1} \left[-\frac{k^2}{m^2} F_y u \right]. \end{aligned} \quad (71)$$

After substituting (71) into (70), one obtains the result in the form

$$\varphi_t = \Phi(\varphi), \quad (72)$$

which can be solved using solvers meant for ODEs.

As the initial condition, a bent sinusoid

$$u(x, y, 0) = \sin(a_x x + \beta \cos(a_y y)), \quad (73)$$

where a_x and a_y define the number of periods per 2π and β changes the amount of "bend" the initial wave has. This idea stems from [88] where a bent sech^2 -type initial condition was used.

The KP equation was numerically solved for equation parameters $\alpha_1 = \alpha_3 = 1$ and $\alpha_2 = 10^{-d_l}$, where $d_l = 0, 1, 1.1, 1.2, \dots, 1.8$ and initial condition parameters $a_x = 2/3, 1, 2$, $a_y = 2/3, 2$, $\beta = 0.2, 0.3, 0.4$ until the final time $t_f = 60$.

3.2 The Burgers' equation

The HWM as well as HOHWM were used to solve the Burgers' equation (4). In Paper IV, the function was expanded into the Haar series with respect to both the spatial as well as temporal coordinates. However, in Papers II and III the HWM and HOHWM were only used along the spatial coordinates.

The homogeneous boundary conditions

$$u(0,t) = u(1,t) = 0 \quad (74)$$

were used for the Burgers' equation. The exact solution (5) was evaluated at $t = 0$ and used as the initial condition in the form of

$$u(x,0) = u_0 \sin \frac{\pi x}{L}, \quad (75)$$

where $u_0 = 1$ is used.

The values of the diffusion parameters $\nu = \frac{1}{10}, \frac{1}{5\pi}, \frac{1}{10\pi}, \frac{1}{100\pi}, \frac{1}{110\pi}, \frac{1}{120\pi}, \frac{1}{160\pi}$ were used in various different articles.

In case the Haar wavelet method was used along both axes, the Burgers' equation (4) can be quasilinearized according to [115] as

$$u_t^{r+1} + (u^{r+1}u_x^r + u^r u_x^{r+1}) - \nu u_{xx}^{r+1} = u^r u_x^r, \quad (76)$$

where r is the iteration step. The HWM can be applied to the quasilinearized Burgers' equation (76) as

$$\begin{aligned} u(x,t) &= \mathbf{R}_2 \cdot \mathbf{A} \cdot \mathbf{P}_{t1} + \mathbf{S}_2, \\ \mathbf{R}_2 &= \mathbf{P}_{x2}^T - \frac{\mathbf{x} - a}{b - a} \cdot \mathbf{P}_{x2}^T(b), \\ \mathbf{S}_2 &= \frac{(b - \mathbf{x}) [u_a(t) - u_a(0)] + (\mathbf{x} - a) [u_b(t) - u_b(0)]}{b - a} + u_0(x), \end{aligned} \quad (77)$$

where $u_a(t)$ and $u_b(t)$ are the left and the right boundary conditions, respectively. For homogeneous boundary conditions, \mathbf{S}_2 simplifies to

$$\mathbf{S}_2 = u_0(x). \quad (78)$$

After substituting (77) into (76) one obtains a system of linear equations to be solved for Haar coefficient matrix \mathbf{A} . It must be noted that since (76) contains u^{r+1} and u_x^{r+1} , the function as well as its first derivative at the previous iteration need to be used in order to find the Haar coefficients for the next iteration. The iteration must be carried out until the change between iterations becomes sufficiently small. The initial condition at all time moments is used as the initial guess (u_r for $r = 0$).

In cases where the Haar wavelet method was used only for the spatial coordinates, no quasilinearization is needed. In such a case, for the HWM

$$\begin{aligned} u &= \mathbf{R}_{x2} \cdot \mathbf{A} + \mathbf{S}_{x2}, \\ \mathbf{R}_{x2} &= \mathbf{P}_{x2} - \mathbf{P}_{x2}(1) \cdot \mathbf{x}, \\ \mathbf{S}_{x2} &= c_l(1 - \mathbf{x}) + c_r \mathbf{x} \end{aligned} \quad (79)$$

is obtained. However, for HOHWM the equation needs to be evaluated at its boundaries as

$$u_t(0,t) + u(0,t)u_x(0,t) - \nu u_{xx}(0,t) = 0, \quad u_t(1,t) + u(1,t)u_x(1,t) - \nu u_{xx}(1,t) = 0. \quad (80)$$

Given the homogeneous boundary conditions (74), $u_t(0, t) = u_t(1, t) = 0$ simplify (80) to

$$u_{xx}(0, t) = 0 \quad u_{xx}(1, t) = 0. \quad (81)$$

This gives

$$\begin{aligned} u &= \mathbf{R}_{x4} \cdot \mathbf{A} + \mathbf{S}_{x4}, \\ \mathbf{R}_{x4} &= \mathbf{P}_{x4} - \mathbf{P}_{x4}(1) \cdot \mathbf{x} + \mathbf{P}_{x2}(1) \cdot \frac{\mathbf{x} - \mathbf{x}^3}{6}, \\ \mathbf{S}_{x4} &= \mathbf{0}, \end{aligned} \quad (82)$$

which can be used to solve the problem numerically using the HOHWM.

3.3 The 2D Burgers' equation

The HWM was used to solve the 2D Burgers' equation (7). Both uniform as well as nonuniform grid approaches were used. The initial and boundary conditions were obtained from the exact solution (8) as

$$u_0(x, y) = u_e(x, y, 0), \quad v_0(x, y) = v_e(x, y, 0) \quad (83)$$

and

$$\begin{aligned} f_0^u(y, t) &= u_e(a, y, t), & f_1^u(y, t) &= u_e(b, y, t), \\ f_0^v(y, t) &= v_e(a, y, t), & f_1^v(y, t) &= v_e(b, y, t), \\ g_0^u(x, t) &= u_e(x, c, t), & g_1^u(x, t) &= u_e(x, d, t), \\ g_0^v(x, t) &= v_e(x, c, t), & g_1^v(x, t) &= v_e(x, d, t), \end{aligned} \quad (84)$$

respectively.

To numerically solve the 2D Burgers' equations, the derivatives within (7), u_{xx} , u_{yy} , v_{xx} and v_{yy} need to be expanded into the Haar wavelet series as per [13]

$$\begin{aligned} \frac{\partial^2 u(x, y)}{\partial x^2} &= \mathbf{A}_x^u \cdot \mathbf{H}_x, & \frac{\partial^2 u(x, y)}{\partial y^2} &= \mathbf{H}_y^T \cdot \mathbf{A}_y^u, \\ \frac{\partial^2 v(x, y)}{\partial x^2} &= \mathbf{A}_x^v \cdot \mathbf{H}_x, & \frac{\partial^2 v(x, y)}{\partial y^2} &= \mathbf{H}_y^T \cdot \mathbf{A}_y^v. \end{aligned} \quad (85)$$

In (85) H_x and H_y denote the Haar wavelet matrices related to the x and y coordinates, respectively, and $A_x^u, A_y^u, A_x^v, A_y^v$ denote the Haar wavelet coefficients for u, v as well as x and y , respectively. After integrating, one arrives at

$$\begin{aligned} u(x, y) &= \mathbf{A}_x^u \cdot \mathbf{R}_{x2} + \mathbf{S}_{x2}^u, & u(x, y) &= \mathbf{R}_{y2} \cdot \mathbf{A}_y^u + \mathbf{S}_{y2}^u, \\ v(x, y) &= \mathbf{A}_x^v \cdot \mathbf{R}_{x2} + \mathbf{S}_{x2}^v, & v(x, y) &= \mathbf{R}_{y2} \cdot \mathbf{A}_y^v + \mathbf{S}_{y2}^v, \end{aligned} \quad (86)$$

where

$$\begin{aligned} \mathbf{R}_{x2} &= \mathbf{P}_{x2} - \mathbf{P}_{x2}(1)\mathbf{x}, & \mathbf{R}_{y2} &= \mathbf{P}_{y2}^T - \mathbf{y}\mathbf{P}_{y2}^T(1), \\ \mathbf{S}_{x2}^u &= [f_1^u(y, t) - f_0^u(y, t)] \cdot \mathbf{x} + f_0^u(y, t), & \mathbf{S}_{y2}^u &= \mathbf{y} \cdot [g_1^u(x, t) - g_0^u(x, t)] + g_0^u(x, t), \\ \mathbf{S}_{x2}^v &= [f_1^v(y, t) - f_0^v(y, t)] \cdot \mathbf{x} + f_0^v(y, t), & \mathbf{S}_{y2}^v &= \mathbf{y} \cdot [g_1^v(x, t) - g_0^v(x, t)] + g_0^v(x, t). \end{aligned} \quad (87)$$

This can be used to transform the 2D Burgers' equation (7) to a form which can be solved using algorithms meant for ODEs.

The 2D Burgers' equation was solved at various different values of the Reynolds number $R = 220, 260, 300, 340$.

3.4 The Korteweg-de Vries equation

The HWM as well as the HOHWM were used to numerically solve the KdV equation (9). Both uniform as well as nonuniform grids were used.

The initial condition was taken from the exact one-soliton solution (10) at $t = 0$ as

$$u(x, 0) = \frac{3c}{\alpha} \operatorname{sech}^2 \left[\frac{1}{2} \sqrt{\frac{c}{\beta}} (x - x_0) \right] \quad (88)$$

or the exact two-soliton solution (11) at $t = 0$ as

$$u(x, 0) = \frac{3(c_B - c_S)}{|\alpha|} \frac{(c_B c_S \operatorname{csch}^2(\xi_B) + c_S \operatorname{sech}^2(\xi_S))}{(\sqrt{c_B} \coth(\xi_B) - \sqrt{c_S} \tanh(\xi_S))^2}, \quad (89)$$

where

$$\begin{aligned} \xi_B &= \frac{1}{2} \sqrt{c_B/\beta} (xt - x_{0B}), \\ \xi_S &= \frac{1}{2} \sqrt{c_S/\beta} (xt - x_{0S}). \end{aligned} \quad (90)$$

Numerical experiments were carried out for $\alpha = 1, 6$, $\beta = 1$ at $c = 1000$, $x_0 = 1/4$ as well as for $\alpha = 6$, $\beta = 4 \cdot 10^{-4}$ at $c = 2$, $x_0 = 3/10$ for the one-soliton initial condition (88). In addition, numerical experiments were carried out for $\alpha = 1$, $c_B = 10000$, $x_{0B} = 1/5$, $c_S = 10000/3$, $x_{0S} = 2/5$, $x \in [0, 1]$, $t \in [0, 0.6 \times 10^{-4}]$ and $\alpha = 6$, $c_B = 10000$, $x_{0B} = 1/5$, $c_S = 10000/3$, $x_{0S} = 2/5$, $x \in [0, 1]$, $t \in [0, 0.6 \times 10^{-4}]$ for the two-soliton initial condition (89). The boundary conditions

$$u(0, t) = u(1, t) = u_x(1, t) = 0, \quad (91)$$

were used in all cases.

For the HWM one obtains

$$\begin{aligned} \mathbf{R}_{x3} &= \mathbf{P}_{x3} + \mathbf{P}_{x2}(1) \cdot (\mathbf{x} - \mathbf{x}^2) + \mathbf{P}_{x3}(1) \cdot (\mathbf{x}^2 - 2\mathbf{x}), \\ \mathbf{S}_{x3} &= 0. \end{aligned} \quad (92)$$

In case of the HOHWM, the equation is evaluated at its boundaries as

$$u_t(0, t) + \alpha u(0, t) u_x(0, t) + u_{xxx}(0, t) = 0, \quad u_t(1, t) + \alpha u(1, t) u_x(1, t) + u_{xxx}(1, t) = 0. \quad (93)$$

Considering the homogeneous boundary conditions (91), we have $u_t(0, t) = u_t(1, t) = 0$ and the above simplifies to

$$u_{xxx}(0, t) = 0, \quad u_{xxx}(1, t) = 0. \quad (94)$$

The addition of (94) gives

$$\begin{aligned} u &= \mathbf{R}_5 \cdot \mathbf{A} + \mathbf{S}_5, \\ \mathbf{R}_{x5} &= \mathbf{P}_{x5} + \frac{1}{2} \mathbf{P}_{x3}(1) \cdot (-\mathbf{x}^4 + 2\mathbf{x}^3 - \mathbf{x}^2) + \frac{1}{2} \mathbf{P}_{x4}(1) \cdot (4\mathbf{x}^4 - 10\mathbf{x}^3 + 6\mathbf{x}^2) \\ &\quad + \frac{1}{2} \mathbf{P}_{x5}(1) \cdot (-6\mathbf{x}^4 + 16\mathbf{x}^3 - 12\mathbf{x}^2), \\ \mathbf{S}_{x5} &= 0 \end{aligned} \quad (95)$$

for the HOHWM.

3.5 The modified Korteweg–de Vries equation

The mKdV equation (13) was numerically solved using the HOHWM. Both uniform as well as nonuniform grid approaches were used for the equation. The homogeneous boundary conditions

$$u(0,t) = u(1,t) = u_x(1,t) = 0 \quad (96)$$

were used. In order to get the initial condition, the exact solution (14) was evaluated at $t = 0$, which gives

$$u(x,0) = \sqrt{-\frac{c}{\alpha\beta}} \operatorname{sech} \left[\sqrt{\frac{c}{\beta}} (x-x_0) \right]. \quad (97)$$

In order to be able to find for the extra integration coefficients introduced by the HOHWM, the equation (13) is evaluated at its boundaries as

$$u_t(0,t) + \alpha u(0,t)u_x(0,t) + u_{xxx}(0,t) = 0, \quad u_t(1,t) + \alpha u(1,t)u_x(1,t) + u_{xxx}(1,t) = 0. \quad (98)$$

The homogeneous boundary conditions (96) mean that $u_t(0,t) = u_t(1,t) = 0$ which simplifies (98) to

$$u_{xxx}(0,t) = 0, \quad u_{xxx}(1,t) = 0. \quad (99)$$

The boundary conditions (96) along with (99) give

$$\begin{aligned} u &= \mathbf{R}_5 \cdot \mathbf{A} + \mathbf{S}_5, \\ \mathbf{R}_5 &= \mathbf{P}_5 + \mathbf{P}_5(1) (\mathbf{x}^2 - 2\mathbf{x}) + \mathbf{P}_4(1) (\mathbf{x} - \mathbf{x}^2) + \mathbf{P}_2(1) \frac{3\mathbf{x}^2 - 2\mathbf{x} - \mathbf{x}^4}{24} \\ \mathbf{S}_5 &= 0. \end{aligned} \quad (100)$$

The equation parameters $\alpha = -1$, $\beta = 10^{-2}$ and the initial condition coefficients $c = 16$ and $x_0 = 0.3$ were used within this thesis. The calculations were carried out until the final time $t_f = \frac{1-2x_0}{c} = 1/40$.

3.6 The Sine–Gordon equation

The numerical experiments involving the sine–Gordon equation (15) were carried out using the HOHWM. Uniform, nonuniform as well as adaptive grid approaches were used. The boundary conditions for the sine–Gordon equation were used as

$$u(0,t) = 0, \quad u(1,t) = \pi. \quad (101)$$

The exact solution (16) was evaluated at $t = 0$ to give

$$u(x,0) = 4\arctan \left[\exp \left(\frac{x-x_0}{\sqrt{1-c^2}} \right) \right] \quad (102)$$

as the initial condition. In it, c is the phase speed of the travelling wave and x_0 is its initial phase.

In order to obtain the extra coefficients introduced by the HOHWM, the equation was evaluated at its boundaries as

$$u_t(0,t) - u_{xx}(0,t) + \sin u(0,t) = 0, \quad u_t(1,t) - u_{xx}(1,t) + \sin u(1,t) = 0. \quad (103)$$

The constant boundary conditions (101) imply that $u_t(0,t) = u_t(1,t) = 0$. That alongside the boundary conditions (101) mean that (103) simplifies to

$$u_{xx}(0,t) = 0, \quad u_{xx}(1,t) = 0. \quad (104)$$

The boundary conditions (101) along with (104) give

$$\begin{aligned}u(x, t) &= \mathbf{R}_4 \cdot \mathbf{A} + \mathbf{S}_4, \\ \mathbf{R}_4 &= \mathbf{P}_4 - \mathbf{P}_4(1) + \mathbf{P}_2(1) \frac{\mathbf{x} - \mathbf{x}^3}{6} \\ \mathbf{S}_4 &= 2\pi\mathbf{x}\end{aligned}\tag{105}$$

for the HOHWM.

The sine-Gordon equation was numerically solved for the parameter $c = 1 - 5 \cdot 10^{-5}$. It must be noted that as $c \rightarrow 1$, the solution resembles a step-function more and more.

4 Numerical results

The results of the numerical experiments carried out within the thesis will be shown and analysed here. First, the 2D spectral analysis results will be discussed in subsection 4.1. The numerical results obtained by the HWM and HOHWM are then discussed in subsection 4.2.

4.1 2D Spectral analysis

The 2D spectral analysis was carried out in case of the KP equation (2). A number of different phenomena were observed. These phenomena will be described in detail in the following subsections. These results were obtained during the construction of the research report [127] which was the basis for Paper I. Some aspects that were not explicitly included in Paper I will also be covered here.

While many different numerical calculations were carried out with different parameter values (see Section 3.2 as well as Table 4.3 in report [127]), only a small subset will be discussed here. The initial condition (73) with parameters $a_x = 1$, $\beta = 0.2, 0.3, 0.4$ and $a_y = 2$ was used along with periodic boundary conditions. Numerical experiments were carried out within the time domain $t \in [0, 60]$. The values of the dispersion parameter were changed in order to see how it affects the solution. Different values for the logarithmic dispersion parameter d_l were used. Within the solution a complex wave structure emerges where solitary waves are localized with respect to both the x and y axes.

4.1.1 Periodicity

It was found that two solitonic structures were formed simultaneously: KdV soliton like solitary waves along the x axis and breather like structures along the y axis. The amplitude spectrum was analysed in order to determine whether or not the solution is (quasi)periodic. In set of Figs. 2-5 amplitude spectrum is presented for $a_x = 1, \beta = 0.4, a_y = 2$ and $d_l = 1, 1.3, 1.5, 1.8$. Fig. 2 shows the first three spectral amplitudes over the integration interval for $d_l = 1$. It shows that $a_1(y, t)$ tends to have maximal values where $a_2(y, t)$ has minimal values. A similar situation can be observed for $d_l = 1.3$, in Fig. 3 where the (quasi)period is simply longer. However, for higher values of $d_l = 1.5, 1.8$ (Figs. 3-5), the situation changes. Periodicity seems to disappear. This has also been shown to happen in case of the KdV equation [135].

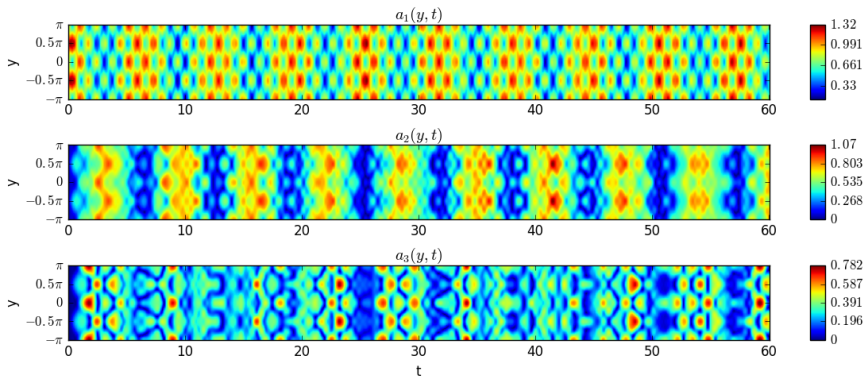


Figure 2 - Spectral amplitudes for the KP equation with parameters $a_x = 1$, $\beta = 0.4$, $a_y = 2$ and $d_l = 1$

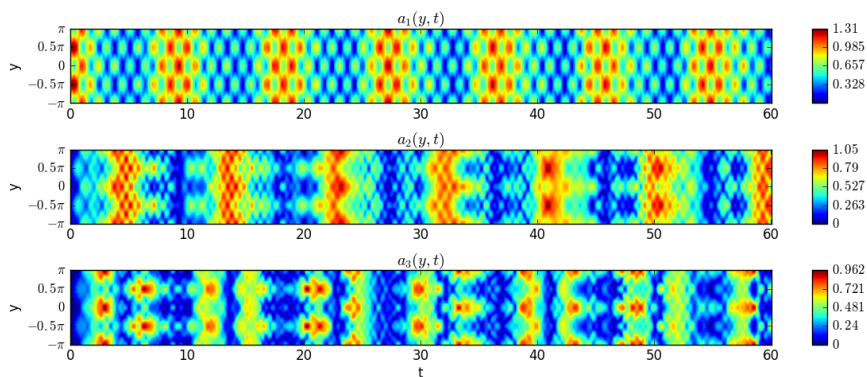


Figure 3 – Spectral amplitudes for the KP equation with parameters $a_x = 1$, $\beta = 0.4$, $a_y = 2$ and $d_l = 1.3$

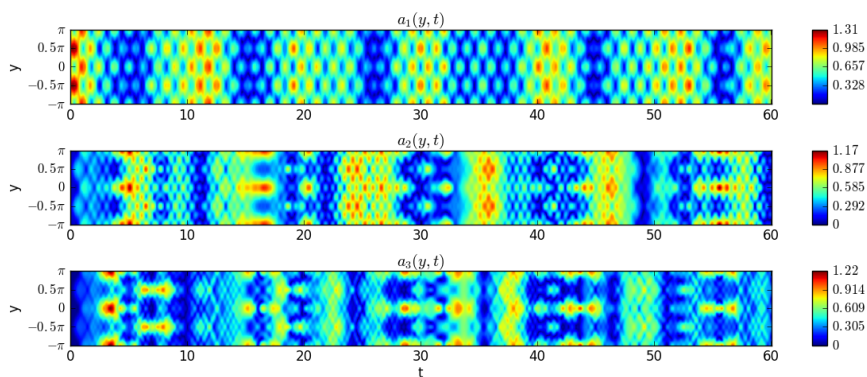


Figure 4 – Spectral amplitudes for the KP equation with parameters $a_x = 1$, $\beta = 0.4$, $a_y = 2$ and $d_l = 1.5$

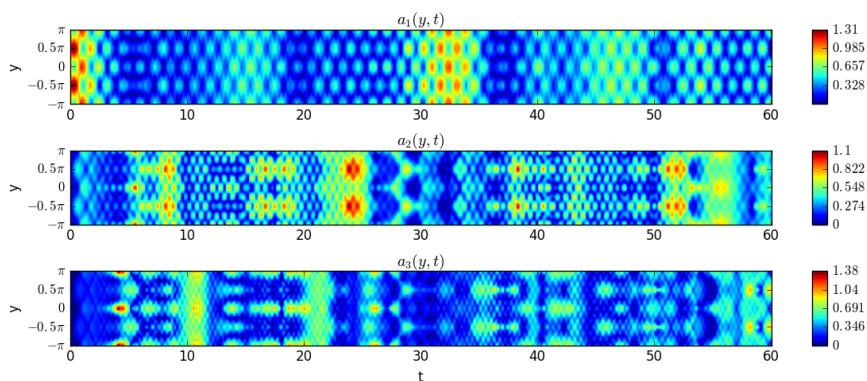


Figure 5 – Spectral amplitudes for the KP equation with parameters $a_x = 1$, $\beta = 0.4$, $a_y = 2$ and $d_l = 1.8$

4.1.2 Recurrence

The concept of recurrence was first introduced in [157]. In general, it states that at the time moment denoted t_R , a wave that is extremely similar to the initial waveform is formed [133]. Spectral amplitudes can be used to track recurrence. One can say that when $t \rightarrow t_R$, $a_k(y, t) \rightarrow a_k(y, 0), \forall k, y$. If recurrence is found at each $t \approx jt_R, j > 1$, the solution can be called quasiperiodic.

The spectral amplitudes in case of the KP equation with the logarithmic dispersion parameter $d_l = 0$ and the initial condition parameters $a_2 = 2, \beta = 0.4$ and $a_y = 2$ are shown in Fig. 6. Since there are an even number of periods of the initial condition over the x axis, the odd numbered spectral amplitudes are all almost zeros and are thus omitted here. One can see that near e.g $t \approx 12.7$, spectral amplitudes look similar to the initial state at $t = 0$. In order to determine the precise time of recurrence, the individual spectral amplitudes $a_k(y, t)$ were averaged over y . The corresponding averages around $t = 12.7$ are presented in Fig. 7, which gives a much clearer picture of local maxima. It must be noted that in Fig. 7, the scale for a_2 is on the left hand side and the scale for $a_4 - a_{10}$ is on the right hand side. Using Fig. 6 one is able to find 6 different time moments where recurrence can be said to have occurred with the first being at $t = 1.6$. These are also marked on Figs. 6 with small arrows. Of those 6 recurrences, the one at $t = 12.7$ turned out to be the one that most closely mimics the initial waveform, see Fig. 8. Due to the complex nature of the interaction process, the wave profile at $t = 12.7$ does not match the initial waveform perfectly. In fact, it is shifted along the x axes by 0.295.

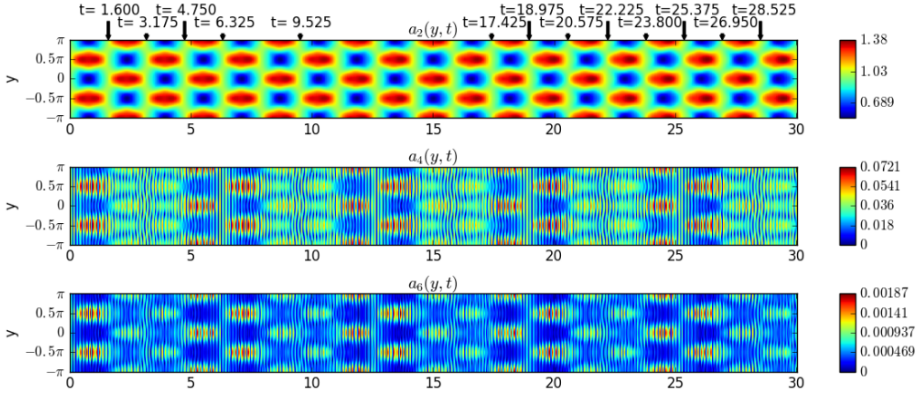


Figure 6 - Spectral amplitudes for the KP equation with parameters $a_x = 2, \beta = 0.4, a_y = 2$ and $d_l = 0$

4.1.3 Temporal symmetries

Temporal symmetries were observed in case of the KP equation in case of $\alpha_2 = 0.1, a_x = a_y = 2$ and are shown in cases where $\beta = 0.2, 0.3$. The spectral amplitudes for such solutions can be seen in Figs. 9 and 10, respectively. That is the same solution that was used for describing recurrence. At closer inspection of spectral amplitudes in Fig. 6 one can observe that the spectral amplitudes around a symmetry time $8.275 < t_s < 8.3$ look as though they have been reflected about the time moment t_s . In order to compare the two sides of t_s they are plotted together in Fig. 11 where the right hand side has been flipped. In fact, a similar situation can be found around $28.4 < t_s < 28.425$ which can be seen in Fig. 12.

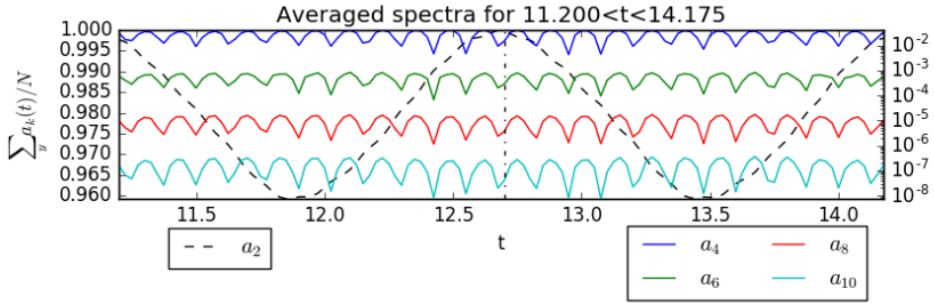


Figure 7 - Averaged spectral amplitudes for the KP equation with parameters $a_x = 2$, $\beta = 0.4$, $a_y = 2$ and $d_l = 0$ around $t = 12.7$

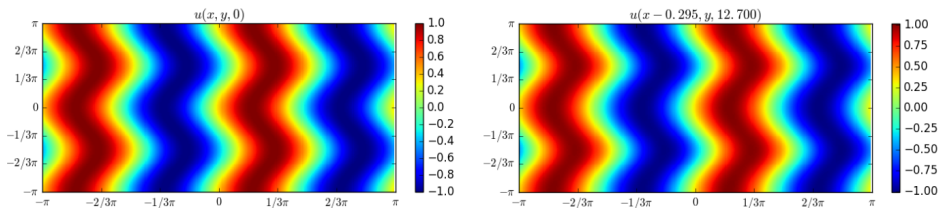


Figure 8 - Recurrence of the initial state in case of the KP equation at $t = 12.7$ (shifted on both axes) and the initial waveform for $a_x = 2$, $\beta = 0.4$, $a_y = 2$ and $d_l = 0$

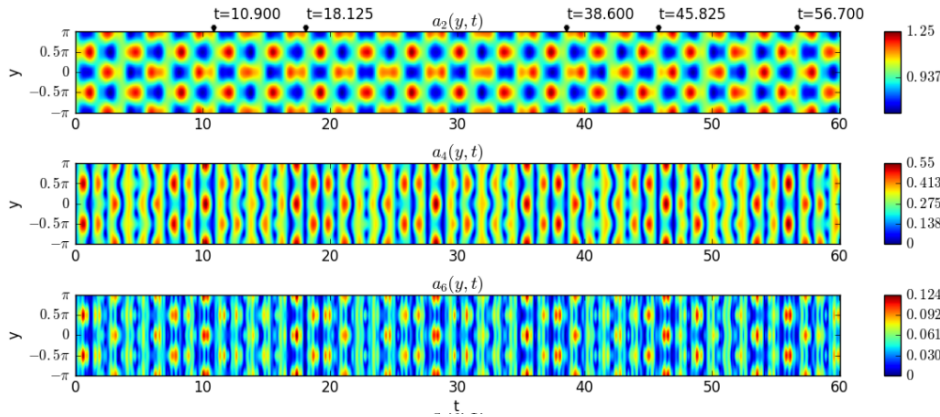


Figure 9 - Spectral amplitudes for the KP equation with parameters $a_x = 2$, $\beta = 0.2$, $a_y = 2$ and $d_l = 1$

4.2 The Haar wavelet method

The results of various case studies are described separately here. The numerical results and their significance are described separately after presenting the results for each model equation.

4.2.1 The Burgers' equation

When the Burgers' equation (4) was solved using the HWM on both the spatial and temporal coordinates, one could also measure the convergence rate. Such results can be seen in Table 1, where the number of grid points is changed on the spatial and temporal axes sep-

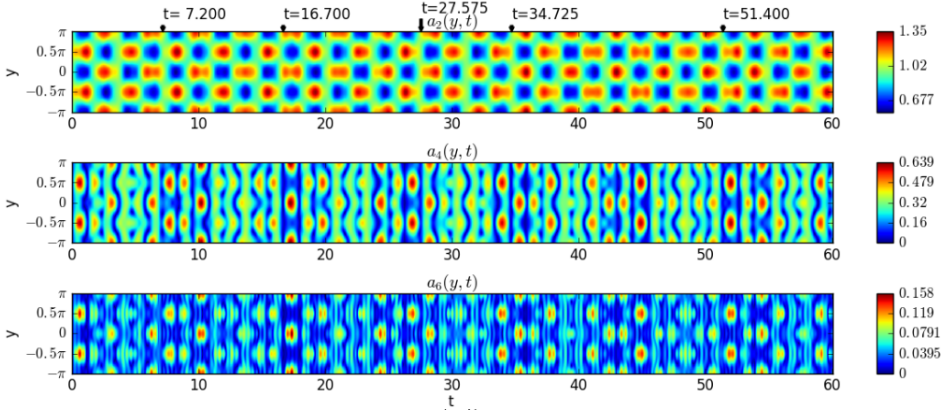


Figure 10 - Spectral amplitudes for the KP equation with parameters $\alpha_x = 2$, $\beta = 0.3$, $\alpha_y = 2$ and $d_l = 1$

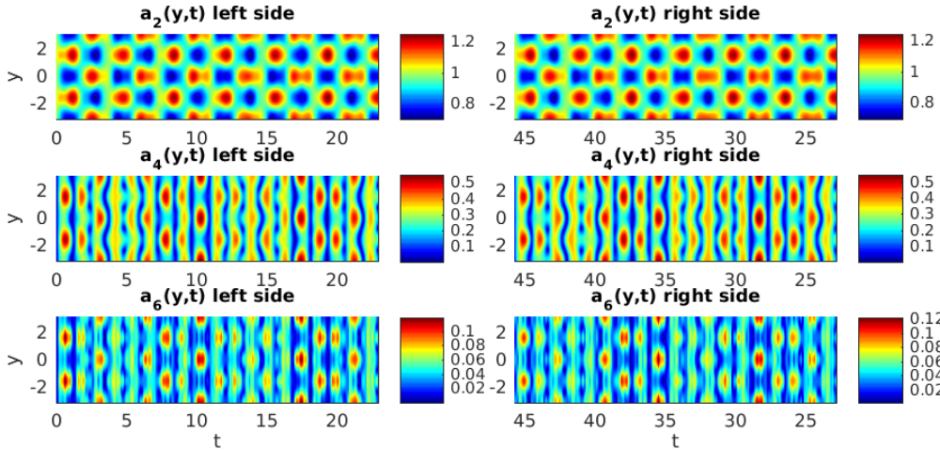


Figure 11 - KP temporal symmetry around the time $t_s \approx 22.875$ for amplitude spectrum in case of $\alpha_x = \alpha_y = 2$, $\beta = 0.2$, $\alpha_2 = 0.1$

arately. The result was evaluated in the middle of the spatial as well as temporal domain in order to find the convergence somewhere off the grid points. The Burgers' equation was also solved numerically for various values of ν for which the maximal deviation from the exact solution can be seen in Table 2

The Burgers' equation was also solved using ODE solvers for temporal derivatives and the HOHWM for spatial ones. In that case, the obtained results are summed up in Tables 3 and 4, the former of which shows the critical time moment t_c which is the maximal time for which $\max_{x,t < t_c} |u(x,t) - u_e(x,t)| < 10^{-3}$; and the latter shows the maximal deviation from the exact solution (5).

The maximal deviations from the exact solution Δu in case of the Burgers' are shown in Table 4 where $N = 2M$ denotes the number of grid points. It must be noted that for $J < 6$ the HOHWM using the uniform grid was unable to successfully calculate the numerical result up to the final time of $t_f = 0.5$. However, even at $J = 6$ the nonuniform grid approach easily outperforms the uniform grid version of the HOHWM. The table also shows that for

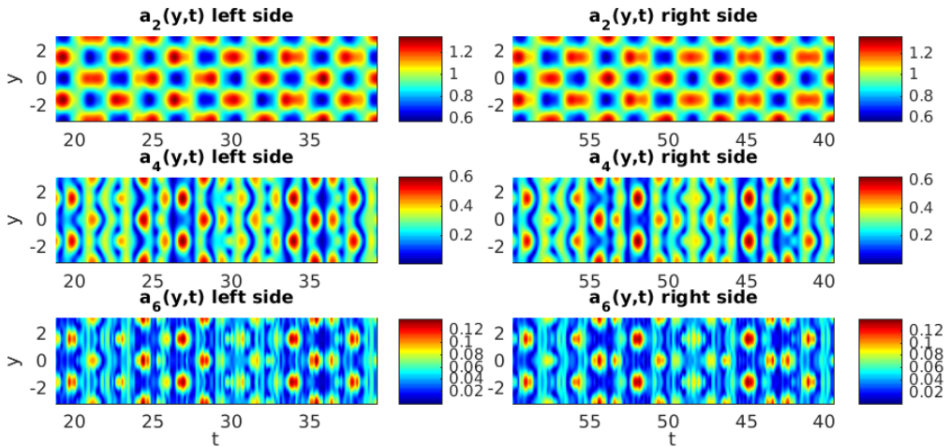


Figure 12 - KP temporal symmetry around the time $39.4 < t_s < 39.425$ for amplitude spectrum in case of $a_x = a_y = 2$, $\beta = 0.3$, $\alpha_2 = 0.1$

Table 1 - Convergence of the HWM in case of the Burgers' equation with $\nu = 1/10$ and $\nu = \frac{1}{10\pi}$ at $u(\frac{1}{2}, \frac{1}{2})$

N_x	N_t	k_i		N_t	N_x	k_i	
		$\nu = 1/10$	$\nu = \frac{1}{10\pi}$			$\nu = 1/10$	$\nu = \frac{1}{10\pi}$
4	16	—	—	4	16	—	—
8	16	—	—	8	16	—	—
16	16	2.5155	3.9938	16	16	2.5914	2.2742
32	16	2.1310	2.4626	32	16	2.0601	2.0625
64	16	2.0328	2.0394	64	16	2.0130	2.0154
128	16	2.0082	2.0103	128	16	2.0031	2.0038
256	16	2.0021	2.0026	256	16	2.0008	2.0010
512	16	2.0005	2.0006	512	16	2.0002	2.0002

Table 2 - Maximum deviation from the exact solution on 16×16 grid with the HWM for $\nu = \frac{1}{10}$, $\nu = \frac{1}{5\pi}$ and $\nu = \frac{1}{10\pi}$; on a 256×16 grid for $\nu = \frac{1}{100\pi}$ and $\nu = \frac{1}{160\pi}$

ν	$\frac{1}{10}$	$\frac{1}{5\pi}$	$\frac{1}{10\pi}$	$\frac{1}{100\pi}$	$\frac{1}{160\pi}$
Δu	0.00168	0.00359	0.01874	0.00612	0.02332

resolution $J > 6$ the accuracy no longer increases significantly.

The HWM results in case of $\nu = \frac{1}{100\pi}$ in Table 2 can also directly be compared to the uniform and nonuniform grid results at the same value of ν in Tables 3 and 4. It is clear that the HOHWM outperforms the HWM even from this simple comparison.

The shape of a typical solution of the Burgers' equation can also be seen in Fig. 13. In the figure, the both the calculated solution as well as the exact solution are shown.

The 2D HWM approach described in Table 1 shows that the convergence of the convergence with respect to either axis of the numerical method is equal to 2 as one would expect according to the literature [110]. Furthermore, Table 2 shows that while the HWM is able to find numerical solutions for the Burgers equation in all the different cases, the maximal deviation from the exact solution increases with the increase of ν when using a

Table 3 – Values of t_c against the resolution J with the HOHWM in the case of the Burgers' equation with $v = \frac{1}{100\pi}, v = \frac{1}{110\pi}, \frac{1}{120\pi}$; parameter q characterises the nonuniformity

v		$\frac{1}{100\pi}$		$\frac{1}{110\pi}$		$\frac{1}{120\pi}$	
J	q	Uniform t_c	Nonuniform t_c	Uniform t_c	Nonuniform t_c	Uniform t_c	Nonuniform t_c
3	0.71	0.2375	0.39	0.1625	0.38	0.1625	0.38
4	0.85	0.2875	0.50	0.275	0.50	0.225	0.50
5	0.92	0.2875	0.50	0.3181	0.50	0.30	0.50
6	0.97	0.3580	0.50	0.3542	0.50	0.3745	0.50
7	0.99	0.50	0.50	0.4646	0.50	0.4143	0.50
8	*	0.50	*	0.50	*	0.50	*

Table 4 – Maximal deviation from the exact solution Δu against the resolution J in the case of the Burgers' equation with $v = \frac{1}{100\pi}, \frac{1}{110\pi}, \frac{1}{120\pi}$; parameter q describes the grid according to (61)

v			$\frac{1}{100\pi}$		$\frac{1}{110\pi}$	
J	N	q	Uniform Δu	Nonuniform Δu	Uniform Δu	Nonuniform Δu
3	16	0.71	—	0.004674	—	0.0066496
4	32	0.95	—	$1.1031 \cdot 10^{-4}$	—	$1.1622 \cdot 10^{-4}$
5	64	0.92	—	$7.0345 \cdot 10^{-6}$	—	$7.3215 \cdot 10^{-6}$
6	128	0.97	0.0418	$5.1019 \cdot 10^{-6}$	0.0875	$5.1855 \cdot 10^{-6}$
7	256	0.99	$6.8360 \cdot 10^{-4}$	$4.0604 \cdot 10^{-6}$	0.001034	$4.8919 \cdot 10^{-6}$
8	512	*	$5.0941 \cdot 10^{-5}$	*	$8.0159 \cdot 10^{-5}$	*

v			$\frac{1}{120\pi}$	
J	N	q	Uniform Δu	Nonuniform Δu
3	16	0.71	—	0.005067
4	32	0.95	—	$1.3072 \cdot 10^{-4}$
5	64	0.92	—	$7.974 \cdot 10^{-6}$
6	128	0.97	0.2021	$3.8774 \cdot 10^{-6}$
7	256	0.99	0.001611	$5.9934 \cdot 10^{-6}$
8	512	*	$1.0959 \cdot 10^{-4}$	*

uniform grid. However, that is not the case when using a nonuniform grid.

The results shown in Tables 2 and 4 show that the uniform grid HOHWM outperforms the HWM (when comparing at $v = \frac{1}{100\pi}$). Furthermore, it is clear that the nonuniform grid HOHWM in turn significantly outperforms the uniform grid HOHWM. In fact, one can get a result of the same (or even better) accuracy using the nonuniform grid with 8 times fewer

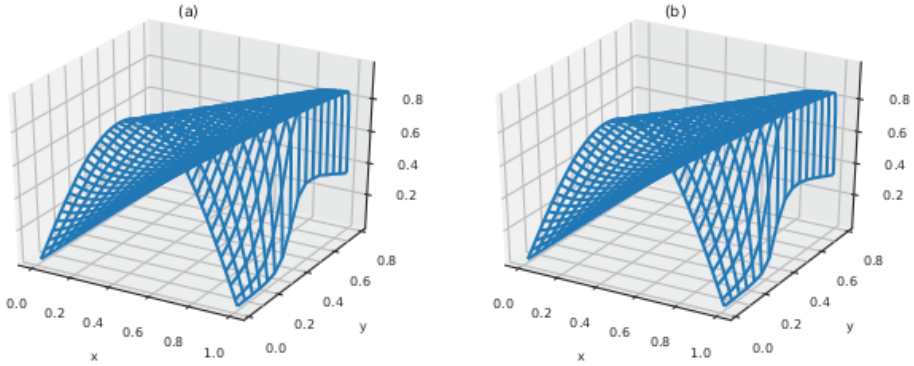


Figure 13 – Typical numerical solution of the Burgers' equation (left) and exact solution (right)

grid points compared to the uniform grid version. Additionally, the maximal deviation from the exact solution in case of the uniform grid HOHWM is 2 orders of magnitude smaller than in the HWM case.

These results demonstrate (i) the advantage of the HOHWM over the HWM and (ii) the usage of the nonuniform grid can give an even more significant gain in accuracy than the switch from the HWM to the HOHWM.

4.2.2 The 2D Burgers' equation

The 2D Burgers' equation (7) was numerically solved using the HWM on its two spatial coordinates and ODE solvers for the temporal derivatives. The maximal deviation from the exact solution was measured and the equation was evaluated at different values of Reynold's number R . In these computations the resolution on both spatial coordinates is kept the same. However, this is not strictly necessary.

Table 5 – Maximal deviations Δu and Δv from exact solution for the 2D Burgers' equation (7) compared to its exact solution (8) at different resolutions and Reynolds numbers with the HWM

J	N	$R = 220$		$R = 260$	
		Δu	Δv	Δu	Δv
2	8	0.0345186	0.0420620	0.0614871	0.0684815
3	16	0.0065951	0.0089431	0.0102949	0.0134474
4	32	0.0018286	0.0015675	0.0026377	0.0025030
5	64	0.0006597	0.0006814	0.0007456	0.0007940
6	128	0.0005707	0.0005707	0.0005952	0.000595

J	N	$R = 300$		$R = 340$	
		Δu	Δv	Δu	Δv
2	8	0.1153377	0.1193631	0.2178892	0.2274026
3	16	0.0153208	0.0185581	0.0230894	0.0253803
4	32	0.0035963	0.0036502	0.0046713	0.0052699
5	64	0.0009196	0.0009025	0.0010940	0.0010823
6	128	0.0005832	0.0005974	0.0005858	0.0006499

The maximal deviations Δu and Δv in Table 5 show that the HWM is capable of handling steep changes in the exact solution in case of two spatial dimensions. A typical solution

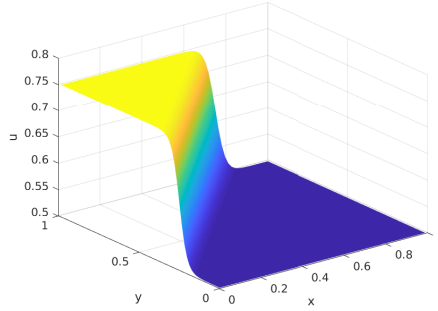


Figure 14 - Calculated u in the case of $R = 340$ and $J = 5$

can be seen in Fig. 14. While the maximal deviation of the exact solution increases as the Reynolds' number R increases, the maximal deviation does not become extremely large within the cases that were numerically evaluated here.

4.2.3 The KdV equation

The KdV equation (9) was solved using the HWM, the uniform grid HOHWM, (static) nonuniform grid HOHWM as well as the adaptive grid HOHWM. In all cases the temporal derivatives were handled using an ODE solver. It was solved for a number of different equation and initial condition parameter values. The first set of solutions were with the uniform grid HWM and HOHWM in case of a 1-soliton exact solution (10). The initial conditions (88) and boundary conditions (91) were used. The maximal deviation from the exact solution Δu as well as the relative maximal deviation $\Delta_{rel}u = \frac{\Delta u}{\max_{x,t}u}$ in such a case can be seen in Tables 6 and 7.

Table 6 - Results for the KdV equation: maximal deviation of the numerical solution from the exact solution $\max\Delta u$ and maximal relative deviation $\max_{rel}\Delta u$ against the resolution parameter J with initial conditions (88) and boundary conditions (91) ($\alpha = 1$, $c = 1000$, $x_0 = 1/4$, $x \in [0, 1]$, $t \in [0, 0.5 \times 10^{-3}]$)

J	N	Δu		$\Delta_{rel}u$	
		HWM	HOHWM	HWM	HOHWM
4	32	134.5414	32.85357	0.0448471	0.0109512
5	64	68.76035	3.316314	0.0229201	0.0011054
6	128	19.26319	0.8202067	0.0064211	0.0002734
7	256	5.066037	0.844972	0.0016887	0.0002817

The next set of solutions were calculated with the uniform grid HWM and HOHWM in case of a 2-soliton exact solution (11). The maximal deviation from the exact solution in this case can be seen in Tables 8 and 9.

A typical example of the numerical solution to the KdV equation in the two cases described above can be seen in Fig. 15.

The final set of results were obtained at different equation parameter values. They were obtained using the HOHWM on a uniform grid, a (static) nonuniform grid as well as an adaptive grid. The same initial conditions and boundary conditions were used as before. According to Paper III, a number of calculations were carried out with different

Table 7 – Results for the KdV equation: maximal deviation of the numerical solution from the exact solution Δu and maximal relative deviation $\max_{rel}\Delta u$ against the resolution parameter J with initial conditions (88) and boundary conditions (91) ($\alpha = 6$, $c = 1000$, $x_0 = 1/4$, $x \in [0, 1]$, $t \in [0, 0.5 \times 10^{-3}]$)

J	N	Δu		$\Delta_{rel}u$	
		HWM	HOHWM	HWM	HOHWM
4	32	22.42356	5.475594	0.0448471	0.0109512
5	64	11.46226	0.5527193	0.0229245	0.0011054
6	128	3.210801	0.1367652	0.0064216	0.0002735
7	256	0.8443429	0.1408244	0.0016887	0.0002816

Table 8 – Results for the KdV equation soliton interaction: maximal deviation of the numerical solution from the exact solution $\max\Delta u$ and maximal relative deviation $\max_{rel}\Delta u$ against the resolution parameter J with initial conditions (89) and boundary conditions (91) ($\alpha = 1$, $c_B = 10000$, $x_{0B} = 1/5$, $c_S = 10000/3$, $x_{0S} = 2/5$, $x \in [0, 1]$, $t \in [0, 0.6 \times 10^{-4}]$)

J	N	Δu		$\Delta_{rel}u$	
		HWM	HOHWM	HWM	HOHWM
4	32	3951164	2246754	131.7054667	74.8918000
5	64	6210848	202544.7	207.0282667	6.7514900
6	128	1567.924	199.7707	0.052264	0.0066590
7	256	542.1262	14.4892	0.0180709	0.0004830

Table 9 – Results for the KdV equation soliton interaction: maximal deviation of the numerical solution from the exact solution $\max\Delta u$ and maximal relative deviation $\max_{rel}\Delta u$ against the resolution parameter J with initial conditions (89) and boundary conditions (91) ($\alpha = 6$, $c_B = 10000$, $x_{0B} = 1/5$, $c_S = 10000/3$, $x_{0S} = 2/5$, $x \in [0, 1]$, $t \in [0, 0.6 \times 10^{-4}]$)

J	N	Δu		$\Delta_{rel}u$	
		HWM	HOHWM	HWM	HOHWM
4	32	215719.2	380037.1	43.1438400	76.0074200
5	64	104514.6	31103.69	20.9029200	6.2207380
6	128	260.845	33.305	0.0521690	0.0066610
7	256	90.35663	2.415028	0.0180713	0.0004830

values for the adaptive grid parameters in order to determine the parameter values corresponding to the most accurate solution. The deviation from the exact 1-soliton solution (10) in this case can be seen in Table 10

Tables 6–9 show that the use of the HOHWM over the HWM significantly increases the accuracy of the numerical results. It is also clear that in the case of the two KdV soliton interaction, a small number of grid points is not sufficient to calculate a numerical result of sufficient accuracy with either the HWM or the HOHWM. However, the HOHWM gives a significantly more accurate result once a sufficient number of grid points is reached.

Table 10 shows that the use of the adaptive grid significantly increases the accuracy of the numerical solution. In fact, 4 times fewer grid points can be used in order to gain a result of the same accuracy when using the HOHWM as opposed to the HWM. Furthermore,

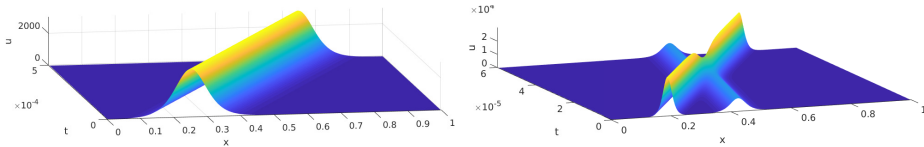


Figure 15 – Typical numerical solution of the KdV equation using the HOHWM. The KdV single soliton solution ($\alpha = 1$, $c = 1000$, $x_0 = 1/4$, $J = 7$ with initial conditions (88) and boundary conditions (91) on the left) and the interaction of KdV solitons ($\alpha = 1$, $c_B = 10000$, $x_{0B} = 1/5$, $c_S = 10000/3$, $x_{0S} = 2/5$, $J = 7$ with initial conditions (89) and boundary conditions (91) on the right)

Table 10 – Maximal deviation from the exact solution Δu against resolution J in the case of the KdV equation with $\alpha = 6$, $\beta = 4 \cdot 10^{-4}$ and $x_0 = 0.3$, $c = 2$, $t_f = 0.2$

J	Uniform grid	Grid (62) with $\gamma = 0.1$	Adaptive grid (63)			
	Δu		Δu	d	e	δ
4	—	—	0.41	0.1	0.004	$6.1679 \cdot 10^{-4}$
5	0.01123	0.001352	0.33	0.05	0.002	$1.5731 \cdot 10^{-5}$
6	0.002541	0.001143	0.4	0.1	0.002	$1.5085 \cdot 10^{-6}$
7	$1.704 \cdot 10^{-4}$	$7.694 \cdot 10^{-5}$	0.3	0.3	0.006	$1.2250 \cdot 10^{-5}$

at a small number of grid points the HWM is unable to successfully numerically solve the problem, whereas the HOHWM is able to do so with quite a small maximum deviation from the exact solution.

4.2.4 The mKdV equation

The mKdV equation (13) was solved using the uniform grid HOHWM, a (static) nonuniform grid as well as an adaptive grid approach. In all cases, the temporal derivatives were evaluated using an ODE solver. The initial conditions (97) and boundary conditions (96) were used. The relevant values of the adaptive grid parameters (d , e and δ) were obtained according to Paper III similar to the KdV equation. The results of such numerical experiments where the maximal deviation from the exact solution is shown can be seen in Table 11.

Table 11 – Maximal deviation from the exact solution Δu against resolution J in the case of the mKdV equation with $\alpha = -1$, $\beta = 10^{-2}$, $c = 16$ and $x_0 = 0.3$, $t_f = 1/40$

J	N	Uniform grid	Grid (62) with $\gamma = 0.1$	Adaptive grid (63)			
		Δu		Δu	d	e	δ
4	32	—	—	0.44	0.2	0.004	0.009246
5	64	0.0719508	0.070632	0.48	0.1	0.002	$1.86 \cdot 10^{-4}$
6	128	0.0117955	0.0052081	0.31	0.2	0.002	$6.1 \cdot 10^{-5}$
7	256	$8.4875 \cdot 10^{-4}$	—	0.3	0.2	0.048	$7.84 \cdot 10^{-4}$

Table 11 shows that while the static nonuniform grid does offer some advantage over the uniform grid HOHWM, most of the gained accuracy comes from the use of the adap-

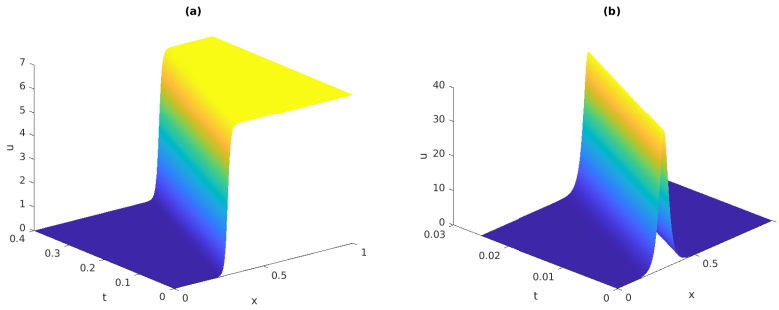


Figure 16 – Typical shape of the solutions of the mKdV (a) and the sine-Gordon (b) equations

tive grid. This is especially evident in case of lower number of grid points, where the uniform grid and static nonuniform grid approach were unable to successfully complete the numerical experiment, whereas the adaptive grid approach was able to do. A typical solution of the mKdV equation is shown in Fig. 16 on the left.

4.2.5 The sine-Gordon equation

The sine-Gordon equation (15) was solved using the uniform grid HOHWM, a (static) nonuniform grid HOHWM as well an adaptive grid. In all cases, the temporal derivatives were evaluated using an ODE solver. The initial conditions (102) and boundary conditions (101) were used. As was the case for the KdV and the mKdV equations, the adaptive grid parameter values were obtained according to Paper III. The maximal deviation from the exact solution (16) was computed in each numerical experiment. Such results can be seen in Table 12

Table 12 – Maximal deviation from the exact solution Δu against resolution J in the case of the sine-Gordon equation with $c = 1 - 5 \cdot 10^{-5}$ and $x_0 = 0.3$, $t_f = \frac{1-2x_0}{c}$

J	N	Uniform grid Δu	Grid (62) with $\gamma = 0.1$ Δu	Adaptive grid (63)			
				d	e	δ	Δu
4	32	1.189817	1.095051	0.33	0.3	0.008	0.033198
5	64	0.4856858	0.3261581	0.32	0.2	0.018	0.0018608
6	128	0.1039031	0.06173826	0.3	0.2	0.018	$1.0331 \cdot 10^{-4}$
7	256	0.01376712	0.006484227	0.3	0.2	0.024	$1.1429 \cdot 10^{-5}$

The results in Table 12 show that while there are some advantages to using a static nonuniform grid, most of the gained accuracy comes from the employment of the adaptive grid approach in this case as well. In fact, one can see that the adaptive grid approach with 64 grid points is more accurate than both the uniform grid and static nonuniform grid approaches in case of 256 grid points. While the uniform and static nonuniform grid are able to solve the problem even at a low number of grid points, the corresponding deviations from the exact solution Δu are large. A typical solution of the sine-Gordon equation is shown in Fig. 16 on the right.

5 Conclusions

The 2D DSA was developed and used in order to gain insight into the character of the numerical solutions of the KP equation. It allowed to discover instances of recurrence as well as (quasi)periodicity more easily and even to detect temporal symmetries.

The HWM was employed for numerical solutions of various model equations: the Burgers' equation, the 2D Burgers' equation and the KdV equation. The Burgers' equation, in particular, was solved in two different ways. In the first, the HWM was used to approximate both the spatial as well as the temporal derivatives; and in the second, only spatial derivatives were approximated using the HWM and the temporal derivatives were approximated using other known approximation methods. For the other model equations, the latter approach was used instead of the former. The various numerical experiments showed the need for a more accurate method.

Thus, the HOHWM was used to evaluate some of the previously mentioned model equations (the Burgers' equation and the KdV equation) in order to obtain an improvement in accuracy. In addition, the mKdV and sine-Gordon equations were also included here and numerically solved using the HOHWM. The HOHWM was shown to be of superior accuracy when compared to the HWM.

Since many of the solutions of the considered PDEs had abrupt changes, a new approach was needed to improve accuracy further. Thus, a nonuniform grid approach was developed that could be used alongside the HOHWM. This approach showed a significant improvement in accuracy in case of problems with abrupt changes within their solutions. The nature of the solution of the Burgers' equation meant that it showed significant improvements over the uniform grid HOHWM. While the accuracy of solutions to the other model equations also increased somewhat, it was not that significant.

Finally, an adaptive grid approach was developed for the HOHWM. This approach involved changing the nonuniform grid in time so that the areas prone to give higher errors have more grid points. The KdV, mKdV and sine-Gordon equations were evaluated using this novel method. The approach was shown to give another significant boost in accuracy over static nonuniform grid approaches for the mentioned model equations.

The model adaptive grid HOHWM (which can simply be called the adaptive HOHWM or AHOHWM) was shown to give significant increase in accuracy given the same number of grid points when compared to the uniform grid as well as static nonuniform grid HOHWM. In fact, it was shown that the same or even better level accuracy can be achieved with 8–16 times fewer grid points. Computationally, the most expensive part of solving an equation is solving the system of algebraic equations. Thus, solving a system of 8–16 times fewer equations gives a significant advantage in computational complexity.

This thesis showed that

- the PsM along with the DSA is a powerful tool for analyzing the behaviour of a 2D evolution equation;
- the accuracy of the HWM can be improved by using the HOHWM;
- the accuracy of the HOHWM can be improved by employing a nonuniform grid approach;
- the accuracy of the nonuniform grid HOHWM can be improved by allowing adaptive grid changes.

List of Figures

1	Haar wavelets on a nonuniform grid for $J = 2$ as described by (31)–(33)	18
2	Spectral amplitudes for the KP equation with parameters $a_x = 1, \beta = 0.4,$ $a_y = 2$ and $d_l = 1$	31
3	Spectral amplitudes for the KP equation with parameters $a_x = 1, \beta = 0.4,$ $a_y = 2$ and $d_l = 1.3$	32
4	Spectral amplitudes for the KP equation with parameters $a_x = 1, \beta = 0.4,$ $a_y = 2$ and $d_l = 1.5$	32
5	Spectral amplitudes for the KP equation with parameters $a_x = 1, \beta = 0.4,$ $a_y = 2$ and $d_l = 1.8$	32
6	Spectral amplitudes for the KP equation with parameters $a_x = 2, \beta = 0.4,$ $a_y = 2$ and $d_l = 0$	33
7	Averaged spectral amplitudes for the KP equation with parameters $a_x = 2,$ $\beta = 0.4, a_y = 2$ and $d_l = 0$ around $t = 12.7$	34
8	Recurrence of the initial state in case of the KP equation at $t = 12.7$ (shifted on both axes) and the initial waveform for $a_x = 2, \beta = 0.4, a_y = 2$ and $d_l = 0$	34
9	Spectral amplitudes for the KP equation with parameters $a_x = 2, \beta = 0.2,$ $a_y = 2$ and $d_l = 1$	34
10	Spectral amplitudes for the KP equation with parameters $a_x = 2, \beta = 0.3,$ $a_y = 2$ and $d_l = 1$	35
11	KP temporal symmetry around the time $t_s \approx 22.875$ for amplitude spec- trum in case of $a_x = a_y = 2, \beta = 0.2, \alpha_2 = 0.1$	35
12	KP temporal symmetry around the time $39.4 < t_s < 39.425$ for amplitude spectrum in case of $a_x = a_y = 2, \beta = 0.3, \alpha_2 = 0.1$	36
13	Typical numerical solution of the Burgers' equation (left) and exact solu- tion (right)	38
14	Calculated u in the case of $R = 340$ and $J = 5$	39
15	Typical numerical solution of the KdV equation using the HOHWM. The KdV single soliton solution ($\alpha = 1, c = 1000, x_0 = 1/4, J = 7$ with ini- tial conditions (88) and boundary conditions (91) on the left) and the in- teraction of KdV solitons ($\alpha = 1, c_B = 10000, x_{0B} = 1/5, c_S = 10000/3,$ $x_{0S} = 2/5, J = 7$ with initial conditions (89) and boundary conditions (91) on the right)	41
16	Typical shape of the solutions of the mKdV (a) and the sine-Gordon (b) equations	42

List of Tables

1	Convergence of the HWM in case of the Burgers' equation with $v = 1/10$ and $v = \frac{1}{10\pi}$ at $u\left(\frac{1}{2}, \frac{1}{2}\right)$	36
2	Maximum deviation from the exact solution on 16×16 grid with the HWM for $v = \frac{1}{10}$, $v = \frac{1}{5\pi}$ and $v = \frac{1}{10\pi}$; on a 256×16 grid for $v = \frac{1}{100\pi}$ and $v = \frac{1}{160\pi}$	36
3	Values of t_c against the resolution J with the HOHWM in the case of the Burgers' equation with $v = \frac{1}{100\pi}$, $v = \frac{1}{110\pi}$, $\frac{1}{120\pi}$; parameter q characterises the nonuniformity	37
4	Maximal deviation from the exact solution Δu against the resolution J in the case of the Burgers' equation with $v = \frac{1}{100\pi}$, $\frac{1}{110\pi}$, $\frac{1}{120\pi}$; parameter q describes the grid according to (61)	37
5	Maximal deviations Δu and Δv from exact solution for the 2D Burgers' equation (7) compared to its exact solution (8) at different resolutions and Reynolds numbers with the HWM	38
6	Results for the KdV equation: maximal deviation of the numerical solution from the exact solution $\max \Delta u$ and maximal relative deviation $\max_{rel} \Delta u$ against the resolution parameter J with initial conditions (88) and boundary conditions (91) ($\alpha = 1$, $c = 1000$, $x_0 = 1/4$, $x \in [0, 1]$, $t \in [0, 0.5 \times 10^{-3}]$)	39
7	Results for the KdV equation: maximal deviation of the numerical solution from the exact solution Δu and maximal relative deviation $\max_{rel} \Delta u$ against the resolution parameter J with initial conditions (88) and boundary conditions (91) ($\alpha = 6$, $c = 1000$, $x_0 = 1/4$, $x \in [0, 1]$, $t \in [0, 0.5 \times 10^{-3}]$)	40
8	Results for the KdV equation soliton interaction: maximal deviation of the numerical solution from the exact solution $\max \Delta u$ and maximal relative deviation $\max_{rel} \Delta u$ against the resolution parameter J with initial conditions (89) and boundary conditions (91) ($\alpha = 1$, $c_B = 10000$, $x_{0B} = 1/5$, $c_S = 10000/3$, $x_{0S} = 2/5$, $x \in [0, 1]$, $t \in [0, 0.6 \times 10^{-4}]$)	40
9	Results for the KdV equation soliton interaction: maximal deviation of the numerical solution from the exact solution $\max \Delta u$ and maximal relative deviation $\max_{rel} \Delta u$ against the resolution parameter J with initial conditions (89) and boundary conditions (91) ($\alpha = 6$, $c_B = 10000$, $x_{0B} = 1/5$, $c_S = 10000/3$, $x_{0S} = 2/5$, $x \in [0, 1]$, $t \in [0, 0.6 \times 10^{-4}]$)	40
10	Maximal deviation from the exact solution Δu against resolution J in the case of the KdV equation with $\alpha = 6$, $\beta = 4 \cdot 10^{-4}$ and $x_0 = 0.3$, $c = 2$, $t_f = 0.2$	41
11	Maximal deviation from the exact solution Δu against resolution J in the case of the mKdV equation with $\alpha = -1$, $\beta = 10^{-2}$, $c = 16$ and $x_0 = 0.3$, $t_f = 1/40$	41
12	Maximal deviation from the exact solution Δu against resolution J in the case of the sine-Gordon equation with $c = 1 - 5 \cdot 10^{-5}$ and $x_0 = 0.3$, $t_f = \frac{1-2x_0}{c}$	42

References

- [1] M. J. Ablowitz. Nonlinear evolution equations, inverse scattering and cellular automata. In P. Olver and D. Sattinger, editors, *Solitons in physics, mathematics, and nonlinear optics*, pages 1–26. Springer, 1990.
- [2] M. J. Ablowitz. *Nonlinear dispersive waves: asymptotic analysis and solitons*. Cambridge University Press, 2011.
- [3] M. J. Ablowitz and D. E. Baldwin. Nonlinear shallow ocean-wave soliton interactions on flat beaches. *Phys. Rev. E*, 86:036305, 2012.
- [4] M. J. Ablowitz, D. J. Kaup, A. C. Newell, and H. Segur. The inverse scattering transform-fourier analysis for nonlinear problems. *Stud. Appl. Math.*, 53(4):249–315, 1974.
- [5] M. J. Ablowitz and H. Segur. *Solitons and the inverse scattering transform*. Siam, 1981.
- [6] E. N. Aksan. A numerical solution of Burgers' equation by finite element method constructed on the method of discretization in time. *Appl. Math. Comput.*, 170(2):895–904, 2005.
- [7] G. Allaire. *Numerical analysis and optimization: an introduction to mathematical modelling and numerical simulation*. Oxford University Press, 2007.
- [8] W. F. Ames. *Numerical methods for partial differential equations*. Academic Press, 2014.
- [9] P. Arminjon and C. Beauchamp. Numerical solution of Burgers' equations in two space dimensions. *Comput. Methods Appl. Mech. Engrg.*, 19(3):351–365, 1979.
- [10] I. Aziz, A. S. Al-Fhaid, et al. An improved method based on Haar wavelets for numerical solution of nonlinear integral and integro-differential equations of first and higher orders. *J. Comput. Appl. Math.*, 260:449–469, 2014.
- [11] I. Aziz et al. New algorithms for the numerical solution of nonlinear Fredholm and Volterra integral equations using Haar wavelets. *J. Comput. Appl. Math.*, 239:333–345, 2013.
- [12] I. Aziz, F. Khan, et al. A new method based on Haar wavelet for the numerical solution of two-dimensional nonlinear integral equations. *J. Comput. Appl. Math.*, 272:70–80, 2014.
- [13] I. Aziz, B. Šarler, et al. Wavelets collocation methods for the numerical solution of elliptic BV problems. *Appl. Math. Model.*, 37(3):676–694, 2013.
- [14] E. Babolian and A. Shamsavaran. Numerical solution of nonlinear Fredholm integral equations of the second kind using Haar wavelets. *J. Comput. Appl. Math.*, 225(1):87–95, 2009.
- [15] A. R. Bahadir. A fully implicit finite-difference scheme for two-dimensional Burgers' equations. *Appl. Math. Comput.*, 137(1):131–137, 2003.

- [16] C. Basdevant, M. Deville, P. Haldenwang, J. M. Lacroix, J. Ouazzani, R. Peyret, P. Orlandi, and A. T. Patera. Spectral and finite difference solutions of the Burgers equation. *Comput. & Fluids*, 14(1):23–41, 1986.
- [17] F. Bashforth and J. C. Adams. *An attempt to test the theories of capillary action: by comparing the theoretical and measured forms of drops of fluid*. Cambridge University Press, 1883.
- [18] M. Basto, V. Semiao, and F. Calheiros. Dynamics and synchronization of numerical solutions of the Burgers equation. *J. Comput. Appl. Math.*, 231(2):793–806, 2009.
- [19] H. Bateman. Some recent researches on the motion of fluids. *Monthly Weather Review*, 43(4):163–170, 1915.
- [20] E. R. Benton and G. W. Platzman. A table of solutions of the one-dimensional Burgers equation. *Quart. Appl. Math.*, 30(2):195–212, 1972.
- [21] S. Bertoluzza. An adaptive collocation method based on interpolating wavelets. In W. Dahmen, A. J. Kurdila, and P. Oswald, editors, *Wavelet Analysis and Its Applications*, volume 6, pages 109–135. Elsevier, 1997.
- [22] G. Beylkin and J. M. Keiser. An adaptive pseudo-wavelet approach for solving non-linear partial differential equations. In W. Dahmen, A. J. Kurdila, and P. Oswald, editors, *Wavelet Analysis and Its Applications*, volume 6, pages 137–197. Elsevier, 1997.
- [23] J. Biazar and H. Aminikhah. Exact and numerical solutions for non-linear Burger's equation by VIM. *Math. Comput. Modelling*, 49(7):1394–1400, 2009.
- [24] G. Biondini and D. Pelinovsky. Kadomtsev–Petviashvili equation. *Scholarpedia*, 3(10):6539, 2008. Available: http://var.scholarpedia.org/article/Kadomtsev-Petviashvili_equation, 2008.
- [25] E. Bour. *Théorie de la déformation des surfaces*. J. Ecole Pol., 1862.
- [26] J. Boussinesq. *Essai sur la théorie des eaux courantes*. Mém. prés par div. savants à la Acad. Sci, 1877.
- [27] P. Bowcock, E. Corrigan, and C. Zambon. Some aspects of jump-defects in the quantum sine-Gordon model. *J. High Energy Phys.*, 2005(08):023, 2005.
- [28] R. N. Bracewell. *The Fourier transform and its applications*. McGraw-Hill New York, 1986.
- [29] C. Brezinski and L. Wuytack. *Numerical analysis: Historical developments in the 20th century*. Elsevier, 2012.
- [30] E. O. Brigham. *The fast Fourier transform and its applications*. Prentice-Hall, Inc., 1988.
- [31] J. M. Burgers. A mathematical model illustrating the theory of turbulence. In R. V. Mises and T. V. Kármán, editors, *Advances in Applied Mechanics*, volume 1, pages 171–199. Academic Press, 1948.

- [32] J. M. Burgers. Statistical problems connected with the solution of a nonlinear partial differential equation. In W. F. Ames, editor, *Nonlinear Problems of Engineering*, pages 123–137. Academic Press, 1964.
- [33] C. Canuto, M. Y. Hussaini, A. Quarteroni, and T. A. Zang. *Spectral methods: fundamentals in single domains*. Springer Science & Business Media, 2007.
- [34] C. Cattani. Haar wavelet-based technique for sharp jumps classification. *Math. Comput. Modelling*, 39(2-3):255–278, 2004.
- [35] C. Cattani. On the existence of wavelet symmetries in archaea DNA. *Comput. Math. Methods Med.*, 2012, 2012.
- [36] C. Cattani and A. Kudreyko. Harmonic wavelet method towards solution of the Fredholm type integral equations of the second kind. *Appl. Math. Comput.*, 215(12):4164–4171, 2010.
- [37] C. Cattani and Y. Y. Rushchitskii. Cubically nonlinear versus quadratically nonlinear elastic waves: Main wave effects. *Internat. Appl. Mech.*, 39(12):1361–1399, 2003.
- [38] C. Cattani, J. J. Rushchitsky, and S. V. Sinchilo. Physical constants for one type of nonlinearly elastic fibrous micro-and nanocomposites with hard and soft nonlinearities. *Internat. Appl. Mech.*, 41(12):1368–1377, 2005.
- [39] S. Chakravarty, T. McDowell, and M. Osborne. Numerical studies of the KP line-solitons. *Commun. Nonlinear Sci. Numer. Simul.*, 44:37–51, 2017.
- [40] S. C. Chapra, R. P. Canale, et al. *Numerical methods for engineers*. Boston: McGraw-Hill Higher Education,, 2010.
- [41] C. F. Chen and C. H. Hsiao. Haar wavelet method for solving lumped and distributed-parameter systems. *IEE Proc. Control Theory Appl.*, 144(1):87–94, 1997.
- [42] A. J. Chorin. On the convergence of discrete approximations to the Navier-Stokes equations. *Math. Comp.*, 23(106):341–353, 1969.
- [43] R. W. Clough. The finite element method in plane stress analysis. In *Proceedings of 2nd ASCE Conference on Electronic Computation, Pittsburgh Pa., Sept. 8 and 9, 1960*, 1960.
- [44] J. D. Cole. On a quasi-linear parabolic equation occurring in aerodynamics. *Quart. Appl. Math.*, 9(3):225–236, 1951.
- [45] J. W. Cooley and J. W. Tukey. An algorithm for the machine calculation of complex Fourier series. *Mathematics of computation*, 19(90):297–301, 1965.
- [46] C. F. Curtiss and J. O. Hirschfelder. Integration of stiff equations. *Proc. Natl. Acad. Sci. USA*, 38(3):235, 1952.
- [47] O. Darrigol. Joseph Boussinesq’s legacy in fluid mechanics. *C. R. Méc.*, 345(7):427–445, 2017.
- [48] J. R. Dormand and P. J. Prince. A family of embedded Runge–Kutta formulae. *J. Comput. Appl. Math.*, 6(1):19–26, 1980.

- [49] P. G. Drazin and R. S. Johnson. *Solitons: an introduction*. Cambridge University Press, 1989.
- [50] P. Dubard and V. B. Matveev. Multi-rogue waves solutions: From the NLS to the KP-I equation. *Nonlinearity*, 26(12):R93–R125, 2013.
- [51] P. R. Eiseman. Adaptive grid generation. *Comput. Methods Appl. Mech. Engrg.*, 64(1-3):321–376, 1987.
- [52] M. Erfanian and A. Mansoori. Solving the nonlinear integro-differential equation in complex plane with rationalized Haar wavelet. *Math. Comput. Simulation*, 165:223–237, 2019.
- [53] L. Euler. *Institutionum calculi integralis*, volume 1. Imp. Acad. imp. Saént, 1768.
- [54] C. A. J. Fletcher. Generating exact solutions of the two-dimensional Burgers' equations. *International Journal for Numerical Methods in Fluids*, 3(3):213–216, 1983.
- [55] A. S. Fokas and L. Y. Sung. The cauchy problem for the Kadomtsev-Petviashvili-I equation without the zero mass constraint. *Math. Proc. Cambridge Philos. Soc.*, 125(1):113–138, 1999.
- [56] B. Fornberg. *A practical guide to pseudospectral methods*. Cambridge University Press, 1998.
- [57] B. Fornberg and D. M. Sloan. A review of pseudospectral methods for solving partial differential equations. *Acta Numer.*, 3:203–267, 1994.
- [58] F. C. Frank and J. H. van der Merwe. One-dimensional dislocations. I. Static theory. *Proc. R. Soc. Lond. Ser. A*, 198(1053):205–216, 1949.
- [59] J. Frenkel and T. Kontorova. On the theory of plastic deformation and twinning. *Izv. Akad. Nauk, Ser. Fiz.*, 1:137–149, 1939.
- [60] A. L. Garcia. *Numerical methods for physics*. Prentice Hall Englewood Cliffs, NJ, 2000.
- [61] C. S. Gardner, J. M. Greene, M. D. Kruskal, and R. M. Miura. Method for solving the Korteweg–de Vries equation. *Phys. Rev. Lett.*, 19:1095–1097, Nov 1967.
- [62] C. S. Gardner, J. M. Greene, M. D. Kruskal, and R. M. Miura. Korteweg–de Vries equation and generalizations. VI. Methods for exact solution. *Comm. Pure Appl. Math.*, 27(1):97–133, 1974.
- [63] C. W. Gear. *Numerical initial value problems in ordinary differential equations*. Prentice Hall PTR, 1971.
- [64] H. H. Goldstine. *A History of Numerical Analysis from the 16th through the 19th Century*, volume 2. Springer Science & Business Media, 2012.
- [65] A. Haar. Zur theorie der orthogonalen funktionensysteme. *Mathematische Annalen*, 71(1):38–53, 1911.
- [66] M. F. Hamilton and C. L. Morfey. Model equations. In M. F. Hamilton and D. T. Blackstock, editors, *Nonlinear acoustics*. Academic Press, San Diego, 1998.

- [67] M. Heideman, D. Johnson, and C. Burrus. Gauss and the history of the fast Fourier transform. *IEEE ASSP Magazine*, 1(4):14–21, 1984.
- [68] H. Hein and L. Feklistova. Computationally efficient delamination detection in composite beams using Haar wavelets. *Mechanical Systems and Signal Processing*, 25(6):2257–2270, 2011.
- [69] A. C. Hindmarsh. ODEPACK, a systematized collection of ODE solvers. *Scientific computing*, pages 55–64, 1983.
- [70] R. Hirota. Exact solution of the modified Korteweg–de Vries equation for multiple collisions of solitons. *J. Phys. Soc. Japan*, 33(5):1456–1458, 1972.
- [71] Y. C. Hon and X. Z. Mao. An efficient numerical scheme for Burgers' equation. *Appl. Math. Comput.*, 95(1):37–50, 1998.
- [72] C. H. Hsiao. State analysis of linear time delayed systems via Haar wavelets. *Math. Comput. Simulation*, 44(5):457–470, 1997.
- [73] C. H. Hsiao. Haar wavelet approach to linear stiff systems. *Math. Comput. Simulation*, 64(5):561–567, 2004.
- [74] E. Isaacson and H. B. Keller. *Analysis of numerical methods*. Courier Corporation, 2012.
- [75] A. Iserles. *A first course in the numerical analysis of differential equations*. Cambridge University Press, 2009.
- [76] P. Jain and D. Holla. Numerical solutions of coupled Burgers' equation. *Internat. J. Non-Linear Mech.*, 13(4):213–222, 1978.
- [77] H. Jeffreys, B. Jeffreys, and B. Swirles. *Methods of mathematical physics*. Cambridge University Press, 1999.
- [78] S. K. Jena and S. Chakraverty. Dynamic behavior of an electromagnetic nanobeam using the Haar wavelet method and the higher-order Haar wavelet method. *Eur. Phys. J. Plus*, 134(10):538, 2019.
- [79] S. K. Jena, S. Chakraverty, and M. Malikan. Implementation of Haar wavelet, higher order Haar wavelet, and differential quadrature methods on buckling response of strain gradient nonlocal beam embedded in an elastic medium. *Engineering with Computers*, pages 1–14, 2019.
- [80] S. K. Jena, S. Chakraverty, M. Ratas, and M. Kris. Application of HOHWM in the stability analysis of nonlocal Euler–Bernoulli beam. *AIP Conference Proceedings*.
- [81] G. Jin, X. Xie, and Z. Liu. The Haar wavelet method for free vibration analysis of functionally graded cylindrical shells based on the shear deformation theory. *Composite Structures*, 108:435–448, 2014.
- [82] R. Jiwari. A Haar wavelet quasilinearization approach for numerical simulation of Burgers' equation. *Comput. Phys. Comm.*, 183(11):2413–2423, 2012.
- [83] B. B. Kadomtsev and V.-I. Petviashvili. On the stability of solitary waves in weakly dispersing media. *Sov. Phys. Dokl.*, 15(6):539–541, 1970.

- [84] C. Y. Kao and Y. Kodama. Numerical study of the KP equation for non-periodic waves. *Math. Comput. Simulation*, 82(7):1185–1218, 2012.
- [85] J. P. Keener and D. W. McLaughlin. Solitons under perturbations. *Phys. Rev. A*, 16(2):777–790, 1977.
- [86] M. Kirs, M. Eerme, D. Bassir, and E. Tungel. Application of HOHWM for vibration analysis of nanobeams. *Key Eng. Mater.*, 799:230–235, 2019.
- [87] M. Kirs and E. Tungel. Evaluation of Haar wavelet method in engineering applications. *AIP Conference Proceedings*, 2116(1):330003, 2019.
- [88] C. Klein, C. Sparber, and P. Markowich. Numerical study of oscillatory regimes in the Kadomtsev–Petviashvili equation. *J. Nonlinear Sci.*, 17(5):429–470, 2007.
- [89] D. J. Korteweg and G. de Vries. On the change of form of long waves advancing in a rectangular canal, and on a new type of long stationary waves. *Phil. Mag.*, 39(240):422–443, 1895.
- [90] S. Kutluay, A. R. Bahadir, and A. Özdeş. Numerical solution of one-dimensional Burgers equation: explicit and exact-explicit finite difference methods. *J. Comput. Appl. Math.*, 103(2):251–261, 1999.
- [91] S. Kutluay, A. Esen, and I. Dag. Numerical solutions of the Burgers' equation by the least-squares quadratic B-spline finite element method. *J. Comput. Appl. Math.*, 167(1):21–33, 2004.
- [92] S. Kutluay, B. A. R., and A. Özdeş. Numerical solution of one-dimensional Burgers equation: explicit and exact-explicit finite difference methods. *J. Comput. Appl. Math.*, 103(2):251–261, 1999.
- [93] P. A. Lagerstrom, J. D. Cole, and L. Trilling. Problems in the theory of viscous compressible fluids. Guggenheim Aeronautical Laboratory, unnumbered report, California Institute of Technology, 1949.
- [94] G. L. Lamb. *Elements of soliton theory*. Wiley-Interscience, 1980.
- [95] Ü. Lepik. Numerical solution of differential equations using Haar wavelets. *Math. Comput. Simulation*, 68(2):127–143, 2005.
- [96] Ü. Lepik. Haar wavelet method for nonlinear integro-differential equations. *Appl. Math. Comput.*, 176(1):324–333, 2006.
- [97] Ü. Lepik. Application of the Haar wavelet transform to solving integral and differential equations. *Proc. Estonian Acad. Sci.*, 56(1):28–46, 2007.
- [98] Ü. Lepik. Numerical solution of evolution equations by the Haar wavelet method. *Appl. Math. Comput.*, 185(1):695–704, 2007.
- [99] Ü. Lepik. Solving integral and differential equations by the aid of non-uniform Haar wavelets. *Appl. Math. Comput.*, 198(1):326–332, 2008.
- [100] Ü. Lepik. Haar wavelet method for solving stiff differential equations. *Math. Model. Anal.*, 14(4):467–481, 2009.

- [101] Ü. Lepik. Solving fractional integral equations by the Haar wavelet method. *Appl. Math. Comput.*, 214(2):468–478, 2009.
- [102] Ü. Lepik. Solving PDEs with the aid of two-dimensional Haar wavelets. *Comput. Math. Appl.*, 61(7):1873–1879, 2011.
- [103] Ü. Lepik and H. Hein. *Haar wavelets: with applications*. Springer, New York, 2014.
- [104] S. H. Lui. *Numerical analysis of partial differential equations*. John Wiley & Sons, 2012.
- [105] J. Majak, M. Pohlak, and M. Eerme. Application of the Haar wavelet-based discretization technique to problems of orthotropic plates and shells. *Mech. Compos. Mater.*, 45(6):631–642, 2009.
- [106] J. Majak, M. Pohlak, M. Eerme, and T. Lepikult. Weak formulation based Haar wavelet method for solving differential equations. *Appl. Math. Comput.*, 211(2):488–494, 2009.
- [107] J. Majak, M. Pohlak, M. Eerme, and B. Shvartsman. Solving ordinary differential equations with higher order Haar wavelet method. *AIP Conference Proceedings*, 2116(1):330002, 2019.
- [108] J. Majak, M. Pohlak, K. Karjust, M. Eerme, J. Kurnitski, and B. S. Shvartsman. New higher order Haar wavelet method: Application to FGM structures. *Composite Structures*, 201:72–78, 2018.
- [109] J. Majak, B. Shvartsman, K. Karjust, M. Mikola, A. Haavajõe, and M. Pohlak. On the accuracy of the Haar wavelet discretization method. *Composites Part B: Engineering*, 80:321–327, 2015.
- [110] J. Majak, B. Shvartsman, M. Kirs, M. Pohlak, and H. Herranen. Convergence theorem for the Haar wavelet based discretization method. *Composite Structures*, 126:227–232, 2015.
- [111] J. Majak, B. Shvartsman, M. Ratas, D. Bassir, M. Pohlak, K. Karjust, and M. Eerme. Higher-order haar wavelet method for vibration analysis of nanobeams. *Materials Today Communications*, 25:101290, 2020.
- [112] H. J. Mikeska. Solitons in a one-dimensional magnet with an easy plane. *J. Phys. D*, 11(1):L29, 1978.
- [113] M. B. Mineev and V. V. Shmidt. Radiation from a vortex in a long Josephson junction placed in an alternating electromagnetic field. *Sov. Phys. JETP*, 52(453):33, 1980.
- [114] L. Molinet, J. C. Saut, and N. Tzvetkov. Remarks on the mass constraint for KP-type equations. *SIAM J. Math. Anal.*, 39(2):627–641, 2007.
- [115] S. S. Motsa, V. M. Magagula, and P. Sibanda. A bivariate Chebyshev spectral collocation quasilinearization method for nonlinear evolution parabolic equations. *The Scientific World Journal*, 2014:581987, 2014.
- [116] T. Musha and H. Higuchi. Traffic current fluctuation and the Burgers equation. *Jpn. J. Appl. Phys.*, 17(5):811–816, 1978.

- [117] J. M. Ortega. Introduction. In J. M. Ortega, editor, *Numerical Analysis*, pages 1–4. Academic Press, 1972.
- [118] S. A. Orszag. Numerical methods for the simulation of turbulence. *The Phys. Fluids*, 12(12):II–250, 1969.
- [119] S. A. Orszag. Comparison of pseudospectral and spectral approximation. *Stud. Appl. Math.*, 51(3):253–259, 1972.
- [120] Ö. Oruç. A non-uniform Haar wavelet method for numerically solving two-dimensional convection-dominated equations and two-dimensional near singular elliptic equations. *Comput. Math. Appl.*, 77(7):1799–1820, 2019.
- [121] Ö. Oruç, F. Bulut, and A. Esen. A Haar wavelet-finite difference hybrid method for the numerical solution of the modified Burgers’ equation. *J. Math. Chem.*, 53(7):1592–1607, 2015.
- [122] L. Petzold. Automatic selection of methods for solving stiff and nonstiff systems of ordinary differential equations. *SIAM J. Sci. Stat. Comput.*, 4(1):136–148, 1983.
- [123] A. D. Polyanin and V. F. Zaitsev. *Handbook of nonlinear partial differential equations*. CRC press, 2004.
- [124] A. Quarteroni, R. Sacco, and F. Saleri. *Numerical mathematics*, volume 37. Springer Science & Business Media, 2010.
- [125] M. Ratas. Application of Haar wavelet method for solving nonlinear evolution equations. *AIP Conference Proceedings*, 2116(1):330004, 2019.
- [126] M. Ratas, S. K. Jena, and S. Chakraverty. Application of Haar wavelet based methods for solving wave propagation problems. *AIP Conference Proceedings*, 2293(1):230002, 2020.
- [127] M. Ratas and A. Salupere. 2D spectral analysis of the KPI equation. Research report Mech319/17, Tallinn University of Technology, Institute of Cybernetics, 2017.
- [128] M. Ratas and A. Salupere. Application of higher order Haar wavelet method for solving nonlinear evolution equations. *Math. Model. Anal.*, 25(2):271–288, 2020.
- [129] M. Ratas, A. Salupere, and J. Majak. Solving nonlinear PDEs using the higher order Haar wavelet method on nonuniform and adaptive grids. *Math. Model. Anal.*, [accepted].
- [130] M. Remoissenet. *Waves called solitons: concepts and experiments*. Springer, 2013.
- [131] J. J. Rushchitsky, C. Cattani, and E. V. Terletska. Wavelet analysis of the evolution of a solitary wave in a composite material. *Internat. Appl. Mech.*, 40(3):311–318, 2004.
- [132] M. Salerno. Discrete model for DNA-promoter dynamics. *Phys. Rev. A*, 44(8):5292, 1991.
- [133] A. Salupere. The pseudospectral method and discrete spectral analysis. In E. Quak and T. Soomere, editors, *Applied Wave Mathematics: Selected Topics in Solids, Fluids, and Mathematical Methods*, pages 301–333. Springer, Berlin, 2009.

- [134] A. Salupere, G. A. Maugin, and J. Engelbrecht. Korteweg–de Vries soliton detection from a harmonic input. *Physics Letters A*, 192(1):5–8, 1994.
- [135] A. Salupere, G. A. Maugin, J. Engelbrecht, and J. Kalda. On the KdV soliton formation and discrete spectral analysis. *Wave Motion*, 23(1):49–66, 1996.
- [136] A. Salupere, P. Peterson, and J. Engelbrecht. Long-time behaviour of soliton ensembles. Part I–Emergence of ensembles. *Chaos Solitons Fractals*, 14(9):1413–1424, 2002.
- [137] A. Salupere, P. Peterson, and J. Engelbrecht. Long-time behaviour of soliton ensembles. Part II–Periodical patterns of trajectories. *Chaos Solitons Fractals*, 15(1):29–40, 2003.
- [138] A. Salupere and M. Ratas. On the application of 2D discrete spectral analysis in case of the KP equation. *Mech. Res. Comm.*, 93:141–147, 2018.
- [139] A. C. Scott, F. Y. F. Chu, and D. W. McLaughlin. The soliton: A new concept in applied science. *Proceedings of the IEEE*, 61(10):1443–1483, 1973.
- [140] L. F. Shampine and M. W. Reichelt. The MATLAB ODE suite. *SIAM J. Sci. Comput.*, 18(1):1–22, 1997.
- [141] G. D. Smith. *Numerical solution of partial differential equations: finite difference methods*. Oxford University Press, 1985.
- [142] M. J. Turner, R. W. Clough, H. C. Martin, and L. J. Topp. Stiffness and deflection analysis of complex structures. *J. Aeronaut. Sci.*, 23(9):805–823, 1956.
- [143] M. Vidyasagar. *Nonlinear systems analysis*, volume 42. Siam, 2002.
- [144] P. Virtanen, R. Gommers, T. E. Oliphant, M. Haberland, T. Reddy, D. Cournapeau, E. Burovski, P. Peterson, W. Weckesser, J. Bright, et al. Scipy 1.0: fundamental algorithms for scientific computing in python. *Nature methods*, 17(3):261–272, 2020.
- [145] J. Wallis. A treatise of algebra, both historical and practical. *Philos. Trans. R. Soc. Lond. Ser. A*, 15(173):1095–1106, 1685.
- [146] M. Wang, X. Li, and J. Zhang. The $\left(\frac{G'}{G}\right)$ -expansion method and travelling wave solutions of nonlinear evolution equations in mathematical physics. *Physics Letters A*, 372(4):417–423, 2008.
- [147] S. Wang, Y. Li, Y. Shao, C. Cattani, Y. Zhang, and S. Du. Detection of dendritic spines using wavelet packet entropy and fuzzy support vector machine. *NS Neurol. Disord. Drug Targets*, 16(2):116–121, 2017.
- [148] Y. Wang, I. M. Navon, X. Wang, and Y. Cheng. 2d Burgers equation with large Reynolds number using POD/DEIM and calibration. *Internat. J. Numer. Methods Fluids*, 82(12):909–931, 2016.
- [149] E. Waring. Problems concerning interpolations. *Philos. Trans. R. Soc. Lond. Ser. A*, 69:59–67, 1779.
- [150] X. Xiang, J. Guoyong, L. Wanyou, and L. Zhigang. A numerical solution for vibration analysis of composite laminated conical, cylindrical shell and annular plate structures. *Composite Structures*, 111:20–30, 2014.

- [151] J. Xie, T. Wang, Z. Ren, J. Zhang, and L. Quan. Haar wavelet method for approximating the solution of a coupled system of fractional-order integral-differential equations. *Math. Comput. Simulation*, 163:80–89, 2019.
- [152] X. Xie, G. Jin, and Z. Liu. Free vibration analysis of cylindrical shells using the Haar wavelet method. *Intern. J. Mech. Sci.*, 77:47–56, 2013.
- [153] X. Xie, G. Jin, Y. Yan, S. X. Shi, and Z. Liu. Free vibration analysis of composite laminated cylindrical shells using the Haar wavelet method. *Composite Structures*, 109:169–177, 2014.
- [154] X. Xie, G. Jin, T. Ye, and Z. Liu. Free vibration analysis of functionally graded conical shells and annular plates using the Haar wavelet method. *Applied Acoustics*, 85:130–142, 2014.
- [155] T. Yoneyama. The Korteweg–de Vries two-soliton solution as interacting two single solitons. *Progress of Theoretical Physics*, 71(4):843–846, 1984.
- [156] N. J. Zabusky. A synergetic approach to problems of nonlinear dispersive wave propagation and interaction. In *Nonlinear partial differential equations*, pages 223–258. Elsevier, 1967.
- [157] N. J. Zabusky and M. D. Kruskal. Interaction of "solitons" in a collisionless plasma and the recurrence of initial states. *Phys. Rev. Lett.*, 15:240–243, Aug 1965.
- [158] H. Zhu, H. Shu, and D. Ding. Numerical solutions of two-dimensional Burgers' equations by discrete Adomian decomposition method. *Computers & Mathematics with Applications*, 60(3):840 – 848, 2010.
- [159] O. C. Zienkiewicz, R. L. Taylor, P. Nithiarasu, and J. Z. Zhu. *The finite element method*. McGraw-hill London, 1977.

Acknowledgements

My thanks go to my supervisors Andrus and Jüri. Both of them helped me immensely during my studies.

I would also like to thank my family for the continued support. I would not have been able to complete this thesis without their help.

And finally, I'd like to thank Kate Estell for all sorts of emotional support as well as being there to proof read my papers from a native English speaker's perspective. This support was essential for the completing of this thesis and the articles within it.

During the PhD studies, financial support was obtained from the Estonian Research Council (IUT 33-24), from the European Regional Development Fund via the Archimedes Foundation's Dora Pluss program and from Estonian Centre of Excellence in Zero Energy and Resource Efficient Smart Buildings and Districts, ZEBE, TK146 funded by the European Regional Development Fund (grant 2014-2020.4.01.15-0016).

Abstract

Numerical analysis of nonlinear wave propagation

Nonlinear partial differential equations (PDEs) arise in many areas of mathematical physics in order to model various physical phenomena. However, in the context of the thesis, nonlinear PDEs that describe wave propagation have been considered. For example, the Korteweg–de Vries and the Kadomtsev–Petviashvili equations can be used in order to model the propagation of long waves of small amplitude in shallow water, the Burgers and the 2D Burgers equations to model shock waves in fluids and traffic flow, the modified Korteweg–de Vries equation to model wave propagation in 1D anharmonic lattices, and the sine–Gordon equation to model one-dimensional crystal dislocations.

Within the thesis, numerous wave propagation problems were numerically solved using the Pseudospectral method (PsM), the Haar wavelet method (HWM) as well as the higher order Haar wavelet method (HOHWM).

2D spectral analysis was used in order to gain extra insights into the behaviour of two dimensional problems. It gave the opportunity to find complex phenomena in the solution that would not have been obvious without its use. The HOHWM was used in order to gain improved accuracy compared to the HWM. The recently developed HOHWM was shown to provide more accurate results for all model equations.

A nonuniform grid approach to the HOHWM was developed. While a nonuniform grid HWM had previously found use, the HOHWM had not been used alongside a nonuniform grid before. The nonuniform grid approach was shown to give significant improvements to accuracy when abrupt changes within the solution were expected and their location was known before computation. While adaptive grids have been used for a long time, they have not seen wide use in combination with the HWM. Furthermore, the HOHWM has never been used alongside an adaptive grid approach.

The novel adaptive HOHWM was developed and shown to be a good candidate for solving nonlinear PDEs with abrupt changes in the solution. The method allowed obtaining results of a better level of accuracy than the uniform or static nonuniform grid HOHWM. This significantly decreases the computational complexity needed to obtain results of a certain accuracy. Thus, the adaptive HOHWM allows one to either obtain a) numerical results of the same accuracy faster while using fewer resources or b) numerical results of greater accuracy using the same amount of resources.

Kokkuvõte

Mittelineaarse lainelevi numbriline analüüs

Mittelineaarseid osatuletistega diferentsiaalvõrrandeid kasutatakse väga erinevate füüsikaliste protsesside ja nähtuste matemaatiliseks modelleerimiseks. Vastavat füüsika haru nimetatakse tihti matemaatiliseks füüsikaks. Käesolevas väitekirjas on vaatluse all mitmed lainelevi kirjeldavad mittelineaarsed osatuletistega diferentsiaalvõrrandid. Näiteks, nii Kortewegi–de Vriesi võrrand kui Kadomtsevi–Petviashvili võrrand kirjeldavad pikkade madala amplituudiga lainete levi madalas vees; Burgersi võrrand ning 2D Burgersi võrrand kirjeldavad lööklainete levi vedelikes ja ka liiklusvoolu; modifitseeritud Kortewegi–de Vriesi võrrand kirjeldab lainelevi anharmoonilises vöres ning sine–Gordoni võrrand kristallide dislokatsioonide levi.

Väitekirjas on lainelevi probleemide lahendamiseks kasutatud mitmeid numbrilisi meetodeid: pseudospektraalmeetodit, Haari lainikute meetodit (HWM) ja kõrgemat järku Haari lainikute meetodit (HOHWM). Kadomtsevi–Petviashvili võrrandi numbriliste lahendite leidmiseks rakendati pseudospektraalmeetodit ning saadud tulemuste analüüsil kasutati kahedimensionaalset diskreetset spektraalanalüüsi. See andis võimaluse täheldada lahendeis peituvaid erinevaid seaduspärasusi, mille leidmine oleks ilma spektraalanalüüsi-
ta olnud keerulisem kui mitte võimatu. Teiste eespool loetletud võrrandite lahendamiseks kasutati Haari lainikute põhinevaid meetodeid. Klassikalise lähenemise korral arendatakse siin Haari ritta võrrandis olev otsitava funktsiooni kõrgeimat järku tuletis ning madalamat järku tuletised arvutatakse saadud Haari rea integreerimise teel. Kirjeldatud lähenemisviisi korral on väitekirjas kasutusel lühend HWM. Täpsemate tulemuste saamiseks on aga võimalik kasutada kõrgemat järku Haari lainikute meetodit. Selle korral arendatakse Haari ritta mitte võrrandis olev otsitava funktsiooni kõrgeimat järku tuletis, vaid sellest veel 2s võrra kõrgemat järku tuletis. Sellise lähenemisviisi korral on väitekirjas kasutusel lühend HOHWM.

Veelgi efektiivsema algoritmi saamiseks töötati välja nii staatilisel ebaühtlasel võrgul kui adaptiivsel võrgul põhinev HOHWM. Ebaühtlast võrku on varasemalt kasutatud küll koos HWM-ga, kuid koos HOHWM-ga seda seni kasutatud ei olnud. Võrrandites, mille lahendites on järsud muutused, annab staatilise ebaühtlase võrgu kasutamine märkimisväärselt täpsuse kasvu (fikseeritud võrgupunktide arvu korral) juhul kui järskude muutuste asukoht ruumis on eelnevalt teada. Adaptiivseid võrke on kasutatud erinevate meetoditega juba pikemat aega, kuid harva on neid kasutatud koos HWM-iga. Käesolevas töös töötati välja uus adaptiivne HOHWM võrrandite jaoks, mille lahendites esinevad järsud muutused, mille asukoht ruumis pole ette teada. See adaptiivne meetod aitab tulemuste täpsust märkimisväärselt parandada, osutudes efektiivsemaks nii ühtlase võrguga HOHWM-st kui staatilise ebaühtlase võrguga HOHWM-st. Võimalus saada sama täpne lahend väiksemate võrgupunktide arvuga vähendab märkimisväärselt arvutuslikku kompleksust. See-
ga annab antud meetod võimaluse leida a) sama täpsusega numbrilisi lahendeid kiiremini ning vähem ressursse kasutades või b) täpsemaid numbrilisi lahendeid samu ressursse kasutades.

Appendix 1

I

A. Salupere and M. Ratas. On the application of 2D discrete spectral analysis in case of the KP equation. *Mech. Res. Comm.*, 93:141–147, 2018



On the application of 2D discrete spectral analysis in case of the KP equation



Andrus Salupere*, Mart Ratas

Department of Cybernetics, School of Science, Tallinn University of Technology, Akadeemia tee 21, Tallinn 12618, Estonia

ARTICLE INFO

Article history:

Received 30 June 2017

Received in revised form 25 August 2017

Accepted 26 August 2017

Available online 31 August 2017

Keywords:

Discrete spectral analysis

Solitons

Recurrence

Numerical integration

Pseudospectral method

ABSTRACT

In case of 1D wave propagation the discrete spectral analysis is very helpful method in order to analyze the space–time behavior of different wave structures. Here we generalize the method to 2D case. The KPI equation is applied as a model equation. For numerical integration the pseudospectral method is applied. We demonstrate how 2D spectral characteristics can be applied for analysis of complicated wave structures that can be formed from different initial pulses in case of the KPI equation. Recurrence phenomenon, temporal periodicity and temporal symmetry of the solution will be discussed.

© 2017 Elsevier Ltd. All rights reserved.

1. Introduction and the problem

Kadomtsev–Petviashvili (KP) equation is used here as a model equation for 2D wave propagation. It is named after Boris Kadomtsev and Vladimir Petviashvili who derived the equation when modeled evolution of long ion-acoustic waves of small amplitude in plasmas under the effect of long transverse perturbations. The resulting KP equation is considered to be the two dimensional generalization of the Korteweg–de Vries (KdV) equation [1,2]. Two different versions of the KP equation can be distinguished. In normalized form they both can be described by

$$(u_t + 6uu_x + u_{xxx})_x + 3\sigma^2 u_{yy} = 0. \quad (1)$$

The case $\sigma^2 = -1$ is called the KPI equation and the case $\sigma^2 = 1$ is called the KP-II equation. The former is used to describe waves in thin films with high surface tension as well as rogue waves and the latter can be used to model water waves with small surface tension [2–4].

Besides the normalised form (1), the KP equation can have various forms depending on problem under consideration. The different values of the coefficients can also be viewed as representing

the environment characteristics [5]. The KPI equation then takes the form of

$$(u_t + \alpha_1 uu_x + \alpha_2 u_{xxx})_x - \alpha_3 u_{yy} = 0, \quad (2)$$

where α_1 , α_2 and α_3 can be called as the nonlinear coefficient, the dispersion coefficient and the transverse perturbation coefficient, respectively. The paper focuses on cases where $\alpha_1 = \alpha_3 = 1$ and only the dispersion coefficient α_2 is changed.

The KP equation is related to various practical problems and is therefore widely studied until today making use of analytical as well as numerical techniques, see e.g. [6–11].

According to a brief definition discrete spectral analysis (DSA) means that discrete Fourier transform (DFT) related spectral characteristics (amplitude spectrum and phase spectrum) are used for analysing of space–time behavior of wave–structures. DSA has been used to analyse the behavior of 1D waves [12–15]. The goal here is to show how DSA can be generalize for 2D waves.

In the present paper KP equation (2) is integrated numerically. For initial condition we use a bended sinusoid:

$$u(x, y, 0) = \sin(a_x x + \beta \cos(a_y y)), \quad (3)$$

where a_x and a_y define the number of periods per 2π , and β is arbitrary parameter. The idea for using the bended sinusoid for initial condition comes from [8] where bended sech²-type initial wave resulted in very interesting 2D wavestructures.

The most immediate result from numerical integration would be a set of 2D wave profiles at different time moments. In order to analyse the time–space behaviour of the solution, one would have

* Corresponding author.

E-mail addresses: salupere@ioc.ee (A. Salupere), Mart.Ratas@ttu.ee (M. Ratas).

to plot a huge amount of 3D surface at different time moments or compose movies. This, however, is often very time consuming to perform, painstaking to follow and does not show all the information about spatio-temporal behavior of waves. That is why DSA should be useful in this case.

The paper is organised as follows: in Section 2 numerical method and in Section 3 ideas of 2D discrete spectral analysis are introduced. Results are discussed in Section 4 and conclusions are drawn in Section 5.

2. Numerical method

For numerical integration of KP equation (2) DFT based Pseudospectral Method (PSM) is used, i.e., spatial derivatives are approximated making use of DFT and for integration with respect of time standard ODE solvers are applied. Making use of properties of the Fourier transform one can approximate spatial derivatives and integrals as follows [16]

$$\begin{aligned} \frac{\partial^n u(x, y)}{\partial x^n} &= F_x^{-1} \left[\left(\frac{ik}{m} \right)^n F_x u \right], \\ \frac{\partial^n u(x, y)}{\partial y^n} &= F_y^{-1} \left[\left(\frac{ik}{m} \right)^n F_y u \right], \\ \int u(x, y) dx &= F_x^{-1} \left[\frac{F_x u}{\frac{ik}{m}} \right] + C(y). \end{aligned} \tag{4}$$

Here F_x and F_y denote the Fourier transform, F_x^{-1} and F_y^{-1} the inverse Fourier transform with respect to variables x and y respectively; wave numbers $k=0, \pm 1, \pm 2, \dots, \pm N/2 - 1, N/2$; i is the imaginary unit and m defines the range of spatial domain ($-m\pi < x \leq m\pi$ and $-m\pi < y \leq m\pi$).

In order to solve a PDE by the PSM, it should have the following form

$$u_t = \Psi(u) \tag{5}$$

and therefore we have to transform the KP equation to appropriate form. At first we introduce variable

$$\varphi = u_x. \tag{6}$$

The KP equation then takes the form

$$\varphi_t = -\alpha_1 (\varphi^2 + u\varphi_x) - \alpha_2 \varphi_{xxx} + \alpha_3 u_{yy}, \tag{7}$$

where

$$\begin{aligned} \varphi_x &= F_x^{-1} \left[\frac{ik}{m} F_x \varphi \right], \quad \varphi_{xxx} = F_x^{-1} \left[-\frac{ik^3}{m^3} F_x \varphi \right], \\ u &= F_x^{-1} \left[\frac{F_x \varphi}{\frac{ik}{m}} \right] + C(y), \quad u_{yy} = F_y^{-1} \left[-\frac{k^2}{m^2} F_y u \right]. \end{aligned} \tag{8}$$

Eqs. (7) and (8) can be solved making use of the PSM. Due to the DFT, boundary conditions must be periodic:

$$u(x, y, 0) = u(x + 2lm\pi, y + 2lm\pi, 0), \quad l = 0, \pm 1, \pm 2, \dots \tag{9}$$

For space grid the number of grid points per space period is N for x as well as for y , i.e., $\Delta_x = \Delta_y = \Delta = 2m\pi/N$.

3. Discrete spectral analysis

In this section, spectral amplitudes (the amplitude spectrum) $a_k(y, t)$ as well as the phase spectrum $\phi_k(y, t)$ are introduced. Spectral amplitudes $a_k(y, t)$ are defined as

$$\begin{aligned} a_k(y, t) &= \frac{2|U(k, y, t)|}{N} \quad k = 1, 2, \dots, \frac{N}{2} - 1, \\ a_k(y, t) &= \frac{|U(k, y, t)|}{N} \quad k = 0, \frac{N}{2}, \end{aligned} \tag{10}$$

where $U(k, y, t) = F_x[u(x, y, t)]$. Phase spectrum is defined as

$$\varphi_k(y, t) = \arg[U(k, y, t)] \tag{11}$$

i.e. $\varphi_k(y, t)$ is the argument of the complex number $U(k, y, t)$. Here the values $k=0, 1, \dots, N/2$ are of interest [12].

If DSA is applied for 1D waves all spectral amplitudes can be shown within a single 2D plot with a different curves referring to each spectral amplitude $a_k(t)$, $k=1, \dots, N/2$. However, in a situation with two spatial dimensions, such a 2D plot would refer to just a single discrete value of y_j , i.e., one has $a_k(y_j, t)$. In order to combat this problem, a new way of looking at spectral analysis was developed. In this depiction, a 3D pseudocolor¹ plot is formed for each spectral amplitude under consideration. Since in most cases, only the first few spectral amplitudes are of interest (the higher spectral amplitudes are usually smaller), this results in only a few different images. An example of such a depiction is shown in Fig. 1, where the horizontal axis refers to the time t while the vertical axis refers to the spatial variable y , and therefore the considered spectral amplitudes are related to the Fourier' transform with respect to variable x . Image of this kind shows how different spectral amplitudes behave in considered time interval. More examples for a_1, \dots, a_5 could be find in Research Report [17].

4. Results and discussion

In this section some results of numerical experiments are presented and discussed. If one takes $\alpha_x = 1$ and $\beta = 0$ in initial condition (3) then the problem is similar to that of the KdV equation with harmonic initial conditions [18]. If to take $\alpha_2 = 0.1$ in (2) then the numerical integration of the KP equation results in train of three solitons, like in the KdV case [17,19].

4.1. Periodicity

In this subsection we consider initial condition (3) with parameters $\alpha_x = 1$, $\beta = 0.4$ and $\alpha_y = 2$. Numerical integration is carried out for $0 \leq t \leq 60$. Different values of the dispersion parameter are used in order to see how it effects on the character of the solution. According to our previous experience [19] we introduce logarithmic dispersion parameter

$$d_l = -\log \alpha_2, \quad \text{i.e.,} \quad \alpha_2 = 10^{-d_l}.$$

Solutions are found for $d_l = 1, 1.1, \dots, 1.8$. Now we use initial conditions with $\beta \neq 0$ and therefore a complex wavestructure emerges: the solution consist of solitary waves that are localized with respect to the x as well as the y axes. A typical waveprofile of such kind is presented in Fig. 2.

Analysis of evolution of waveprofiles demonstrates coexistence of two different wavestructures. Along the x axis KdV soliton like solitary waves are propagating and along the y axis breather like structure is formed. However, in order to estimate is the behaviour

¹ In a pseudocolor plot each value is given a distinct color – this is similar to maps that indicate height with colors.

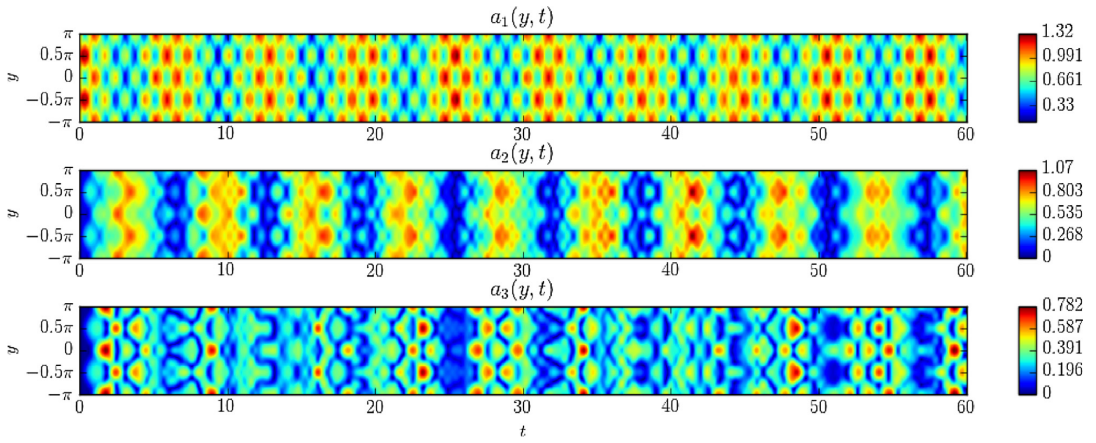


Fig. 1. Spectral amplitudes in case of the initial condition (3), parameters $a_x = 1$, $\beta = 0.4$, $a_y = 2$ and logarithmic dispersion parameter $d_l = 1$.

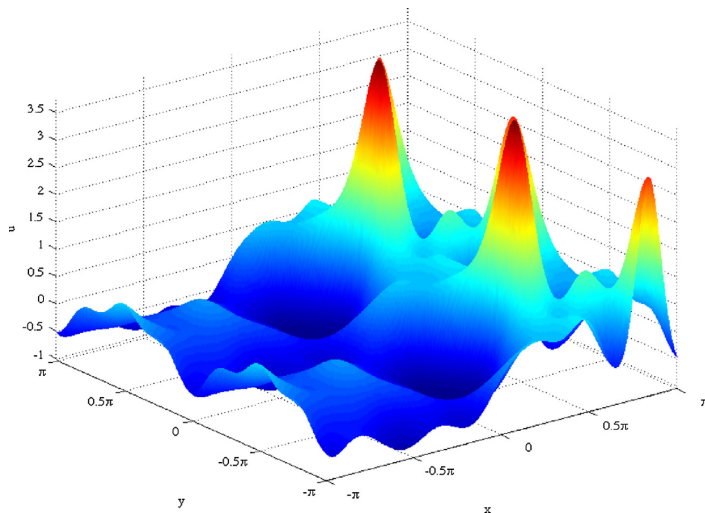


Fig. 2. Solution for $d_l = 1.4$ at $t = 19$ ($a_x = 1$, $\beta = 0.4$, $a_y = 2$).

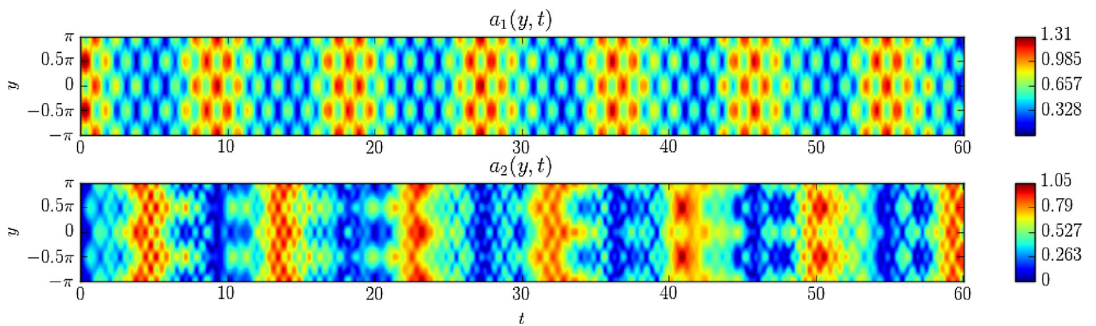


Fig. 3. Spectral amplitudes in case of the initial condition (3), parameters $a_x = 1$, $\beta = 0.4$, $a_y = 2$ and logarithmic dispersion parameter $d_l = 1.3$.

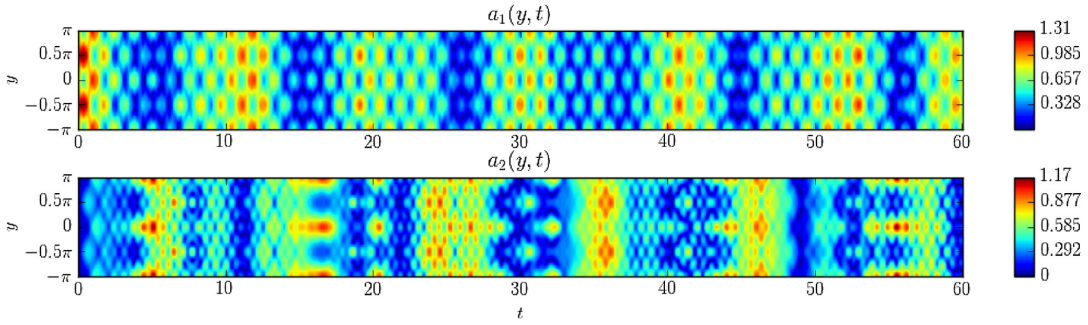


Fig. 4. Spectral amplitudes in case of the initial condition (3), parameters $\alpha_x = 1$, $\beta = 0.4$, $a_y = 2$ and logarithmic dispersion parameter $d_l = 1.5$.

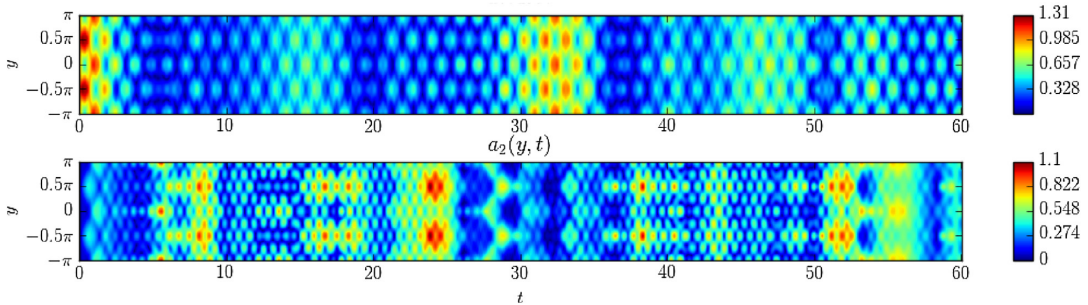


Fig. 5. Spectral amplitudes in case of the initial condition (3), parameters $\alpha_x = 1$, $\beta = 0.4$, $a_y = 2$ and logarithmic dispersion parameter $d_l = 1.8$.

of the solution (quasi)periodic with respect to time one has to analyse the amplitude spectrum. In Fig. 1 the first three spectral amplitudes are plotted over the integration interval. It is clear, that $a_1(y, t)$ tends to have maximal values and $a_2(y, t)$ simultaneously minimal values regularly over the time interval $0 \leq t \leq 60$. In Figs. 3–5 the first two spectral amplitudes are plotted for $d_l = 1.3$, $d_l = 1.5$, and $d_l = 1.8$. For $d_l = 1.3$ the behaviour of $a_1(y, t)$ and $a_2(y, t)$ is similar to the $d_l = 1$ case. Only the length of the (quasi)period is longer. If the value of d_l is rising then the situation changes dramatically and the periodicity disappear. This is not surprising, because the same happened in case of 1D waves in case of the KdV equation [19]. In the Research Report [17] five first spectral amplitudes $a_k(y, t)$, $k = 1, \dots, 5$ are presented for all $d_l = 1, 1.1, \dots, 1.8$.

4.2. Recurrence

Recurrence was first introduced by Zabusky and Kruskal [18]. In general recurrence means that at a certain time moment (let us denote this by t_R) a wave extremely similar to the initial one is formed [12]. It is possible to use spectral amplitudes to track recurrence. When $t \rightarrow t_R$, $a_k(y, t) \rightarrow a_k(y, 0)$, $\forall k, y$. If recurrence takes place at each $t_{R_j} \approx j t_R$, $j = 2, 3, \dots$, the solution is called quasiperiodic.

As an example of the recurrence phenomenon we consider here the case where the initial condition parameters $\alpha_x = 2$, $\beta = 0.4$ and $a_y = 2$ and logarithmic dispersion parameter $d_l = 1$. In case $\alpha_x = 2$ spectral amplitudes $a_k(y, t) \approx 0$ for $k = 1, 3, 5, \dots$ and only even number spectral amplitudes are important. In Research Report [17] the recurrence phenomenon is studied making use of some other sets of parameters as well.

From Fig. 6 one can see that near $t \approx 7$ spectral amplitudes look similar to the initial state at $t = 0$. In order to determine the recurrence time more precisely, the individual spectral amplitudes are averaged over y . Corresponding averaged spectral amplitude curves

are presented in Fig. 7 which is much easier to read in sense of the recurrence. In this figure only three lowest spectral amplitudes are presented – according to the Research Report [17] the contribution of others is negligible when the recurrence is studied. One has to pay attention to the fact that the scale for a_2 is on the left side and for a_4 and a_6 on the right side of the axis. In [17] also curves for a_8 and a_{10} can be found. The averaged spectrum allows (in case of a sinusoidal initial condition) to find time moments when recurrence could occur using local maxima of the lowest spectral amplitude. From Fig. 7 we found that the recurrence occur six times in the considered case and the first recurrence takes place at $t = 7.15$. These time moments are shown by little arrows in Figs. 6 and 7. Fig. 7 is very similar to the amplitude spectrum in 1D case. The latter was used for finding the recurrence time in KdV-type systems [12,14,15,19]. In these papers among other topics super recurrence is discussed. If several recurrences are detected then all recurrences which are closer to the initial state than the first one are called superrecurrences. In the present case the first recurrence is the worst and therefore all others can be called superrecurrences. The closest to the initial state is the recurrence at $t = 16.6$. In Fig. 8 waveprofiles at $t = 0$ and $t = 16.6$ are presented by pseudocolor plots. Due to complex interactions the waveprofile is not restored entirely and not in the initial position, but is shifted along x as well as y axis by 1.669 and $\pi/2$, respectively.

Recurrence related numerical experiments were carried out for different values of logarithmic dispersion parameter d_l and initial condition parameter β . We did not find proper recurrence for $d_l > 1.0$. The influence of parameter β is as follows: if the value of d_l is fixed, then the higher the value of β the faster the first recurrence occurs and the shorter the time intervals between successive recurrence times.

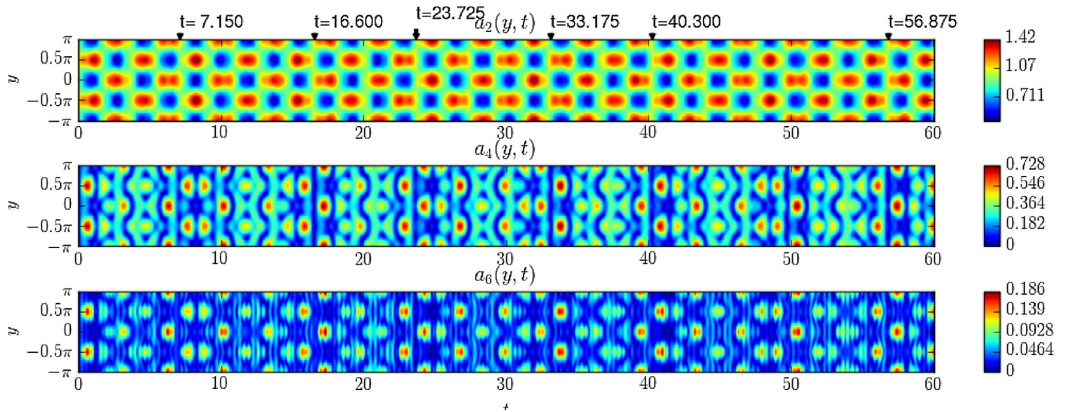


Fig. 6. Spectral amplitudes in case of the initial condition (3), parameters $a_x = 2$, $\beta = 0.4$, $a_y = 2$ and logarithmic dispersion parameter $d_l = 1$.

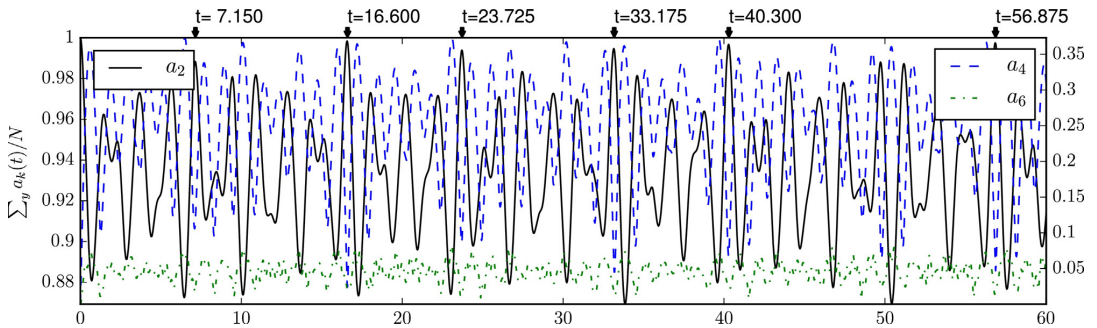


Fig. 7. Averaged spectral amplitudes in case of the initial condition (3), parameters $a_x = 2$, $\beta = 0.4$, $a_y = 2$ and logarithmic dispersion parameter $d_l = 1$.

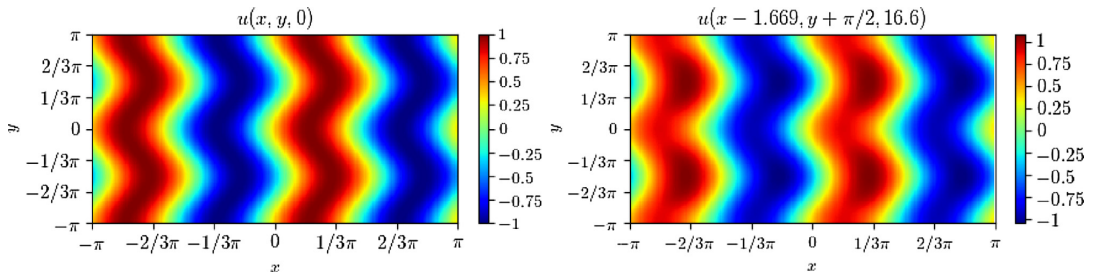


Fig. 8. Recurrence of the initial state: waveprofile at $t = 16.6$ and the initial waveprofile for $a_x = 2$, $\beta = 0.4$, $a_y = 2$ and $d_l = 1$. Note that the waveprofile at $t = 16.6$ is shifted along both coordinate axis.

4.3. Temporal symmetries

In order to observe phenomenon of temporal symmetry we consider solutions of the KP equation with the same set of parameters what was used when the recurrence phenomenon was discussed, i.e., $\alpha_2 = 0.1$, $a_x = a_y = 2$ and $\beta = 0.4$. Corresponding spectral amplitudes are plotted in Fig. 6. When taking a closer look at spectrum, it is evident that the spectral amplitudes around $8.275 < t_5 < 8.3$ look as though they are reflected with respect of that time moment t_5 (symmetry time). In Fig. 9 the left and the right side are plotted side by side with the temporal axes of the right one flipped for

comparison. A similar temporal symmetry can be observed around symmetry time $28.4 < t_5 < 28.425$ for the same solution, see Fig. 10. It is clear that there are slight differences between the left and the right sides in last two figures, but the differences are rather small. At the same time one can observe temporal antisymmetry for the phase spectrum (see Fig. 11).

5. Conclusions

The present paper is dedicated to application of DSA for analysing of 2D wave propagation. The KPI equation is considered

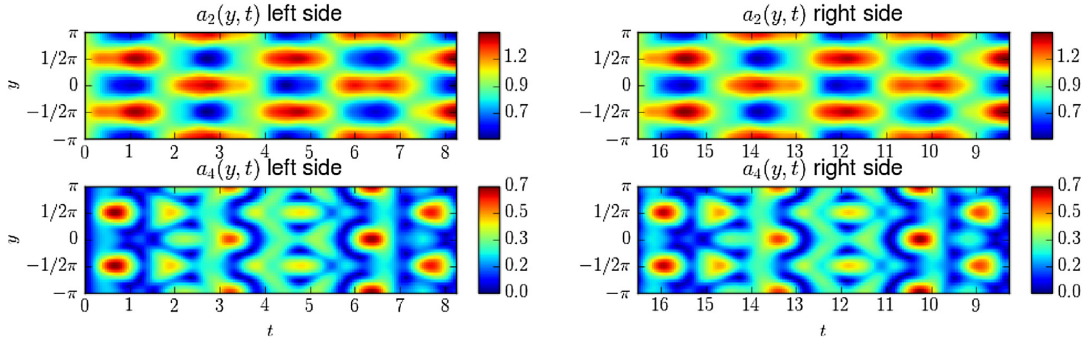


Fig. 9. Temporal symmetry around the time $8.275 < t_s < 8.3$ for amplitude spectrum.

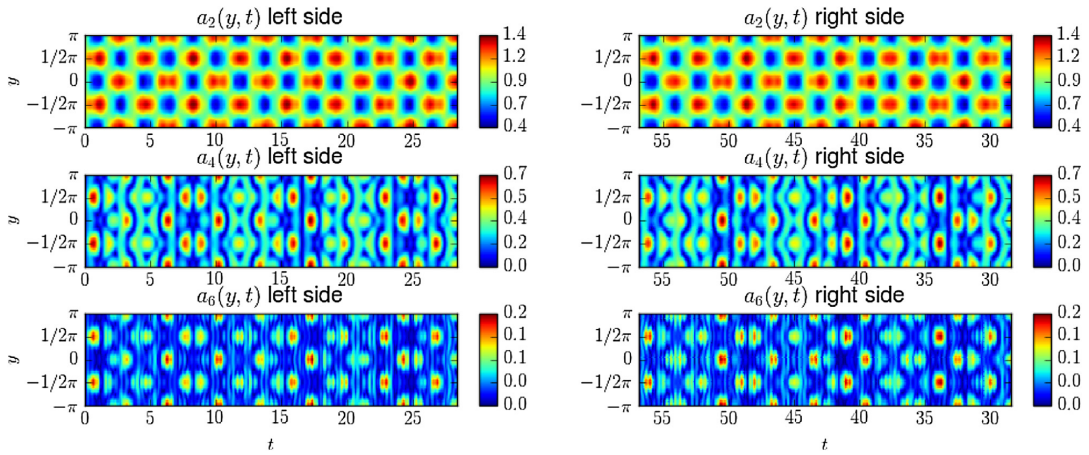


Fig. 10. Temporal symmetry around the time $28.4 < t_s < 28.425$ for amplitude spectrum.

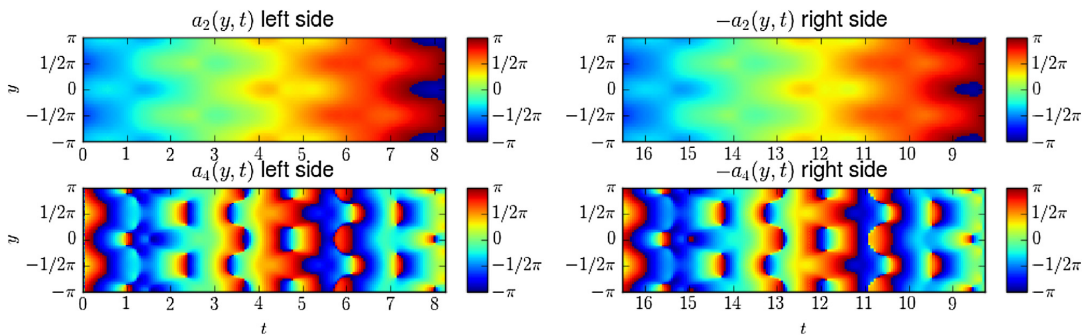


Fig. 11. Temporal antisymmetry around the time $8.275 < t_s < 8.3$ for phase spectrum.

as a model equation, which is solved numerically by PSM. Due to the banded sinusoidal type initial conditions complex wavestru-
 ctures emerge here: soliton trains (similar to the KdV solitons) are
 propagating along x axis and breather like solitonic structures are
 formed along y axis. If one is interested in studying of the character
 of time-space behaviour of such wavestru-
 ctures then it is practically impossible to detect any regularity if to examine only the
 waveprofiles. We demonstrate that similarly to the 1D waves the
 DFT related spectral characteristics can carry additional informa-

tion about the internal structure of 2D waves and that DSA is a very
 helpful tool for analysing spatio-temporal behaviour of 2D waves.
 At first, we demonstrated in Section 4.1 how to understand whether
 or not the solution has (quasi)periodic behaviour making use of
 DSA. Secondly, in Section 4.2 we demonstrated how the recurrence
 phenomenon can be detected making use of DSA. Thirdly, we used
 DSA in order to demonstrate the existence of temporal symmetries.
 The KPI equation and banded sinusoidal initial wave were consid-
 ered here only as an example. The same procedure can be applied

to (numerical) solutions of any 2D wave equations in order to shed more light upon their internal structure.

Acknowledgements

One of the authors (A.S.) is grateful for the possibility to collaborate with Gérard A. Maugin during long years and for many fruitful discussions. This research was supported by the Estonian Research Council (project IUT 33-24).

References

- [1] B.B. Kadomtsev, V.I. Petviashvili, On the stability of solitary waves in weakly dispersing media, *Sov. Phys. Dokl.* 15 (6) (1970) 539–541.
- [2] G. Biondini, D. Pelinovsky, Kadomtsev–Petviashvili equation, *Scholarpedia* 3 (10) (2008) 6539, <http://dx.doi.org/10.4249/scholarpedia.6539>, revision #91398, (accessed 07.08.17).
- [3] P. Dubard, V.B. Matveev, Multi-rogue waves solutions: from the NLS to the KP-I equation, *Nonlinearity* 26 (12) (2013) R93.
- [4] M.J. Ablowitz, *Nonlinear Dispersive Waves: Asymptotic Analysis and Solitons*, vol. 47, Cambridge University Press, Cambridge, 2011.
- [5] A.V. Porubov, G.A. Maugin, V.V. Mareev, Amplification of two-dimensional strain solitary waves, in: D. Kajiwara (Ed.), *Proceeding of the RIAM Symposium no. 16ME-S1 “Physics and Mathematical Structures of Nonlinear Waves”*, 2004, pp. 6–11.
- [6] A.S. Fokas, L.-Y. Sung, The inverse spectral method for the KP I equation without the zero mass constraint, *Math. Proc. Camb. Philos. Soc.* 125 (01) (1999) 113–138.
- [7] L. Molinet, J.-C. Saut, N. Tzvetkov, Remarks on the mass constraint for KP-type equations, *SIAM J. Math. Anal.* 39 (2) (2007) 627–641.
- [8] C. Klein, C. Sparber, P. Markowich, Numerical study of oscillatory regimes in the Kadomtsev–Petviashvili equation, *J. Nonlinear Sci.* 17 (5) (2007) 429–470.
- [9] C.-Y. Kao, Y. Kodama, Numerical study of the KP equation for non-periodic waves, *Math. Comput. Simul.* 82 (7) (2012) 1185–1218.
- [10] M.J. Ablowitz, D.E. Baldwin, Nonlinear shallow ocean-wave soliton interactions on flat beaches, *Phys. Rev. E* 86 (3) (2012) 036305.
- [11] S. Chakravarty, T. McDowell, M. Osborne, Numerical studies of the KP line-solitons, *Commun. Nonlinear Sci. Numer. Simul.* 44 (2017) 37–51.
- [12] A. Salupere, The pseudospectral method and discrete spectral analysis, in: E. Quak, T. Soomere (Eds.), *Applied Wave Mathematics: Selected Topics in Solids, Fluids, and Mathematical Methods*, Springer, Berlin, 2009, pp. 301–333.
- [13] A. Salupere, M. Lints, J. Engelbrecht, On solitons in media modelled by the hierarchical KdV equation, *Arch. Appl. Mech.* 84 (2014) 1583–1593.
- [14] O. Ilison, A. Salupere, Propagation of sech^2 -type solitary waves in higher-order KdV-type systems, *Chaos Solitons Fractals* 26 (2) (2005) 453–465.
- [15] L. Ilison, A. Salupere, Propagation of sech^2 -type solitary waves in hierarchical KdV-type systems, *Math. Comput. Simul.* 79 (11) (2009) 3314–3327.
- [16] D.T. Steinmoeller, M. Statna, K.G. Lamb, Fourier pseudospectral methods for 2D Boussinesq-type equations, *Ocean Modell.* 52 (2012) 76–89.
- [17] M. Ratas, A. Salupere, 2D spectral analysis of the KPI equation, *Research Report Mech 319/17*, Department of Cybernetics, School of Science, Tallinn University of Technology, 2017 www.ioc.ee/~salupere/lae/Mech_319_17.pdf.
- [18] N.J. Zabusky, M.D. Kruskal, Interaction of solitons in a collisionless plasma and the recurrence of initial states, *Phys. Rev. Lett.* 15 (1965) 240–243.
- [19] A. Salupere, G. Maugin, J. Engelbrecht, J. Kalda, On the KdV soliton formation and discrete spectral analysis, *Wave Motion* 23 (1996) 49–66.

Appendix 2

II

M. Ratas and A. Salupere. Application of higher order Haar wavelet method for solving nonlinear evolution equations. *Math. Model. Anal.*, 25(2):271-288, 2020



Application of Higher Order Haar Wavelet Method for Solving Nonlinear Evolution Equations

Mart Ratas and Andrus Salupere

Department of Cybernetics, School of Science, Tallinn University of Technology

12618 Tallinn, Estonia

E-mail(*corresp.*): mart.ratas@ttu.ee

Received August 29, 2019; revised February 3, 2020; accepted February 7, 2020

Abstract. The recently introduced higher order Haar wavelet method is treated for solving evolution equations. The wave equation, the Burgers' equations and the Korteweg-de Vries equation are considered as model problems. The detailed analysis of the accuracy of the Haar wavelet method and the higher order Haar wavelet method is performed. The obtained results are validated against the exact solutions.

Keywords: Haar wavelets, evolution equations, higher order wavelet expansion.

AMS Subject Classification: 37M05; 65T60; 35Q51.

1 Introduction

From the mathematical viewpoint evolution equations under consideration are partial differential equations (PDEs). In case of numerical solution of PDEs one has to approximate the partial derivatives with respect to time and space coordinates. Local or global methods can be used for these approximations. The finite difference method is the most typical example of local methods. In the case of global methods, usually the function itself is approximated as a sum of basis functions (for example trigonometric functions). However, trigonometric functions are not the only choice for basis functions. For example, in [64] mixed Laguerre-Legendre interpolation approximation is applied. One of the more popular global methods is the fast Fourier transform (FFT) related pseudospectral method [20, 22, 55, 56, 58, 59]. In the present paper another global approach is applied: Haar wavelets are used for approximation of partial derivatives.

Copyright © 2020 The Author(s). Published by VGTU Press

This is an Open Access article distributed under the terms of the Creative Commons Attribution License (<http://creativecommons.org/licenses/by/4.0/>), which permits unrestricted use, distribution, and reproduction in any medium, provided the original author and source are credited.

Recently, the higher order Haar wavelet method (HOHWM) has been developed by Majak et. al. [42] as an improvement of the Haar wavelet method (HWM) originally introduced by Chen and Hsiao in [15]. The HWM has been proposed for solving differential equations [15, 27, 51] as well as a wide class of integro-differential and integral equations [5, 7, 8, 14, 35, 37, 63]. According to HWM, as proposed in [15, 27], the highest order derivative included in the differential equation is expanded into the series of Haar functions. This approach is based on the fact that the Haar functions are given in form of quadratic waves which are not differentiable. A different approach was introduced in [13], according to which the quadratic waves can be regularized. However, the latter approach appears more complicated and has not found wider use. In addition to the apparant simpler implementation, the former approach has commonly been utilized in studies related to the development and application of HWM. In pioneering works by Lepik [33, 34, 35, 36, 37, 38], integration techniques for HWM were developed. A thorough overview of HWM and its application in different research areas can be found in the monograph [39]. The weak formulation based HWM was introduced by Majak et. al. in [41]. The complexity issues of strong and weak formulation based HWM are also discussed in the latter study.

One of the most common areas of application for HWM appears to be engineering. This specific field includes solid mechanics [35, 36, 38], composites [26, 28, 40, 66, 68, 69], etc. Additionally, free vibration analysis of the multi-layer composite plate was performed in [40] and in [28, 66, 67, 68, 69] the HWM was adopted for free vibration analysis of composite laminated conical and cylindrical shell, and annular plate structures.

The fractional differential and integro-differential equations form a challenging application area for new numerical methods. This also applies to HWM. Due to their specific nature, less coverage by numerical methods and commercial software has been observed. In a pioneering study the Caputo derivatives are utilized and the differential equations are converted to integral equations including integer order derivatives [37]. Thus, the wavelet expansion is applied to derivatives of integer order. An alternate approach was employed in [44, 53, 60, 62] where the fractional derivatives are expanded directly to wavelet series.

Recent developments in this area have lead to HWM being treated for multidimensional case [3, 4, 6] as well an adaptive wavelet method [23]. Other developoments include nonuniform HWM [48], application in inverse problems [21], identification of software piracy [47], etc.

The key factors of any numerical method are the accuracy and convergence. These are studied for HWM in [43, 45, 65]. The convergence theorem is proven in [45], which also shows that the order of convergence of the HWM approach based on [15] is equal to two. The latter result gives an incentive to further improve HWM. In the comparative study [30] it was shown that HWM proposed in [15, 27] is not competitive with other simple strong formulation based methods used in engineering like differential quadrature method and finite difference method. Motivated by the latter conclusions Majak et.al. developed HOHWM in [42].

In the current study the HOHWM is treated for solving evolution equations. In addition, the wave equation was chosen as the first model equation for its simplicity. The Burgers' equation [10,11] has previously been studied using the HWM [29, 36, 41, 49] and also has an analytical solution, thus the possibility of comparison made it a decent choice for a model equation. It finds applications in modeling of turbulence [10] and traffic [46], as well as in weak non-stationary shock wave in real fluids [31] and in nonlinear acoustics [24]. The HWM has also previously been applied to the Korteweg-de Vries (KdV) equation in [50, 52]. The KdV equation was derived in order to describe the movement of long unidirectional shallow water waves in a rectangular channel but has been found to model different nonlinear phenomena nowadays [18,19,54]. A detailed analysis of the improved accuracy of HOHWM over HWM is performed for all three model equations.

The article is structured as follows. Firstly, the Haar wavelet family is introduced in Section 2. Secondly, the model equations used are described in Section 3. Section 4 outlines the HWM and HOHWM. The analysis of the results is presented in Section 5 and conclusions are drawn in the final section.

2 Haar wavelet family

In the following the Haar wavelet family is defined utilizing the notation introduced by Lepik in [38]. $2M$ subintervals of equal length $\Delta x = (B - A)/(2M)$ form the integration domain $x \in [A, B]$. The maximum level of resolution J is defined as $J = \log_2(M)$. The Haar wavelet family for a fixed M can be described as

$$h_i(x) = \begin{cases} 1, & \text{for } x \in [\xi_1(i), \xi_2(i)), \\ -1, & \text{for } x \in [\xi_2(i), \xi_3(i)), \\ 0, & \text{elsewhere,} \end{cases} \tag{2.1}$$

where

$$\begin{aligned} \xi_1(i) &= A + 2k\mu\Delta x, \quad \xi_2(i) = A + (2k + 1)\mu\Delta x, \quad \xi_3(i) = A + 2(k + 1)\mu\Delta x, \\ \mu &= M/m, \quad m = 2^j, \quad \Delta x = (B - A)/(2M). \end{aligned} \tag{2.2}$$

In (2.1) and (2.2) $j = 0, 1, \dots, J$ is the dilation parameter, $k = 0, 1, \dots, m - 1$ is translation parameter, m corresponds to the maximum number of square waves in the interval $x \in [A, B]$ for the given dilation and index i is calculated from $i = m + k + 1$. Therefore (2.2) corresponds to $i \geq 2$ since $m \geq 1$ and $k \geq 0$. The scaling function $h_1(x) = 1$ is constant, in this case the values $m = 0, \xi_1 = A, \xi_2 = B, \xi_3 = B$ are considered. The other Haar functions contain a single square wave each. The Haar functions are orthogonal to each other and therefore form a good transform basis

$$\int_A^B h_i(x)h_l(x)dx = \begin{cases} 2^{-j}, & i = l = 2^j + k, \\ 0, & i \neq l. \end{cases}$$

Thus, any square integrable function $f(x)$ can be expanded into Haar wavelets as

$$f(x) = \sum_{i=1}^{\infty} a_i h_i(x), \tag{2.3}$$

where a_i denote the Haar coefficients.

According to [38] the integrals of the Haar functions (2.1) of order n can be calculated analytically as follows

$$p_{n,i}(x) = \begin{cases} 0, & \text{for } x \in [A, \xi_1(i)), \\ \frac{(x-\xi_1(i))^n}{n!}, & \text{for } x \in [\xi_1(i), \xi_2(i)), \\ \frac{(x-\xi_1(i))^n - 2(x-\xi_2(i))^n}{n!}, & \text{for } x \in [\xi_2(i), \xi_3(i)), \\ \frac{(x-\xi_1(i))^n - 2(x-\xi_2(i))^n + (x-\xi_3(i))^n}{n!}, & \text{for } x \in [\xi_3(i), B). \end{cases} \tag{2.4}$$

Within the present paper the matrix form of the above formulation is used. Therefore, the elements of $(2M) \times (2M)$ matrix \mathbf{H} , are given as values of the Haar functions

$$H_{il} = h_i(x_l) \tag{2.5}$$

at collocation points $x_l = (l - 1/2)\Delta x$. The $(2M) \times (2M)$ matrix \mathbf{P}_n with elements

$$(P_n)_{il} = p_{n,i}(x_l), \tag{2.6}$$

denotes the n th integral of the Haar wavelet matrix for a given resolution J .

Using (2.5) and (2.6) and considering the coefficient vector \mathbf{a} one obtains $\mathbf{f}(\mathbf{x}) = \mathbf{a} \cdot \mathbf{H}$ instead of (2.3) and

$$\underbrace{\int \dots \int_A}_{n} \mathbf{H} \underbrace{d\xi \dots d\xi}_n = \mathbf{P}_n.$$

It must be noted, that the matrices \mathbf{H} and \mathbf{P}_n depend on vector \mathbf{x} of collocation points. The statements in (2.4) imply that in boundary points A and B hold

$$(P_n(A))_i = 0, \quad \forall n > 0, \quad \forall i, \tag{2.7}$$

$$(P_n(B))_i = p_{n,i}(B) = \frac{(B - \xi_1(i))^n - 2(B - \xi_2(i))^n + (B - \xi_3(i))^n}{n!}. \tag{2.8}$$

$\mathbf{P}_n(0)$ and $\mathbf{P}_n(B)$ form column vectors which will be used when forming a system of equations that satisfy the boundary conditions. These expressions can often be simplified due to equation (2.7).

3 Model equations

The wave equation

$$u_{tt} = c^2 u_{xx}, \tag{3.1}$$

subject to the initial and boundary conditions

$$u(x, 0) = u_0(x), \quad u_t(x, 0) = v_0(x), \quad u(A, t) = u_l(t), \quad u(B, t) = u_r(t),$$

was considered as the first model equation. The particular exact solution used was a travelling wave solution of the form

$$u(x, t) = \left(1 + e^{c_1(x-ct-x_0)}\right)^{-1}, \tag{3.2}$$

where c_1 is a parameter that varies the steepness of the shockwave, c is its travelling speed and x_0 its initial phase.

As the second model equation, the Burgers' equation

$$u_t + uu_x = \nu u_{xx} \tag{3.3}$$

was chosen. Here ν is the diffusion coefficient. The Burgers' equation subjected to the initial and boundary conditions

$$u(x, 0) = u_0(x), \quad u(A, t) = u_l(t), \quad u(B, t) = u_r(t),$$

was considered. Its analytical solution has been found in the form of

$$u(x, t) = \frac{2\nu\pi}{L} \frac{\sum_{n=1}^{\infty} \exp(-E_n t) n I_n(R_0/(2\pi)) \sin(n\pi x/L)}{I_0(R_0/(2\pi)) + 2 \sum_{n=1}^{\infty} \exp(-E_n t) I_n(R_0/(2\pi)) \cos(n\pi x/L)}, \tag{3.4}$$

where $R_0 = u_0 L/\nu$ is the Reynolds number, $E_n = \nu n^2 \pi^2/L^2$, I_n represents the modified Bessel functions of first kind and $L = B - A$ is the x domain range [9, 16].

The third model equation was chosen to be the KdV equation of the form

$$u_t + \alpha uu_x + u_{xxx} = 0 \tag{3.5}$$

subjected to the initial and boundary conditions

$$u(x, 0) = u_0(x), \quad u(A, t) = u_l(t), \quad u(B, t) = u_r(t), \quad u_x(A, t) = u_{l,x}(t).$$

An exact one soliton solution for the KdV equation (3.5) is known in the form of

$$u(x, t) = \frac{3c}{\alpha} \operatorname{sech}^2\left(\frac{1}{2}\sqrt{c}(x - ct - x_0)\right), \tag{3.6}$$

where c is the speed of the travelling soliton, α is the nonlinear coefficient in the equation and x_0 denotes the initial phase. There exists also a two-soliton solution [1, 32, 57, 70] in the form

$$u(x, t) = \frac{3(c_B - c_S)}{|\alpha|} \frac{(c_B c_S \operatorname{sch}^2(\xi_B) + c_S \operatorname{sech}^2(\xi_S))}{(\sqrt{c_B} \coth(\xi_B) - \sqrt{c_S} \tanh(\xi_S))^2}, \tag{3.7}$$

where $\xi_B = \frac{1}{2}\sqrt{c_B}(x - c_B t - x_{0B})$, $\xi_S = \frac{1}{2}\sqrt{c_S}(x - c_S t - x_{0S})$, and c_B and c_S are the speeds of the bigger and smaller soliton, respectively, x_{0B} and x_{0S} are the initial phases for the bigger and smaller soliton, respectively and α is the nonlinear parameter. Using (3.7) soliton interactions can be observed.

4 Haar wavelet methods

In many numerical studies [2, 12, 25, 41], spatial derivatives are expanded into Haar wavelet series while finite difference type schemes are used for integration with respect to time. In the present study, MATLAB's *ode45* [61] solver based on Runge–Kutta (4,5) formula [17] is used for integration with respect to time. This allows one to calculate the value of the function at each time moment from its values at previous time moments without the need to expand both axes into the Haar series. The latter often results in extremely large matrices which can get computationally expensive.

The well known HWM involves expanding in the Haar wavelet series the highest order derivative present within the equation. One then obtains for the n th spatial derivative

$$\mathbf{u}_{n,x}(\mathbf{x}) = \mathbf{a} \cdot \mathbf{H}_x, \quad (4.1)$$

where the subscript notes the axis along which the HWM (as well as the HOHWM) is deployed and \mathbf{a} is the Haar wavelet coefficient vector. After integrating n times one arrives at the function itself as

$$\mathbf{u}(\mathbf{x}) = \mathbf{a} \cdot \mathbf{P}_{xn} + \sum_{i=0}^{n-1} \left(c_i \frac{\mathbf{x}^i}{i!} \right),$$

where the unknown coefficients c_i can be calculated by using the boundary conditions and \mathbf{x}^i denotes the collocation vector with its elements raised to the power of i . The superscript of the vector of collocation points will refer to the element wise multiplication throughout the rest of the present study.

When it comes to the HOHWM, one needs to start with a derivative of a higher order than that which is present in the equation. In general, an additional $2s$ derivatives are used. However, in the current study, only $s = 1$ is considered. Thus, one starts with

$$\mathbf{u}_{(n+2),x}(\mathbf{x}) = \mathbf{a} \cdot \mathbf{H}_x \quad (4.2)$$

and after integration arrives at

$$\mathbf{u}(\mathbf{x}) = \mathbf{a} \cdot \mathbf{P}_{x(n+2)} + \sum_{i=0}^{n+2} \left(c_i \frac{\mathbf{x}^i}{i!} \right),$$

where two extra coefficients, c_n and c_{n+1} are introduced. In order to calculate those extra coefficients, some extra information is needed. In the present study the equation is evaluated at the boundary.

When the unknown coefficients c_i have been obtained, the function u can be described as

$$\begin{aligned} \mathbf{u}(\mathbf{x}, t) &= \mathbf{a} \cdot \mathbf{R}_{xn} + \mathbf{S}_{xn}, & \text{for HWM,} \\ \mathbf{u}(\mathbf{x}, t) &= \mathbf{a} \cdot \mathbf{R}_{x(n+2)} + \mathbf{S}_{x(n+2)}, & \text{for HOHWM,} \end{aligned}$$

where \mathbf{R}_{xm} is a matrix and \mathbf{S}_{xm} a vector obtained only from the Haar matrices and boundary conditions. They both depend on x . \mathbf{S}_{xm} can also depend on t

(depending on the boundary conditions). Thus for the k th derivative ($k < m$) of u one can write

$$\begin{aligned} \mathbf{u}_{kx}(\mathbf{x}, t) &= \mathbf{a} \cdot \mathbf{R}_{x(n-k)} + \mathbf{S}_{x(n-k)}, & \text{for HWM,} \\ \mathbf{u}_{kx}(\mathbf{x}, t) &= \mathbf{a} \cdot \mathbf{R}_{x(n+2-k)} + \mathbf{S}_{x(n+2-k)}, & \text{for HOHWM.} \end{aligned} \tag{4.3}$$

It must be noted that $\mathbf{R}_{x0} = \mathbf{H}_x$ and $\mathbf{S}_{x0} = 0$ due to (4.1) and (4.2) in case of HWM. Once \mathbf{R}_{xm} and \mathbf{S}_{xm} have been found, one can arrive at

$$\mathbf{a} = (u(x, t) - \mathbf{S}_{xm}) \cdot \mathbf{R}_{xm}^{-1}, \tag{4.4}$$

where $m = n$ (HWM) or $m = n + 2$ (HOHWM). Equation (4.4) can be used to find the wavelet coefficient vector \mathbf{a} from the previous iteration.

Finally, the equation in question will need to be arranged in the form $u_t = f(u, u_x, u_{xx}, \dots, u_{nx})$ or $u_{tt} = f(u, u_x, u_{xx}, \dots, u_{nx})$. Then, (4.4) can be used to calculate \mathbf{a} , after which (4.3) can be used to substitute u and its derivatives into the right hand side of the equation in question. This routine has to be followed for each time step.

In the following subsections, the numerical approach is described for each model equation. Firstly, the HWM is described. Then the extra conditions to find the extra coefficients added by HOHWM are introduced. Finally, HOHWM is described. The domain is fixed as $A = 0$ and $B = 1$.

4.1 Wave equation

Given constant boundary conditions

$$u(0, t) = 1, \quad u(1, t) = 0, \tag{4.5}$$

one obtains

$$\mathbf{R}_{x2} = \mathbf{P}_{x2} - \mathbf{P}_{x2}(1) \cdot \mathbf{x}, \quad \mathbf{S}_{x2} = c_l(1 - \mathbf{x}) + c_r \mathbf{x} \tag{4.6}$$

for HWM. For HOHWM the equation is evaluated at the boundary points as

$$u_{tt}(0, t) = c^2 u_{xx}(0, t), \quad u_{tt}(1, t) = c^2 u_{xx}(1, t).$$

Since the boundary conditions (4.5) are constant in time $u_t(0, t) = u_t(1, t) = u_{tt}(0, t) = u_{tt}(1, t) = 0$. Thus one arrives at

$$u_{xx}(0, t) = 0, \quad u_{xx}(1, t) = 0. \tag{4.7}$$

The addition of (4.7) gives

$$\mathbf{R}_{x4} = \mathbf{P}_{x4} - \mathbf{P}_{x4}(1) \cdot x - \mathbf{P}_{x2}(1) \cdot (\mathbf{x}^3 - 1), \quad \mathbf{S}_{x4} = 1 - \mathbf{x}.$$

4.2 Burgers' equation

Given the homogeneous boundary conditions

$$u(0, t) = 0, \quad u(1, t) = 0, \tag{4.8}$$

one again obtains the same results (4.6) for HWM. However, for HOHWM the equation is again evaluated at the boundary points as

$$\begin{aligned} u_t(0, t) + u(0, t)u_x(0, t) - \nu u_{xx}(0, t) &= 0, \\ u_t(1, t) + u(1, t)u_x(1, t) - \nu u_{xx}(1, t) &= 0. \end{aligned} \tag{4.9}$$

Since the boundary conditions (4.8) are homogeneous $u_t(0, t) = u_t(1, t) = 0$ and (4.9) simplifies to

$$u_{xx}(0, t) = 0 \quad u_{xx}(1, t) = 0. \tag{4.10}$$

The addition of (4.10) gives

$$\mathbf{R}_{x4} = \mathbf{P}_{x4} - \mathbf{P}_{x4}(1) \cdot \mathbf{x} + \mathbf{P}_{x2}(1) \cdot \frac{\mathbf{x} - \mathbf{x}^3}{6}, \quad \mathbf{S}_{x4} = 0.$$

4.3 KdV equation

Given homogeneous boundary conditions

$$u(0, t) = u(1, t) = u_x(1, t) = 0, \tag{4.11}$$

for HWM one obtains

$$\mathbf{R}_{x3} = \mathbf{P}_{x3} + \mathbf{P}_{x2}(1) \cdot (\mathbf{x} - \mathbf{x}^2) + \mathbf{P}_{x3}(1) \cdot (\mathbf{x}^2 - 2\mathbf{x}), \quad \mathbf{S}_{x3} = 0.$$

For HOHWM the equation is yet again evaluated at the boundary points as

$$u_t(0, t) + \alpha u(0, t)u_x(0, t) + u_{xxx}(0, t) = 0, \quad u_t(1, t) + \alpha u(1, t)u_x(1, t) + u_{xxx}(1, t) = 0.$$

Since the boundary conditions (4.11) are homogeneous $u_t(0, t) = u_t(1, t) = 0$ and the above simplifies to

$$u_{xxx}(0, t) = 0, \quad u_{xxx}(1, t) = 0. \tag{4.12}$$

The addition of (4.12) gives

$$\begin{aligned} \mathbf{R}_{x5} = & \mathbf{P}_{x5} + \frac{1}{2}\mathbf{P}_{x3}(1) \cdot (-\mathbf{x}^4 + 2\mathbf{x}^3 - \mathbf{x}^2) + \frac{1}{2}\mathbf{P}_{x4}(1) \cdot (4\mathbf{x}^4 - 10\mathbf{x}^3 + 6\mathbf{x}^2) \\ & + \frac{1}{2}\mathbf{P}_{x5}(1) \cdot (-6\mathbf{x}^4 + 16\mathbf{x}^3 - 12\mathbf{x}^2), \\ \mathbf{S}_{x5} = & 0. \end{aligned}$$

5 Numerical results

Numerical experiments were carried out for equations (3.1), (3.3) and (3.5) with both HWM and HOHWM for different values of the resolution parameter J . The results were compared to the corresponding exact solutions (3.2), (3.4) and (3.6), respectively. The maximal deviation of the calculated result with respect to the exact solution is traced. In case of the Burgers' equation, the time at which calculations become insufficiently accurate was measured in addition to

the deviation. This is because given the near-singular behaviour of the exact solution at the boundary at the low values of ν used the integration scheme can become unstable. In case of the KdV equation, since the absolute value of the solution can be rather large, maximum relative deviation is traced in addition to maximum deviation. The results of HWM are compared with HOHWM.

Calculations for wave equation were carried out with initial condition from the exact solution (3.2) at $t = 0$ as

$$u_0(x) = \left(1 + e^{c_1(x-x_0)}\right)^{-1} \tag{5.1}$$

and the boundary conditions (4.5). In case of HOHWM the additional conditions (4.7) were added. The maximum deviation from the exact solution in case of $c = 1/2$ and $x_0 = 1/4$ for $c_1 = 60, 70, 80$ within the domain $x \in [0, 1]$, $t \in [0, 1]$ can be seen in Table 1.

Table 1. Results for the wave equation: maximal deviation of the numerical solution from the exact solution $\max \Delta u$ against the resolution parameter J with initial conditions (5.1) and boundary conditions (4.5) ($c = 1/2$, $x_0 = 1/4$, $x \in [0, 1]$, $t \in [0, 1]$, $c_1 = 60, 70, 80$).

J	2M	max Δu					
		$c_1 = 60$		$c_1 = 70$		$c_1 = 80$	
		HWM	HOHWM	HWM	HOHWM	HWM	HOHWM
3	16	0.1336325	0.1106219	0.1799650	0.1614320	0.2428010	0.2203232
4	32	0.1127782	0.0480090	0.1420468	0.0695581	0.1687752	0.0912491
5	64	0.0522854	0.0077165	0.0744285	0.0138613	0.0987152	0.0220050
6	128	0.0159480	0.0006604	0.0242365	0.0013906	0.0342071	0.0025845
7	256	0.0042292	0.0000415	0.0066610	0.0000903	0.0098198	0.0001786

Table 2. Results for the Burgers' equation: maximal time t_f at which the numerical solutions deviates from the exact solution less than 10^{-3} against the resolution parameter J with initial conditions (5.2) and boundary conditions (4.8) ($x \in [0, 1]$, $t \in [0, 1]$, $\nu = \frac{1}{100\pi}, \frac{1}{110\pi}, \frac{1}{120\pi}$).

J	2M	t_f					
		$\nu = \frac{1}{100\pi}$		$\nu = \frac{1}{110\pi}$		$\nu = \frac{1}{120\pi}$	
		HWM	HOHWM	HWM	HOHWM	HWM	HOHWM
3	16	0.1625	0.2375	0.1625	0.2375	0.1625	0.2375
4	32	0.225	0.2875	0.225	0.275	0.225	0.275
5	64	0.275	0.2875	0.275	0.3181	0.2625	0.3
6	128	0.3106	0.3580	0.308	0.3542	0.3038	0.3475
7	256	0.3400	0.5	0.3364	0.4646	0.3317	0.4143
8	512	0.3801	0.5	0.3671	0.5	0.3657	0.5

The Burgers' equation was solved for diffusion coefficient values of $\nu = \frac{1}{100\pi}, \frac{1}{110\pi}, \frac{1}{120\pi}$ within the domain $x \in [0, 1]$, $t \in [0, t_f]$. The initial condition

$$u_0(x) = \sin(\pi x) \tag{5.2}$$

and boundary conditions (4.8) were used. In case of HOHWM the additional conditions (4.10) were added. Due to the near-singular nature of the solution, the numerical solution can get unstable near the steep slope. Thus the time at which sufficient accuracy was lost t_f^n is shown instead of the maximum error. The numerical result was taken to be sufficiently accurate if the maximum deviation with respect to the exact solution was smaller than 10^{-3} . Corresponding results can be seen in Table 2. Figure 1 shows how the maximum error behaves in time for different resolutions at different values of ν .

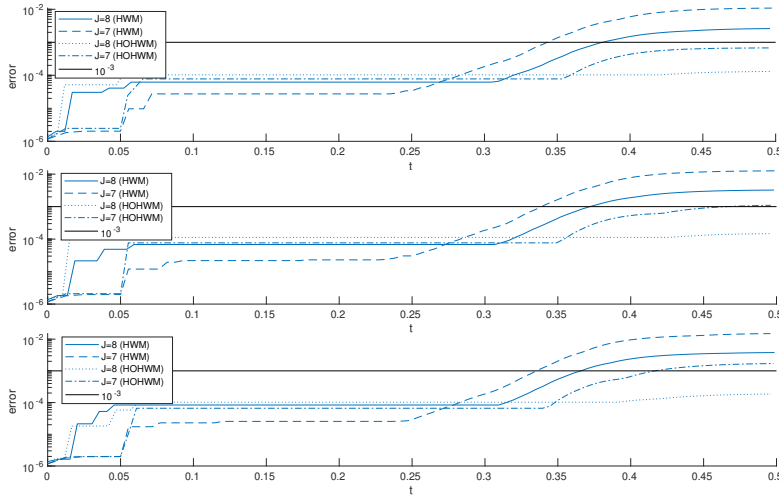


Figure 1. Maximum deviation in case of Burgers' equation for $\nu = \frac{1}{100\pi}$ (top), $\nu = \frac{1}{110\pi}$ (middle) and $\nu = \frac{1}{120\pi}$ (bottom).

The KdV equation was numerically solved for the nonlinear parameter values $\alpha = 1, 6$ with $c = 1000$ and $x_0 = 1/4$ within the domain $x \in [0, 1]$, $t \in [0, 0.5 \times 10^{-3}]$. The initial condition

$$u_0(x) = \frac{3c}{\alpha} \operatorname{sech}^2 \left(\frac{1}{2} \sqrt{c}(x - x_0) \right) \tag{5.3}$$

and boundary conditions (4.11) were used. In case of HOHWM the additional conditions (4.12) were added. The maximum deviation from the exact solution can be seen in Table 3.

In case of the KdV equation, the two-soliton exact solution (3.7) was also used. In this case the initial condition was taken from the exact solution as

$$u_0(x) = \frac{3(c_B - c_S) \left(c_B c_S \operatorname{sch}^2 \frac{\sqrt{c_B}(x-x_{0B})}{2} + c_S \operatorname{sech}^2 \frac{\sqrt{c_S}(x-x_{0S})}{2} \right)}{|\alpha| \left(\sqrt{c_B} \coth \frac{\sqrt{c_B}(x-x_{0B})}{2} - \sqrt{c_S} \tanh \frac{\sqrt{c_S}(x-x_{0S})}{2} \right)^2}. \tag{5.4}$$

Boundary conditions (4.11) as well as additional conditions (4.12) were used in this case as well. The results of these calculations can be found in Tables 5 and 6.

Table 3. Results for the KdV equation: maximal deviation of the numerical solution from the exact solution $\max\Delta u$ and maximal relative deviation $\max_{rel}\Delta u$ against the resolution parameter J with initial conditions (5.3) and boundary conditions (4.11) ($\alpha = 1, c = 1000, x_0 = 1/4, x \in [0, 1], t \in [0, 0.5 \times 10^{-3}]$).

J	$2M$	$\max\Delta u$		$\max_{rel}\Delta u$	
		HWM	HOHWM	HWM	HOHWM
4	32	134.5414	32.85357	0.0448471	0.0109512
5	64	68.76035	3.316314	0.0229201	0.0011054
6	128	19.26319	0.8202067	0.0064211	0.0002734
7	256	5.066037	0.844972	0.0016887	0.0002817

Table 4. Results for the KdV equation: maximal deviation of the numerical solution from the exact solution $\max\Delta u$ and maximal relative deviation $\max_{rel}\Delta u$ against the resolution parameter J with initial conditions (5.3) and boundary conditions (4.11) ($\alpha = 6, c = 1000, x_0 = 1/4, x \in [0, 1], t \in [0, 0.5 \times 10^{-3}]$).

J	$2M$	$\max\Delta u$		$\max_{rel}\Delta u$	
		HWM	HOHWM	HWM	HOHWM
4	32	22.42356	5.475594	0.0448471	0.0109512
5	64	11.46226	0.5527193	0.0229245	0.0011054
6	128	3.210801	0.1367652	0.0064216	0.0002735
7	256	0.8443429	0.0016887	0.0016887	0.0002816

Typical numerical results for the wave equation, the Burgers' equation and the KdV equation can be seen in Figure 2.

In case of both the Burgers' equation as well as the KdV equation the steep slope can be observed. The soliton interaction and subsequent phase shift can also be observed in case of the KdV interaction.

Table 5. Results for the KdV equation soliton interaction: maximal deviation of the numerical solution from the exact solution $\max\Delta u$ and maximal relative deviation $\max_{rel}\Delta u$ against the resolution parameter J with initial conditions (5.4) and boundary conditions (4.11) ($\alpha = 1, c_B = 10000, x_{0B} = 1/5, c_S = 10000/3, x_{0S} = 2/5, x \in [0, 1], t \in [0, 0.6 \times 10^{-4}]$).

J	$2M$	$\max\Delta u$		$\max_{rel}\Delta u$	
		HWM	HOHWM	HWM	HOHWM
4	32	3951164	2246754	131.7054667	74.8918000
5	64	6210848	202544.7	207.0282667	6.7514900
6	128	1567.924	199.7707	0.052264	0.0066590
7	256	542.1262	14.4892	0.0180709	0.0004830

Tables 1–6 show that HOHWM generally gives a more accurate result than HWM. In case of the wave equation (Table 1), the increase in c_1 (which translates into an increase in the slope) also increases the error of both methods while HOHWM remains more accurate. The Burgers' equation at the values of ν that were used introduces such a steep slope that at lower resolutions,

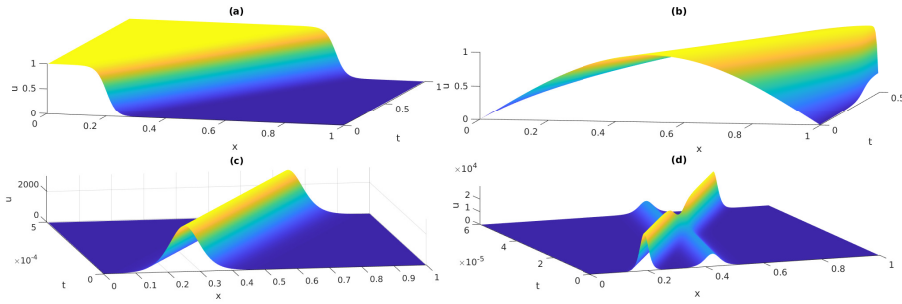


Figure 2. Typical calculated results for HOHWM. (a) Wave equation ($c_1 = 60, J = 7$ with boundary conditions (4.5) and initial condition (5.1)); (b) Burgers' equation ($\nu = \frac{1}{100\pi}, J = 7$ with boundary conditions (4.8) and initial condition (5.2)); (c) KdV single soliton solution ($\alpha = 1, c = 1000, x_0 = 1/4, J = 7$ with boundary conditions (4.11) and initial conditions (5.3)); (d) Interaction of KdV solitons ($\alpha = 1, c_B = 10000, x_{0B} = 1/5, c_S = 10000/3, x_{0S} = 2/5, J = 7$ with boundary conditions (4.11) and initial conditions (5.4)).

Table 6. Results for the KdV equation soliton interaction: maximal deviation of the numerical solution from the exact solution $\max \Delta u$ and maximal relative deviation $\max_{rel} \Delta u$ against the resolution parameter J with initial conditions (5.4) and boundary conditions (4.11) ($\alpha = 6, c_B = 10000, x_{0B} = 1/5, c_S = 10000/3, x_{0S} = 2/5, x \in [0, 1], t \in [0, 0.6 \times 10^{-4}]$).

J	$2M$	$\max \Delta u$		$\max_{rel} \Delta u$	
		HWM	HOHWM	HWM	HOHWM
4	32	215719.2	380037.1	43.1438400	76.0074200
5	64	104514.6	31103.69	20.9029200	6.2207380
6	128	260.845	33.305	0.0521690	0.0066610
7	256	90.35663	2.415028	0.0180713	0.0004830

neither method is able to successfully calculate the solution. This is due to the fact that the collocation points are used and at a low resolution, no collocation point falls within the slope. However, it is clear that HOHWM is able to perform calculations further in time before diminishing in accuracy, making it advantageous here as well. Figure 1 shows that HOHWM remains stable for a longer time than HWM since the former does not reach such high error throughout the integration.

In case of the one soliton solutions of the KdV equation, HOHWM again shows a higher accuracy than HWM. It can be noted from Tables 3 and 4 that the HOHWM is more accurate at $J = 5$ ($2M = 64$) than HWM is at $J = 7$ ($2M = 256$).

While the results are not directly comparable with [50] due to the difference in domain as well as values of c and differences in presenting error analysis, some comparison can be made. The maximum relative deviation from the exact solution can be compared. Such a comparison between [50] and results in Table 4 is carried out in Table 7. While the result with HWM is not as accurate as that of [50] the results with HOHWM surpass the referenced results.

Table 7. Comparison to [50]: maximal relative deviation from the exact solution at $J = 7$.

[50]	HWM	HOHWM
0.00041236	0.001688031	0.0002817978

The KdV soliton interactions show an interesting phenomenon, however. From Tables 5 and 6 one can see that at lower resolutions neither method can successfully solve the problem. This is caused by the fact that one now has two relatively localized solitary waves and at lower resolutions no collocation point falls within these localized solitary waves. However, at higher resolutions, one can clearly see the advantages of HOHWM over HWM as the former shows a significant boost in accuracy.

6 Conclusions

The HOHWM has been adapted for solving partial differential equations numerically. The results obtained by the widely used HWM were compared with those obtained by the HOHWM. The Burgers' equation and the KdV equation were considered as model equations.

Our numerical experiments demonstrated that both methods, the HWM and the HOHWM, were able to provide numerical solutions that are in good agreement with the exact analytical solutions. The detailed comparison of the accuracy of the HWM and the HOHWM was performed in Section 5. It is shown that HOHWM can be preferred where high accuracy is required. Furthermore, the HOHWM can also be preferred in cases where high accuracy is not required by applying the method at a lower resolution in comparison with HWM.

Solving the system of algebraic equations is the most computationally expensive task within Haar wavelet based methods. However, the algebraic systems of equations are of the same dimension and have the same symmetric properties for the HWM as well as for the HOHWM. Even though some expressions needed to evaluate are more complex in case of HOHWM, in general it can be concluded that the numerical complexity of the HOHWM is only slightly higher than that of the HWM at the same resolution. It would be more pragmatic to estimate computational complexity of the solution providing the same accuracy, however. For example, in the case of single KdV-soliton solution (Tables 3 and 4), one can use HWM with 256 collocation points or HOHWM with 64 collocation points in order to obtain the same degree of accuracy. Solving a 64×64 algebraic system is substantially computationally cheaper than solving a 256×256 system. Therefore, it is possible to obtain the results with the same accuracy as HWM with lower computational cost by applying HOHWM.

The Fourier transform related pseudospectral method is known as a powerful tool for numerical solution of evolution equations because it is able to produce high accuracy at relatively low number of collocation points [22]. However,

this method has a disadvantage: because of the nature of the Fourier transform one must apply periodic boundary conditions. Haar wavelet related methods do not have such a disadvantage and one can solve PDEs numerically applying arbitrary boundary conditions in case of the HWM and arbitrary time independent boundary conditions in case of the HOHWM. In order to use time dependent boundary conditions with HOHWM a different numerical scheme must be applied to approximate the temporal derivatives.

Acknowledgements

This research was supported by the Estonian Research Council (IUT 33-24).

References

- [1] M.J. Ablowitz. Nonlinear evolution equations, inverse scattering and cellular automata. In P.J. Olver and D.H. Sattinger(Eds.), *Solitons in Physics, Mathematics, and Nonlinear Optics*, pp. 1–26. Springer, 1990.
- [2] U. Andersson, B. Engquist, G. Ledfelt and O. Runborg. A contribution to wavelet-based subgrid modeling. *Appl. Comput. Harmon. Anal.*, **7**(2):151–164, 1999. <https://doi.org/10.1006/acha.1999.0264>.
- [3] I. Aziz and R. Amin. Numerical solution of a class of delay differential and delay partial differential equations via Haar wavelet. *Appl. Math. Model*, **40**(23):10286–10299, 2016. <https://doi.org/10.1016/j.apm.2016.07.018>.
- [4] I. Aziz and I. Khan. Numerical solution of diffusion and reaction–diffusion partial integro-differential equations. *Int. J. Comput. Methods*, **15**(06):1850047, 2018. <https://doi.org/10.1016/j.apm.2016.07.018>.
- [5] I. Aziz and Siraj-ul-Islam. New algorithms for the numerical solution of nonlinear Fredholm and Volterra integral equations using Haar wavelets. *Comput. Appl. Math.*, **239**:333–345, 2013. <https://doi.org/10.1016/j.cam.2012.08.031>.
- [6] I. Aziz, Siraj-ul-Islam and M. Asif. Haar wavelet collocation method for three-dimensional elliptic partial differential equations. *Comput. Math. Appl.*, **73**(9):2023–2034, 2017. <https://doi.org/10.1016/j.camwa.2017.02.034>.
- [7] I. Aziz, Siraj-ul-Islam and F. Khan. A new method based on Haar wavelet for the numerical solution of two-dimensional nonlinear integral equations. *Comput. Appl. Math.*, **272**:70–80, 2014. <https://doi.org/10.1016/j.cam.2014.04.027>.
- [8] E. Babolian and A. Shamsavaran. Numerical solution of nonlinear Fredholm integral equations of the second kind using Haar wavelets. *Comput. Appl. Math.*, **225**(1):87–95, 2009. <https://doi.org/10.1016/j.cam.2008.07.003>.
- [9] E.R. Benton and G.W. Platzman. A table of solutions of the one-dimensional Burgers equation. *Quart. Appl. Math.*, **30**(2):195–212, 1972. <https://doi.org/10.1090/qam/306736>.
- [10] J.M. Burgers. A mathematical model illustrating the theory of turbulence. In Richard Von Mises and Theodore Von Kármán(Eds.), *Advances in Applied Mechanics*, volume 1, pp. 171–199. Academic Press, 1948. [https://doi.org/10.1016/S0065-2156\(08\)70100-5](https://doi.org/10.1016/S0065-2156(08)70100-5).
- [11] J.M. Burgers. Statistical problems connected with the solution of a nonlinear partial differential equation. In William F. Ames(Ed.), *Nonlinear Problems of*

- Engineering*, pp. 123–137. Academic Press, 1964. <https://doi.org/10.1016/B978-1-4832-0078-1.50015-8>.
- [12] C. Cattani. Haar wavelets based technique in evolution problems. *Proc. Estonian Acad. Sci. Phys. Math.*, **53**(1):45–63, 2004.
- [13] C. Cattani. Harmonic wavelets towards the solution of non-linear PDE. *Comput. Math. Appl.*, **50**(8-9):1191–1210, 2005. <https://doi.org/10.1016/j.camwa.2005.07.001>.
- [14] C. Cattani and A. Kudreyko. Harmonic wavelet method towards solution of the Fredholm type integral equations of the second kind. *Appl. Math. Comput.*, **215**(12):4164–4171, 2010. <https://doi.org/10.1016/j.amc.2009.12.037>.
- [15] C.F. Chen and C. H. Hsiao. Haar wavelet method for solving lumped and distributed-parameter systems. *IEE Proc. Control Theory Appl.*, **144**(1):87–94, 1997. <https://doi.org/10.1049/ip-cta:19970702>.
- [16] J.D. Cole. On a quasi-linear parabolic equation occurring in aerodynamics. *Quart. Appl. Math.*, **9**(3):225–236, 1951. <https://doi.org/10.1090/qam/42889>.
- [17] J.R. Dormand and P.J. Prince. A family of embedded Runge-Kutta formulae. *J. Comput. Appl. Math.*, **6**(1):19–26, 1980. [https://doi.org/10.1016/0771-050X\(80\)90013-3](https://doi.org/10.1016/0771-050X(80)90013-3).
- [18] P.G. Drazin. *Solitons*, volume 85 of *London Mathematical Society Lecture Note Series*. Cambridge University Press, 1983.
- [19] P.G. Drazin and R.S. Johnson. *Solitons: an introduction*. Cambridge University Press, 1989. <https://doi.org/10.1002/zamm.19900700817>.
- [20] J. Engelbrecht and A. Salupere. On the problem of periodicity and hidden solitons for the KdV model. *Chaos*, **15**:015114, 2005. <https://doi.org/10.1063/1.1858781>.
- [21] S. Foadian, R. Pourgholi, S.H. Tabasi and J. Damirchi. The inverse solution of the coupled nonlinear reaction–diffusion equations by the Haar wavelets. *Int. J. Comput. Math.*, **96**(1):105–125, 2019. <https://doi.org/10.1080/00207160.2017.1417593>.
- [22] B. Fornberg. *A Practical Guide to Pseudospectral Methods*. Cambridge University Press, Cambridge, 1998. <https://doi.org/10.1017/CBO9780511626357>.
- [23] Y. Ge, S. Li, Y. Shi and L. Han. An adaptive wavelet method for solving mixed-integer dynamic optimization problems with discontinuous controls and application to alkali–surfactant–polymer flooding. *Eng. Optim.*, **51**(6):1028–1048, 2019. <https://doi.org/10.1080/0305215X.2018.1508573>.
- [24] M.F. Hamilton and D. T. Blackstock(Eds.). *Nonlinear acoustics*. Academic Press, San Diego, 1998.
- [25] G. Hariharan, K. Kannan and K.R. Sharma. Haar wavelet method for solving fishers equation. *Appl. Math. Comput.*, **211**(2):284–292, 2009. <https://doi.org/10.1016/j.amc.2008.12.089>.
- [26] H. Hein and L. Feklistova. Computationally efficient delamination detection in composite beams using Haar wavelets. *Mech. Syst. Signal Process.*, **25**(6):2257–2270, 2011.
- [27] C.H. Hsiao. State analysis of linear time delayed systems via Haar wavelets. *Math. Comput. Simulation*, **44**(5):457–470, 1997. [https://doi.org/10.1016/S0378-4754\(97\)00075-X](https://doi.org/10.1016/S0378-4754(97)00075-X).

- [28] G. Jin, X. Xie and Z. Liu. The Haar wavelet method for free vibration analysis of functionally graded cylindrical shells based on the shear deformation theory. *Compos. Struct.*, **108**:435–448, 2014. <https://doi.org/10.1016/j.compstruct.2013.09.044>.
- [29] R. Jiwari. A Haar wavelet quasilinearization approach for numerical simulation of Burgers equation. *Comput. Phys. Comm.*, **183**(11):2413–2423, 2012. <https://doi.org/10.1016/j.cpc.2012.06.009>.
- [30] M. Kirs, K. Karjust, I. Aziz, E. Õunapuu and E. Tungal. Free vibration analysis of a functionally graded material beam: evaluation of the Haar wavelet method. *Proc. Estonian Acad. Sci.*, **67**(1):1–9, 2018.
- [31] P.A. Lagerstrom, J.D. Cole and L. Trilling. Problems in the theory of viscous compressible fluids. Guggenheim Aeronautical Laboratory, unnumbered report, California Institute of Technology, 1949.
- [32] G. L. Lamb Jr. *Elements of Soliton Theory*. John Wiley & Sons, 1980.
- [33] Ü. Lepik. Numerical solution of differential equations using Haar wavelets. *Math. Comput. Simulation*, **68**(2):127–143, 2005. <https://doi.org/10.1016/j.matcom.2004.10.005>.
- [34] Ü. Lepik. Haar wavelet method for nonlinear integro-differential equations. *Appl. Math. Comput.*, **176**(1):324–333, 2006. <https://doi.org/10.1016/j.amc.2005.09.021>.
- [35] Ü. Lepik. Application of the Haar wavelet transform to solving integral and differential equations. *Proc. Estonian Acad. Sci. Phys. Math.*, **56**(1):28–46, 2007. <https://doi.org/10.1117/12.736416>.
- [36] Ü. Lepik. Numerical solution of evolution equations by the Haar wavelet method. *Appl. Math. Comput.*, **185**(1):695–704, 2007. <https://doi.org/10.1016/j.amc.2006.07.077>.
- [37] Ü. Lepik. Solving fractional integral equations by the Haar wavelet method. *Appl. Math. Comput.*, **214**(2):468–478, 2009. <https://doi.org/10.1016/j.amc.2009.04.015>.
- [38] Ü. Lepik. Solving PDEs with the aid of two-dimensional Haar wavelets. *Comput. Math. Appl.*, **61**(7):1873–1879, 2011. <https://doi.org/10.1016/j.camwa.2011.02.016>.
- [39] Ü. Lepik and H. Hein. *Haar wavelets: with applications*. Springer, 2014. <https://doi.org/10.1007/978-3-319-04295-4>.
- [40] J. Majak, M. Pohlak and M. Eerme. Application of the Haar wavelet-based discretization technique to problems of orthotropic plates and shells. *Mech. Compos. Mater.*, **45**(6):631–642, 2009. <https://doi.org/10.1007/s11029-010-9119-0>.
- [41] J. Majak, M. Pohlak, M. Eerme and T. Lepikult. Weak formulation based Haar wavelet method for solving differential equations. *Appl. Math. Comput.*, **211**(2):488–494, 2009. <https://doi.org/10.1016/j.amc.2009.01.089>.
- [42] J. Majak, M. Pohlak, K. Karjust, M. Eerme, J. Kurnitski and B.S. Shvartsman. New higher order Haar wavelet method: Application to FGM structures. *Compos. Struct.*, **201**:72–78, 2018. <https://doi.org/10.1016/j.compstruct.2018.06.013>.
- [43] J. Majak, B. Shvartsman, K. Karjust, M. Mikola, A. Haavaj oe and M. Pohlak. On the accuracy of the Haar wavelet discretization method. *Compos. Part B*, **80**:321–327, 2015. <https://doi.org/10.1016/j.compositesb.2015.06.008>.

- [44] J. Majak, B. Shvartsman, M. Pohlak, K. Karjust, M. Eerme and E. Tungel. Solution of fractional order differential equation by the Haar Wavelet method. numerical convergence analysis for most commonly used approach. *AIP Conference Proceedings*, **1738**(1):480110, 2016. <https://doi.org/10.1063/1.4952346>.
- [45] J. Majak, B.S. Shvartsman, M. Kirs, M. Pohlak and H. Herranen. Convergence theorem for the Haar wavelet based discretization method. *Compos. Struct.*, **126**:227–232, 2015. <https://doi.org/10.1016/j.compstruct.2015.02.050>.
- [46] T. Musha and H. Higuchi. Traffic current fluctuation and the Burgers equation. *Jpn. J. Appl. Phys.*, **17**(5):811–816, 1978. <https://doi.org/10.1143/JJAP.17.811>.
- [47] S. Nazir, S. Shahzad, R. Wirza, R. Amin, M. Ahsan, N. Mukhtar, Iván. García-Magariño and J. Lloret. Birthmark based identification of software piracy using Haar wavelet. *Math. Comput. Simulation*, 2019. <https://doi.org/10.1016/j.matcom.2019.04.010>.
- [48] Ö. Oruç. A non-uniform Haar wavelet method for numerically solving two-dimensional convection-dominated equations and two-dimensional near singular elliptic equations. *Comput. Math. Appl.*, **77**(7):1799–1820, 2019. <https://doi.org/10.1016/j.camwa.2018.11.018>.
- [49] Ö. Oruç, F. Bulut and A. Esen. A Haar wavelet-finite difference hybrid method for the numerical solution of the modified Burgers equation. *J. Math. Chem.*, **53**(7):1592–1607, 2015. <https://doi.org/10.1007/s10910-015-0507-5>.
- [50] Ö. Oruç, F. Bulut and A. Esen. Numerical solution of the KdV equation by Haar wavelet method. *Pramana - J. Phys.*, **87**(6):94, Nov 2016. <https://doi.org/10.1007/s12043-016-1286-7>.
- [51] Ö. Oruç, F. Bulut and A. Esen. Numerical solutions of regularized long wave equation by Haar wavelet method. *Mediterr. J. Math.*, **13**(5):3235–3253, 2016. <https://doi.org/10.1007/s00009-016-0682-z>.
- [52] Ö. Oruç, F. Bulut and A. Esen. A numerical treatment based on Haar wavelets for coupled KdV equation. *Int. J. Optim. Control*, **7**(2):195–204, 2017. <https://doi.org/10.11121/ijocta.01.2017.00396>.
- [53] Ö. Oruç, A. Esen and F. Bulut. A Haar wavelet approximation for two-dimensional time fractional reaction–subdiffusion equation. *Eng. Comput.*, **35**(1):75–86, Jan 2019. ISSN 1435-5663. <https://doi.org/10.1007/s00366-018-0584-8>.
- [54] M. Remoissenet. *Waves called solitons: concepts and experiments*. Springer, 2013.
- [55] A. Salupere. The pseudospectral method and discrete spectral analysis. In Ewald Quak and Tarmo Soomere(Eds.), *Applied Wave Mathematics: Selected Topics in Solids, Fluids, and Mathematical Methods*, pp. 301–333. Springer, 2009.
- [56] A. Salupere, J. Engelbrecht, O. Ilison and L. Ilison. On solitons in microstructured solids and granular materials. *Math. Comput. Simulation*, **69**:502–513, 2005. <https://doi.org/10.1016/j.matcom.2005.03.015>.
- [57] A. Salupere, P. Peterson and J. Engelbrecht. Long-time behaviour of soliton ensembles. Part I—Emergence of ensembles. *Chaos Solitons Fractals*, **14**(9):1413–1424, 2002. [https://doi.org/10.1016/S0960-0779\(02\)00069-3](https://doi.org/10.1016/S0960-0779(02)00069-3).
- [58] A. Salupere and M. Ratas. On the application of 2D discrete spectral analysis in case of the kp equation. *Mech. Research Comm.*, **93**:141–147, 2018. <https://doi.org/10.1016/j.mechrescom.2017.08.010>.

- [59] I. Sertakov, J. Engelbrecht and J. Janno. Modelling 2D wave motion in microstructured solids. *Mech. Research Comm.*, **56**:42 – 49, 2014. <https://doi.org/10.1016/j.mechrescom.2013.11.007>.
- [60] A. Setia, B. Prakash and A.S. Vatsala. Haar based numerical solution of Fredholm–Volterra fractional integro-differential equation with nonlocal boundary conditions. In *AIP Conference Proceedings*, volume 1798, p. 020140. AIP Publishing, 2017. <https://doi.org/10.1063/1.4972732>.
- [61] L.F. Shampine and M.W. Reichelt. The MATLAB ODE suite. *SIAM J. Sci. Comput.*, **18**(1):1–22, 1997. <https://doi.org/10.1137/S1064827594276424>.
- [62] X. Si, C. Wang, Y. Shen and L. Zheng. Numerical method to initial-boundary value problems for fractional partial differential equations with time-space variable coefficients. *Appl. Math. Model.*, **40**(7-8):4397–4411, 2016. <https://doi.org/10.1016/j.apm.2015.11.039>.
- [63] Siraj-ul-Islam, I. Aziz and A.S. Al-Fhaid. An improved method based on Haar wavelets for numerical solution of nonlinear integral and integro-differential equations of first and higher orders. *Comput. Appl. Math.*, **260**:449–469, 2014. <https://doi.org/10.1016/j.cam.2013.10.024>.
- [64] T.J. Wang and T. Sun. Mixed pseudospectral method for heat transfer. *Math. Mod. Anal.*, **21**(2):199–219, 2016. <https://doi.org/10.3846/13926292.2016.1146925>.
- [65] N. Wichailukkanaa, B. Novapruteepa and C. Boonyasiriwatc. A convergence analysis of the numerical solution of boundary-value problems by using two-dimensional Haar wavelets. *ScienceAsia*, **42**(5):346–355, 2016. <https://doi.org/10.2306/scienceasia1513-1874.2016.42.346>.
- [66] X. Xiang, J. Guoyong, L. Wanyou and L. Zhigang. A numerical solution for vibration analysis of composite laminated conical, cylindrical shell and annular plate structures. *Compos. Struct.*, **111**:20–30, 2014. <https://doi.org/10.1016/j.compstruct.2013.12.019>.
- [67] X. Xie, G. Jin and Z. Liu. Free vibration analysis of cylindrical shells using the Haar wavelet method. *Int. J. Mech. Sci.*, **77**:47–56, 2013. <https://doi.org/10.1016/j.ijmecsci.2013.09.025>.
- [68] X. Xie, G. Jin, Y. Yan, S.X. Shi and Z. Liu. Free vibration analysis of composite laminated cylindrical shells using the Haar wavelet method. *Compos. Struct.*, **109**:169–177, 2014. <https://doi.org/10.1016/j.compstruct.2013.10.058>.
- [69] X. Xie, G. Jin, T. Ye and Z. Liu. Free vibration analysis of functionally graded conical shells and annular plates using the Haar wavelet method. *Appl. Acoust.*, **85**:130–142, 2014. <https://doi.org/10.1016/j.apacoust.2014.04.006>.
- [70] T. Yoneyama. The Korteweg–de Vries two-soliton solution as interacting two single solitons. *Progr. Theoret. Phys.*, **71**(4):843–846, 1984. <https://doi.org/10.1143/PTP.71.843>.

Appendix 3

III

M. Ratas, A. Salupere, and J. Majak. Solving nonlinear PDEs using the higher order Haar wavelet method on nonuniform and adaptive grids. *Math. Model. Anal.*, [accepted]

Solving nonlinear PDEs using the higher order Haar wavelet method on nonuniform and adaptive grids

Mart Ratas^a, Andrus Salupere^a and Jüri Majak^b

^a*Department of Cybernetics, School of Science, Tallinn University of Technology*

12618 Tallinn, Estonia

^b*Department of Mechanical and Industrial Engineering, School of Engineering, Tallinn University of Technology*

19086 Tallinn, Estonia

E-mail(*corresp.*): mart.ratas@taltech.ee

Received September 2, 2020; revised September 2, 2020; published online Mxx 1, 20xx

Abstract. The higher order Haar wavelet method (HOHWM) is used with a nonuniform grid to solve nonlinear partial differential equations numerically. The Burgers' equation, the Korteweg–de Vries equation, the modified Korteweg–de Vries equation and the sine–Gordon equation are used as model equations. Adaptive as well as nonadaptive nonuniform grids are developed and used to solve the model equations numerically. The numerical results are compared to the known analytical solutions as well as to the numerical solutions obtained by application of the HOHWM on a uniform grid. The proposed methods of using nonuniform grid are shown to significantly increase the accuracy of the HOHWM at the same number of grid points.

Keywords: Numerical simulation, Haar wavelet method, higher order wavelet expansion, nonlinear PDEs, nonuniform grid, adaptive grid.

AMS Subject Classification: 37M05, 65T60, 35Q51, 35G31, 65M50.

1 Introduction

Wavelet based numerical methods have seen wide use since the 1990s [12, 13]. Since then, numerous papers on wavelet based numerical methods have been published with applications in various types of Partial Differential Equations (PDEs) of mathematical physics [20, 22, 39, 46, 57, 59, 62]. Haar wavelets deserve a special mention among other wavelets, however. They are made up of pairs of piecewise constant functions and are therefore mathematically the simplest of all the wavelet families. They can be integrated analytically arbitrary times.

The Haar Wavelet Method (HWM) was originally proposed in [27] for solving differential equations. It was later extended for solving a wide class of integro-differential and integral equations [4, 5, 6, 7, 24, 54, 58]. According to this method, the highest order derivative included in the differential equations is expanded into the Haar series. Lepik developed the integration techniques for the HWM in [53, 54, 55, 58, 59]. A thorough overview of the HWM and its applications can be found in [60]. The weak formulation based HWM was introduced and complexity issues of the strong as well as weak formulation based HWM were discussed in [62].

One of the most common areas of application for the HWM seems to be engineering. The method has been used in solid mechanics [54, 55, 59], analysis and modelling of composite structures [25, 26, 40, 78], free vibration analysis [45, 61, 88, 89], solving fractional differential equations [17, 74] as well as many other areas, e.g [70, 71, 72, 73]. In addition to engineering, Haar wavelets have found application in various research areas from informatics to medicine [21, 23, 87].

Recently, the higher order Haar wavelet method (HOHWM) has been developed [64] as an improvement of the HWM. The HOHWM has been found to increase accuracy as well as convergence over the regular HWM [43, 44, 47, 63, 64]. In case of the HWM the highest derivative present within the differential equation is expanded into the Haar series. However, the HOHWM proposes that a derivative of $2s$ higher order is expanded into the Haar series. This procedure introduces $2s$ extra integration coefficients, although, in case of $s = 1$, the equation can be evaluated at its boundary in order to solve for those extra coefficients. Therefore, this paper focuses on the use of the HOHWM over the conventional HWM.

The nonuniform Haar wavelets were first introduced in [31]. They were first used to solve integral and differential equations by Lepik [56]. The nonuniform Haar wavelets have since been used in multiresolution analysis [3], boundary value problems [33], fractional order problems [65, 79] as well as two dimensional problems [69]. An overview of uniform and non-uniform wavelet based methods can be found in [49].

In order to deal with PDEs with rapid solution variation, adaptive grids have been developed [11, 16, 32, 76]. They have seen use in many areas, including astrophysics and turbulence problems in hydrodynamics [36, 48, 82, 84], among others. The general idea of adaptive grids is to be able to reshape the grid in such a way that areas with large variations have more grid points. Such a system uses error estimates as weight functions to determine where the grid needs to be more concentrated. Adaptivity can be achieved by changing the number of grid points or the movement of grid points. Since the HWM and the HOHWM require a fixed number of grid points, movement of grid points is considered within this paper. With a fixed number of grid points resolution is raised locally at the expense of decreased resolution in other regions. The effect of the decreased resolution can be minor if the other regions previously have more grid points than are needed for the required accuracy. The basic premise of an adaptive grid is that when moving from coordinate grid ξ to s with a weight function of w , $w ds = c d\xi$ holds for a proportionality constant c .

In the current study, the HOHWM is used to solve nonlinear partial differential equations which have abrupt changes in their solutions. The benefits of the nonuniform grid can best be observed in solutions with such abrupt changes. To the best knowledge of the authors, this is the first time the HOHWM is used on a nonuniform grid. The Burgers' equation [18, 19] and the Korteweg–de Vries (KdV) equation were chosen as model equations because they have previously been studied using the HOHWM on the uniform grid [77] and have analytical solutions [2, 8, 50, 68] which make comparisons easy to draw. The Burgers' equation finds applications in modelling of turbulence [18] and traffic flow [67] as well as in nonlinear acoustics [38] and non-stationary shock waves in fluids [51]. The KdV equation was first used as a description of the propagation of long unidirectional shallow water waves in a rectangular channel, but it has been used to model different nonlinear phenomena since then [30]. The modified Korteweg–de Vries equation (mKdV) was chosen as a model equation because of its close relation to the KdV equation as well as the existence of an analytical solution [1, 42]. The mKdV equation finds use in modelling of behaviour of anharmonic lattices [42]. The sine–Gordon equation was chosen as the last model equation because of the existence of an analytical traveling wave solution [52] and the fact that its analytical solution is not asymptotically homogeneous like those of the KdV and mKdV. The sine–Gordon equation was originally developed to describe surfaces with constant mean curvature [14] and has also seen use in one-dimensional crystal dislocation theory [35, 34] as well as in many other fields [15, 66, 81, 80]. In the current study, the adaptive grid with a constant number of grid points according to the constrained least-squares statement defined in [32] is used.

This paper is structured as follows. Firstly, the spatial discretisation and nonuniform grids are described in Section 2. Section 3 focuses on the Haar wavelet family and describes how it is used in the HOHWM. Model equations and their corresponding exact solutions are introduced in Section 4, and the nonuniform HOHWM is applied to them in Section 5. The numerical results are discussed in Section 6 and conclusions are drawn in the final section.

2 Discretization

The Haar wavelet method is used along the spatial axis only within this paper. The *ODEPACK* [41] provided by *SciPy* [85] is used for integration with respect to time. It automatically switches between Adams and BDF [9, 29, 37] solvers according to [75]. Since this involves calculating the value of the function at each moment in time, this allows for adaptive changes to the grid.

The collocation method is used alongside the HOHWM. As such, the collocation points lie in the middle of an adjacent pair of grid points. Given the domain $x \in [A, B]$, the $2M + 1$ grid points can be described as

$$x^g(l), \quad l = 0, 1, \dots, 2M, \quad x^g(l+1) > x^g(l) \forall l, \quad x^g(0) = A, \quad x^g(2M) = B. \quad (2.1)$$

The $2M$ collocation points can be obtained as

$$x(l) = \frac{x^g(l) + x^g(l+1)}{2}, \quad l = 0, 1, \dots, 2M-1. \quad (2.2)$$

Within this paper, three different approaches are used for numerical differentiation with respect to the space coordinate. Two of those approaches are static (the space grid does not change during usage) and the third is adaptive (the space grid changes during operation).

2.1 Nonuniform grids

The first type of nonuniform grid for domain $x \in [0, 1]$ follows the formula

$$x^g(l) = \frac{q^l - 1}{q^{2M} - 1}, \quad l = 0, 1, \dots, 2M, \quad (2.3)$$

where q is an arbitrary constant. It is clear that for $q < 1$ the above leads to a grid which concentrates grid points around 1 and that in case of $q > 1$ the grid points are concentrated around 0. It is also clear that given $q \rightarrow 1$ the grid (2.3) becomes uniform. This type of grid is most applicable for cases where the characteristic behaviour of a solution tends to concentrate near a boundary. The same type of nonuniform grid was used in [69].

The second type of nonuniform grid for domain $x \in [0, 1]$ is perhaps a little simpler. It follows the formula

$$x^g(l) = \begin{cases} 0, & l = 0 \\ \frac{(l-1)(1-2\gamma)}{2M-2} + \gamma, & 0 < l < 2M, \\ 1, & l = 2M \end{cases} \quad (2.4)$$

where γ is the gap parameter. It describes how far from either boundary the coarse part of the grid ends and the finer part begins. Such a grid is most applicable for cases where the characteristic behaviour of a solution stays in the middle of the domain, yet its exact position cannot be determined.

2.2 Adaptive grid

In the current paper the adaptive grid based on the constrained least-squares statement [32] is used. According to it, when changing the grid, the new grid x^* will have grid points such that

$$x_{k+1}^* - x_k^* = \frac{1}{\sum_{i=1}^{N-1} \frac{1}{w_{i+1/2}}} (x_{max}^* - x_{min}^*), \quad k = 1, \dots, N-1, \quad (2.5)$$

where x_{min}^* and x_{max}^* denote the minimal and maximal grid point, respectively and w is the weight function. It must be noted, that $w_{i+1/2}$ is used. In the current paper, the weight function is calculated at collocation points, which lie in the middle of two subsequent grid points according to (2.2) and thus the

values at the collocation points can directly be used. For the weight function, either the function itself or its first derivative is scaled and a constant e is added (to ensure the weights never reach 0). The weight function from the function u is thus obtained as

$$w = |u|^d + e, \quad (2.6)$$

where d is the scaling factor and e is the offset. Similarly, when using the derivative one obtains

$$w = |u_x|^d + e. \quad (2.7)$$

The algorithm (2.5) is carried out iteratively as many times as necessary for conversion of the grid points. During each iteration, the weights are estimated at the new collocation points by interpolation.

In case of the adaptive grid, a new grid is only calculated if the characteristic point in the numerical result (i.e the maximal point of the function or its derivative) has moved by δ . This helps to save on CPU time.

3 Haar wavelet family

In the following, the Haar wavelet family is defined utilizing the notation introduced by Lepik in [56] and Oruç in [69]. The integration domain $[A, B]$ can be divided into $2M$ subintervals. The maximal level of resolution J is defined as $M = 2^J$. The base Haar wavelet family can be described as

$$h_i(x) = \begin{cases} 1 & \text{for } x \in [\xi_1(i), \xi_2(i)), \\ -c_i & \text{for } x \in [\xi_2(i), \xi_3(i)), \\ 0 & \text{elsewhere,} \end{cases} \quad (3.1)$$

where

$$\begin{aligned} \xi_1(i) &= x^g(2k\mu), & \xi_2(i) &= x^g((2k+1)\mu), \\ \xi_3(i) &= x^g(2(k+1)\mu), & \mu &= M/m. \end{aligned} \quad (3.2)$$

The coefficient c_i is calculated from

$$\int_A^B h_i(x) dx = 0, \quad (3.3)$$

which gives

$$c_i = \frac{\xi_2(i) - \xi_1(i)}{\xi_3(i) - \xi_2(i)}. \quad (3.4)$$

In (3.1)–(3.3), $k = 0, 1, \dots, m-1$ is the translation parameter. The parameter $m = 2^j$ corresponds to the maximum number of rectangular waves that can be sequentially deployed in the interval $[A, B]$ for the given dilation parameter $j = 0, 1, \dots, J$. The index i is calculated from $i = m + k + 1$. While the scaling function $h_1(x) = 1$ is constant, the other Haar functions contain a single rectangular wave. Since the scaling function $h_1(x)$ does not include a wave, in its case $m = 0, \xi_1 = A, \xi_2 = B, \xi_3 = B$. A general example of the Haar wavelets for $J = 2$ on a nonuniform grid is shown in Fig. 1. In this figure locations where

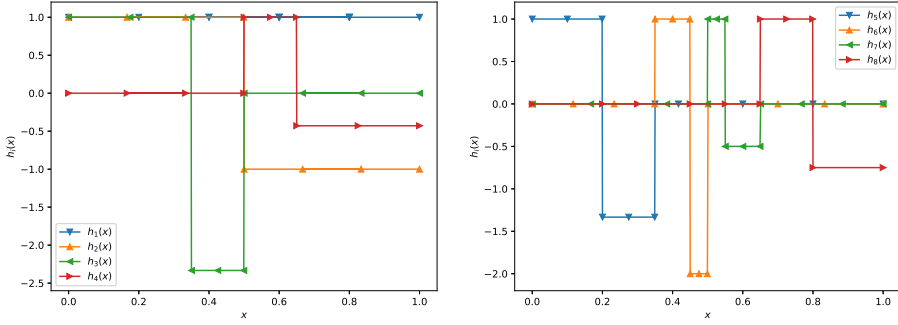


Figure 1. Haar wavelets on a nonuniform grid for $J = 2$ as described by (3.2)–(3.4)

the vertical lines cross the x axis along with the two boundary points form the grid points.

The Haar functions are orthogonal to each other and therefore form a good transform basis

$$\int_A^B h_i(x)h_l(x)dx = \begin{cases} 2^{-j} & i = l, \\ 0 & i \neq l. \end{cases} \quad (3.5)$$

Thus, any square integrable function $f(x)$ can be expanded into Haar wavelets as

$$f(x) = \sum_{i=1}^{\infty} a_i h_i(x), \quad (3.6)$$

where a_i are the Haar coefficients.

The integrals of order n of the Haar functions (3.1) can be calculated analytically as [59]

$$p_{n,i}(x) = \begin{cases} 0 & \text{for } x \in [A, \xi_1(i)), \\ \frac{[x - \xi_1(i)]^n}{n!} & \text{for } x \in [\xi_1(i), \xi_2(i)), \\ \frac{[x - \xi_1(i)]^n - (1 + c_i)[x - \xi_2(i)]^n}{n!} & \text{for } x \in [\xi_2(i), \xi_3(i)), \\ \frac{[x - \xi_1(i)]^n - (1 + c_i)[x - \xi_2(i)]^n}{n!} + \frac{c_i[x - \xi_3(i)]^n}{n!} & \text{for } x \in [\xi_3(i), B). \end{cases} \quad (3.7)$$

Within this article the matrix form of the above formulation is used. Therefore, the elements of $(2M) \times (2M)$ matrix \mathbf{H} , are given as values of the Haar functions

$$H_{il} = h_i(x_l), \quad (3.8)$$

in collocation points $x_l = (l - 1/2)\Delta x$. The $(2M) \times (2M)$ matrix \mathbf{P}_n with elements

$$(P_n)_{il} = p_{n,i}(x_l), \quad (3.9)$$

denotes the n th integral of the Haar wavelet matrix for a given resolution J . Using (3.8) and (3.9) and considering the vector $\mathbf{a} = (a_1, a_2, \dots, a_{2M})$ one obtains

$$f(x) = \mathbf{a} \cdot \mathbf{H} \quad (3.10)$$

instead of (3.6) and

$$\underbrace{\int \dots \int_A}_n \mathbf{H} \underbrace{d\xi \dots d\xi}_n = \mathbf{P}_n. \quad (3.11)$$

It must be noted, that the matrices \mathbf{H} and \mathbf{P}_n depend on space coordinate x and that the vector \mathbf{a} is finite in a discrete setting.

It implies from (3.7) that in boundary points A and B hold

$$[P_n(A)]_i = 0 \quad \forall n > 0, \quad \forall i \quad (3.12)$$

and

$$[P_n(B)]_i = p_{n,i}(B) = \frac{[B - \xi_1(i)]^n - (1 - c_i)[B - \xi_2(i)]^n + c_i[B - \xi_3(i)]^n}{n!}. \quad (3.13)$$

Due to equation (3.12) the boundary conditions for particular problems are often simplified.

4 Model equations

The four model equations along with their corresponding exact solutions are described here. The Burgers' equation

$$u_t + uu_x - \nu u_{xx} = 0, \quad (4.1)$$

where ν is the viscosity parameter, was used as the first model equation. Its analytical solution has been shown to be

$$u_e(x, t) = \frac{2\nu\pi}{L} \frac{\sum_{n=1}^{\infty} \exp(-E_n t) n I_n(R') \sin(n\pi x/L)}{I_0(R') + 2 \sum_{n=1}^{\infty} \exp(-E_n t) I_n(R') \cos(n\pi x/L)}, \quad (4.2)$$

where $R' = R_0/(2\pi)$ and $R_0 = u_0 L/\nu$ is the Reynolds number, $E_n = \nu n^2 \pi^2/L^2$, I_n represents the modified Bessel functions of first kind and $L = B - A$ is the x domain range [2, 8, 10, 28, 50].

The KdV equation

$$u_t + \alpha uu_x + \beta u_{xxx} = 0, \quad (4.3)$$

where α is the nonlinear parameter and β is the dispersion parameter, was used as the second model equation. The analytical solution for the KdV equation has been found in the form

$$u_e(x, t) = \frac{3c}{\alpha} \operatorname{sech}^2 \left[\frac{1}{2} \sqrt{\frac{c}{\beta}} (x - ct - x_0) \right], \quad (4.4)$$

where c is the phase speed of the travelling soliton and x_0 denotes the initial phase [68].

The sine–Gordon equation, the third model equation,

$$u_{tt} - u_{xx} + \sin u = 0 \quad (4.5)$$

has been shown to have an analytical solution in the form

$$u_e(x, t) = 4\arctan \left[\exp \left(\frac{x - ct - x_0}{\sqrt{1 - c^2}} \right) \right], \quad (4.6)$$

where c is the speed at which the phase of the travelling wave propagates and x_0 denotes the initial phase [52].

Finally, the mKdV equation

$$u_t + 6\alpha u^2 u_x + \beta u_{xxx} = 0, \quad (4.7)$$

where α is the nonlinear coefficient and β is the dispersion coefficient, was used as the fourth model equation. The analytical solution for the mKdV equation has been found in the form

$$u_e(x, t) = \sqrt{\frac{c}{\alpha\beta}} \operatorname{sech} \left[\sqrt{\frac{c}{\beta}} (x - ct - x_0) \right], \quad (4.8)$$

where x_0 denotes the initial phase and c is the phase speed of the travelling wave [42, 1, 86, 83].

5 The Higher order Haar wavelet method

This section will give an overview of how the HOHWM is applied for spatial integration in case of each specific model equation within this paper. Firstly, the general steps are described and then the results specific to each model equation are provided.

With the HOHWM, according to [64], the derivative of $n + 2s$ order, where n is the maximal spatial derivative present within the equation, is expanded into the Haar series for a fixed time moment t_j . Thus,

$$u_{(n+2s)x}(x, t_j) = \mathbf{a} \cdot \mathbf{H} \quad (5.1)$$

is obtained. In order to obtain the function u , equation (5.1) is integrated $n + 2s$ times to obtain

$$u(x, t_j) = \mathbf{a} \cdot \mathbf{P}_{n+2s} + \sum_{i=0}^{n+2s-1} c_i \frac{\mathbf{x}^i}{i!}, \quad (5.2)$$

where c_i are unknown coefficients. In equation (5.2), \mathbf{x}^i denotes an element wise power of the vector \mathbf{x} . Since the equation has n spatial derivatives, these provide n conditions that can be evaluated in order to solve for the unknown coefficients c_i . However, $2s$ additional coefficients are introduced by the HOHWM

(in comparison to the HWM) which must be obtained using some supplementary information.

In the present paper $s = 1$ is used. This gives

$$u_{(n+2)x}(x, t_j) = \mathbf{a} \cdot \mathbf{H}. \quad (5.3)$$

Integrating $n + 2$ times yields

$$u(x, t_j) = \mathbf{a} \cdot \mathbf{P}_{n+2} + \sum_{i=0}^{n+1} c_i \frac{\mathbf{x}^i}{i!}. \quad (5.4)$$

Using the n boundary conditions as well as evaluating the differential equation at its boundaries (A and B) one obtains the $n + 2$ equations needed to solve for the $n + 2$ unknown coefficients c_i . Some of these coefficients can depend on the Haar wavelet coefficients vector \mathbf{a} . After solving for the unknown coefficients and inserting the results into expression (5.4) one obtains the result in the form of

$$u(x, t_j) = \mathbf{a} \cdot \mathbf{R}_{n+2} + \mathbf{S}_{n+2}, \quad (5.5)$$

where \mathbf{R}_{n+2} and \mathbf{S}_{n+2} are matrices which only depend on the boundary conditions and the grid. Thus the values for these can be calculated right after the grid has been specified.

5.1 The Burgers' equation

For the given homogeneous boundary conditions

$$u(0, t) = 0, \quad u(1, t) = 0, \quad (5.6)$$

the equation (4.1) is evaluated at the boundary points as

$$\begin{aligned} u_t(0, t) + u(0, t)u_x(0, t) - \nu u_{xx}(0, t) &= 0, \\ u_t(1, t) + u(1, t)u_x(1, t) - \nu u_{xx}(1, t) &= 0. \end{aligned} \quad (5.7)$$

Since the boundary conditions (5.6) are homogeneous $u_t(0, t) = u_t(1, t) = 0$ and (5.7) simplifies to

$$u_{xx}(0, t) = 0 \quad u_{xx}(1, t) = 0. \quad (5.8)$$

The addition of (5.8) gives

$$\begin{aligned} \mathbf{R}_4 &= \mathbf{P}_4 - \mathbf{P}_4(1) \cdot \mathbf{x} + \mathbf{P}_2(1) \cdot \frac{\mathbf{x} - \mathbf{x}^3}{6}, \\ \mathbf{S}_4 &= 0 \end{aligned} \quad (5.9)$$

The initial condition was taken from the exact solution (4.2). It can be shown that at $t = 0$ the solution simplifies to

$$u(x, 0) = u_0 \sin\left(\frac{\pi x}{L}\right), \quad (5.10)$$

which is used as the initial condition. Within the context of this paper $u_0 = 1$ is used.

5.2 The KdV equation

For the given homogeneous boundary conditions

$$u(0, t) = u(1, t) = u_x(1, t) = 0, \quad (5.11)$$

the equation (4.3) is evaluated at the boundary points as

$$\begin{aligned} u_t(0, t) + \alpha u(0, t)u_x(0, t) + u_{xxx}(0, t) &= 0, \\ u_t(1, t) + \alpha u(1, t)u_x(1, t) + u_{xxx}(1, t) &= 0. \end{aligned} \quad (5.12)$$

Since the boundary conditions (5.11) are homogeneous $u_t(0, t) = u_t(1, t) = 0$ and the above simplifies to

$$u_{xxx}(0, t) = 0, \quad u_{xxx}(1, t) = 0. \quad (5.13)$$

The addition of (5.13) gives

$$\begin{aligned} \mathbf{R}_5 &= \mathbf{P}_5 + \frac{1}{2}\mathbf{P}_3(1) \cdot (-\mathbf{x}^4 + 2\mathbf{x}^3 - \mathbf{x}^2) + \frac{1}{2}\mathbf{P}_4(1) \cdot (4\mathbf{x}^4 - 10\mathbf{x}^3 + 6\mathbf{x}^2) \\ &\quad + \frac{1}{2}\mathbf{P}_x(1) \cdot (-6\mathbf{x}^4 + 16\mathbf{x}^3 - 12\mathbf{x}^2), \\ \mathbf{S}_5 &= 0. \end{aligned} \quad (5.14)$$

The initial condition was taken from the exact solution (4.4) at $t = 0$. This gives

$$u(x, 0) = \frac{3c}{\alpha} \operatorname{sech}^2 \left[\frac{1}{2} \sqrt{\frac{c}{\beta}} (x - x_0) \right], \quad (5.15)$$

which is used as the initial condition with specified values for c , x_0 as well as for α and β .

5.3 The sine-Gordon equation

For given constant boundary conditions

$$u(0, t) = 0, \quad u(1, t) = \pi \quad (5.16)$$

the equation (4.5) is evaluated at the boundary points as

$$u_t(0, t) - u_{xx}(0, t) + \sin u(0, t) = 0, \quad u_t(1, t) - u_{xx}(1, t) + \sin u(1, t) = 0. \quad (5.17)$$

Since the boundary conditions (5.16) are constant $u_t(0, t) = u_t(1, t) = 0$ and the above simplifies to

$$u_{xx}(0, t) = 0, \quad u_{xx}(1, t) = 0. \quad (5.18)$$

The addition of (5.18) gives

$$\begin{aligned} \mathbf{R}_4 &= \mathbf{P}_4 - \mathbf{P}_4(1) + \mathbf{P}_2(1) \frac{\mathbf{x} - \mathbf{x}^3}{6} \\ \mathbf{S}_4 &= 2\pi\mathbf{x}. \end{aligned} \quad (5.19)$$

The initial condition was taken from the exact solution (4.6). It is evaluated at $t = 0$ to give

$$u(x, 0) = 4\arctan \left[\exp \left(\frac{x - x_0}{\sqrt{1 - c^2}} \right) \right], \quad (5.20)$$

which is used as the initial condition with specified value of phase speed c .

5.4 The mKdV equation

Given homogeneous boundary conditions

$$u(0, t) = u(1, t) = u_x(1, t) = 0, \quad (5.21)$$

the equation (4.7) is evaluated at the boundary points as

$$\begin{aligned} u_t(0, t) + 6\alpha [u(0, t)]^2 u_x(0, t) + u_{xxx}(0, t) &= 0, \\ u_t(1, t) + 6\alpha [u(1, t)]^2 u_x(1, t) + u_{xxx}(1, t) &= 0. \end{aligned} \quad (5.22)$$

Since the boundary conditions (5.21) are homogeneous $u_t(0, t) = u_t(1, t) = 0$ and the above simplifies to

$$u_{xxx}(0, t) = 0, \quad u_{xxx}(1, t) = 0. \quad (5.23)$$

The addition of (5.23) gives

$$\begin{aligned} \mathbf{R}_5 &= \mathbf{P}_5 + \mathbf{P}_5(1) (\mathbf{x}^2 - 2\mathbf{x}) + \mathbf{P}_4(1) (\mathbf{x} - \mathbf{x}^2) + \mathbf{P}_2(1) \frac{3\mathbf{x}^2 - 2\mathbf{x} - \mathbf{x}^4}{24} \\ \mathbf{S}_5 &= 0. \end{aligned} \quad (5.24)$$

The initial condition was taken from the exact solution (4.8) at $t = 0$. This gives

$$u(x, 0) = \sqrt{\frac{c}{\alpha\beta}} \operatorname{sech} \left[\sqrt{\frac{c}{\beta}} (x - x_0) \right], \quad (5.25)$$

which is used as the initial condition with specified values for coefficients c , x_0 as well as parameters α and β .

6 Analysis of numerical results

6.1 Optimal values for parameters d and δ

Given the adaptive grid described by (2.5) it becomes evident that the accuracy of the method depends the values of parameters d , e and δ . In order to find out which values for the parameters to use for each model equation, a series of calculations were conducted using numerous different combinations of values for the parameters d , e and δ . Within this subsection, only results in the case of the sine–Gordon equation at $J = 4$ are described in detail. Only the parameter intervals for which the best results are obtained are shown for the other model equations. The maximal deviation from the exact solution

$$\Delta u = \max_{x,t} |u(x, t) - u_e(x, t)| \quad (6.1)$$

was used as a measure of success for a given set of parameters. The sine–Gordon equation at different resolutions as well as the other model equations were handled in a similar manner and the detailed results are omitted for conciseness sake.

The sine–Gordon equation (4.5) was numerically solved at $J = 4$ with parameter values varying from $d = 0.1, 0.11, \dots, 0.85$, $e = 0.05, 0.1, 0.2, 0.3, 0.4, 0.5$ and $0.001 < \delta < 0.05$. The maximum deviation from the exact solution (4.6) was calculated and compared between the various numerical experiments. Such numerical results are shown in Fig. 2.

Figure 2 demonstrates that the optimal values are located in the region where $\delta < 0.02$ and $0.15 < d < 0.4$ for all considered values of parameter e . According to the detailed analysis the best results were obtained for $d = 0.33$, $e = 0.3$ and $\delta = 0.008$. With those parameter values the maximum deviation from the exact solution was $\Delta u = 0.033198$. This makes the relative deviation 0.53%. The highest deviation from the exact solution was found on the wavefront of the solution (near $x - ct - x_0 = 0$). The parameter values between which the best results were obtained for the KdV, the sine–Gordon and the mKdV equations are shown in Table 1.

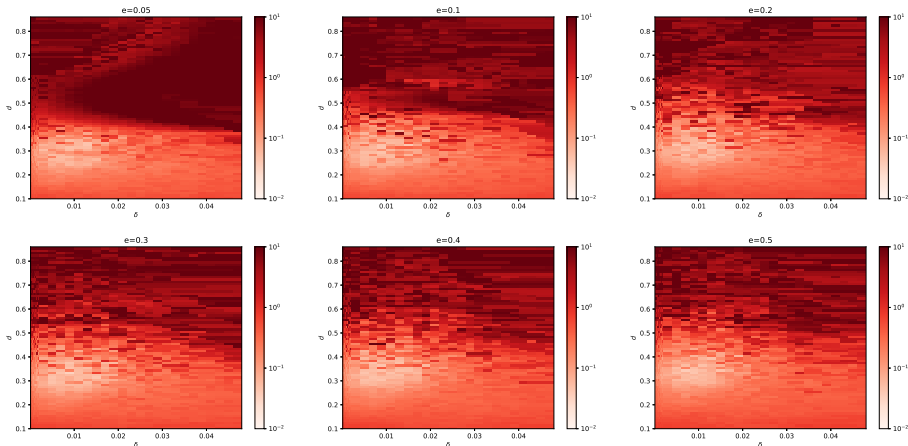


Figure 2. Maximum deviation from exact solution of the sine–Gordon equation with $c = 1 - 5 \cdot 10^{-5}$ at $J = 4$ using the adaptive grid (2.5) for various grid parameters

Table 1. Adaptive grid (2.5) parameter values that resulted in the best results for the various model equations at different resolutions

Equation	$J = 4$			$J = 5$			$J = 6$		
	d range min	d range max	δ range max	d range min	d range max	δ range max	d range min	d range max	δ range max
KdV	0.3	0.5	0.01	0.3	0.4	0.01	0.3	0.5	0.005
sine–Gordon	0.15	0.4	0.02	0.3	0.4	0.02	0.3	0.4	0.025
mKdV	0.3	0.4	0.01	0.45	0.55	0.005	0.3	0.4	0.02

Table 2. Values of t_f against the resolution J in the case of the Burgers' equation with $\nu = \frac{1}{100\pi}, \nu = \frac{1}{110\pi}, \frac{1}{120\pi}$; parameter q characterises the nonuniformity of the grid

ν		$\frac{1}{100\pi}$		$\frac{1}{110\pi}$		$\frac{1}{120\pi}$	
J	q	Uniform t_f	Nonuniform t_f	Uniform t_f	Nonuniform t_f	Uniform t_f	Nonuniform t_f
3	0.71	0.2375	0.39	0.1625	0.38	0.1625	0.38
4	0.85	0.2875	0.50	0.275	0.50	0.225	0.50
5	0.92	0.2875	0.50	0.3181	0.50	0.30	0.50
6	0.97	0.3580	0.50	0.3542	0.50	0.3745	0.50
7	0.99	0.50	0.50	0.4646	0.50	0.4143	0.50
8	*	0.50	*	0.50	*	0.50	*

Table 3. Maximal deviation from the exact solution Δu against the resolution J in the case of the Burgers' equation with $\nu = \frac{1}{100\pi}, \frac{1}{110\pi}, \frac{1}{120\pi}$

ν			$\frac{1}{100\pi}$		$\frac{1}{110\pi}$	
J	N	q	Uniform Δu	Nonuniform Δu	Uniform Δu	Nonuniform Δu
3	16	0.71	—	0.004674	—	0.0066496
4	32	0.85	—	$1.1031 \cdot 10^{-4}$	—	$1.1622 \cdot 10^{-4}$
5	64	0.92	—	$7.0345 \cdot 10^{-6}$	—	$7.3215 \cdot 10^{-6}$
6	128	0.97	0.0418	$5.1019 \cdot 10^{-6}$	0.0875	$5.1855 \cdot 10^{-6}$
7	256	0.99	$6.8360 \cdot 10^{-4}$	$4.0604 \cdot 10^{-6}$	0.001034	$4.8919 \cdot 10^{-6}$
8	512	*	$5.0941 \cdot 10^{-5}$	*	$8.0159 \cdot 10^{-5}$	*

ν			$\frac{1}{120\pi}$	
J	N	q	Uniform Δu	Nonuniform Δu
3	16	0.71	—	0.005067
4	32	0.85	—	$1.3072 \cdot 10^{-4}$
5	64	0.92	—	$7.974 \cdot 10^{-6}$
6	128	0.97	0.2021	$3.8774 \cdot 10^{-6}$
7	256	0.99	0.001611	$5.9934 \cdot 10^{-6}$
8	512	*	$1.0959 \cdot 10^{-4}$	*

6.2 Discussion of numerical results

The Burgers' equation (4.1) was numerically solved for various values of parameter ν at various resolutions J . The numerical solutions were compared to the exact solution (4.2). The nonuniform grid (2.3) was used for this problem since the solution is known for creating a steep decline near its boundary $x = 1$. The time moment $t_f = \max(0.5, t_c)$ was determined by obtaining the value of critical time moment t_c which is the maximal time t for which $\max_{x, t < t_c} |u(x, t) - u_e(x, t)| < 10^{-3}$. These numerical results were compared with the uniform grid results previously published in [77]. Such numerical results are shown in Table 2. As the resolutions J increases, the value of the nonuniformity parameter q at which the best results were obtained approaches

Table 4. Maximal deviation from the exact solution Δu against resolution J in the case of the KdV equation with $\alpha = 6$, $\beta = 4 \cdot 10^{-4}$ and $x_0 = 0.3$, $c = 2$, $t_f = 0.2$

J	Uniform grid	Grid (2.4) with $\gamma = 0.1$	Adaptive grid (2.5)			
	Δu	Δu	Δu	d	e	δ
4	—	—	$6.1679 \cdot 10^{-4}$	0.41	0.1	0.004
5	0.01123	0.001352	$1.5731 \cdot 10^{-5}$	0.33	0.05	0.002
6	0.002541	0.001143	$1.5085 \cdot 10^{-6}$	0.4	0.1	0.002
7	$1.704 \cdot 10^{-4}$	$7.694 \cdot 10^{-5}$	$1.2250 \cdot 10^{-5}$	0.3	0.3	0.006

1. This is because otherwise there would be too many grid points gathered near the boundary of the domain which leads to numerically singular matrices because the grid points or the respective Haar wavelet function values are numerically equal. It is clear that for $J > 6$ the advantages of a nonuniform grid vanish simply because of the abundance of collocation points. In fact, none of the nonuniform grids used outperformed the uniform grid in this case, which is why such results are not included in Table 2. Such cases are marked with * in the table as well as subsequent tables.

The maximal deviations from the exact solution Δu in case of the Burgers' equation are shown in Table 3 where $N = 2M$ denotes the number of collocation points. It must be noted that for $J < 6$ the HOHWM using the uniform grid was unable to successfully calculate the numerical result up to the final time of $t_f = 0.5$. However, even at $J = 6$ the nonuniform grid approach easily outperforms the uniform grid version of the HOHWM. The table also shows that for resolution $J > 4$ the accuracy no longer increases significantly in the case of the nonuniform grid.

The KdV equation (4.3) was solved at various resolutions J and the numerical results were compared to the exact solution (4.4). The uniform grid results from [77] were used and new results with the nonuniform grid (2.4) and the adaptive grid (2.5) were calculated. The numerical result itself was used as the basis for the weight function in the adaptive grid for this model equation. The maximal deviation from the exact solution for the numerical experiments are shown in Table 4. It must be noted that the values of d , e and δ for which the best numerical accuracy was obtained vary from resolution to resolution.

When dealing with the sine-Gordon equation (4.5), the uniform grid, nonuniform grid (2.4) as well as the adaptive grid (2.5) were used. In this case, the first spatial derivative was used as the basis for the weight function. The numerical results were compared to the exact solution (4.6). The maximal deviation from the exact solution Δu for the different grids can be seen in Table 5.

Finally, the mKdV equation (4.7) was numerically solved using the uniform grid, the nonuniform grid (2.4) as well as the adaptive grid (2.5). The numerical result itself was used for the weight function in the adaptive grid for this equation. The obtained numerical results were compared to the exact solution (4.8). The maximal deviation from the exact solution Δu for the different grids at different resolutions can be seen in Table 6.

Tables 2–6 show that the nonuniform grid always outperformed the uniform grid version of the HOHWM. This is especially clear given that in some cases

Table 5. Maximal deviation from the exact solution Δu against resolution J in the case of the sine-Gordon equation with $c = 1 - 5 \cdot 10^{-5}$ and $x_0 = 0.3$, $t_f = \frac{1-2x_0}{c}$

J	N	Uniform grid	Grid (2.4) with $\gamma = 0.1$	Adaptive grid (2.5)			
		Δu	Δu	Δu	d	e	δ
4	32	1.189817	1.095051	0.033198	0.33	0.3	0.008
5	64	0.4856858	0.3261581	0.0018608	0.32	0.2	0.018
6	128	0.1039031	0.06173826	$1.0331 \cdot 10^{-4}$	0.3	0.2	0.018
7	256	0.01376712	0.006484227	$1.1429 \cdot 10^{-5}$	0.3	0.2	0.024

Table 6. Maximal deviation from the exact solution Δu against resolution J in the case of the mKdV equation with $\alpha = 1$, $\beta = 10^{-2}$, $c = 16$ and $x_0 = 0.3$, $t_f = 1/40$

J	N	Uniform grid	Grid (2.4) with $\gamma = 0.1$	Adaptive grid (2.5)			
		Δu	Δu	Δu	d	e	δ
4	32	—	—	0.009246	0.44	0.2	0.004
5	64	0.0719508	0.070632	$1.86 \cdot 10^{-4}$	0.48	0.1	0.002
6	128	0.0117955	0.0052081	$6.1 \cdot 10^{-5}$	0.31	0.2	0.002
7	256	$8.4875 \cdot 10^{-4}$	—	$7.84 \cdot 10^{-4}$	0.3	0.2	0.048

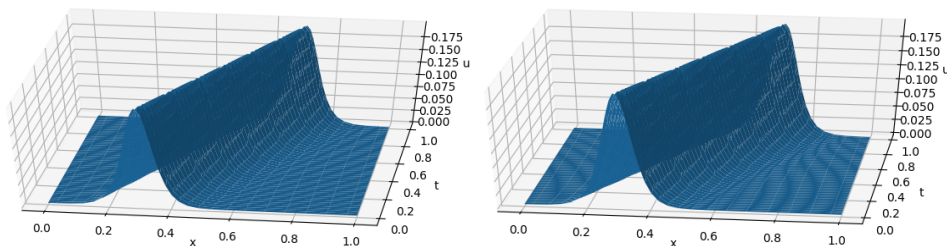


Figure 3. Example of how the adaptive grid changes with the changes in the waveform in case of the KdV equation: calculated solution (left) and exact solution (right)

the uniform and static nonuniform grid approaches in Tables 4 and 6 are unable to successfully finish the integration. Furthermore, Tables 4–6 show that the adaptive grid outperforms the static nonuniform grid as well. It is clear from Tables 2 and 3 that the same (or even better) accuracy obtained with the uniform at 256 or 512 grid points is achieved with only 32 grid points by employing the nonuniform grid (2.3). Similarly, Tables 4–6 clearly show that the same (or even better) accuracy obtained with the uniform grid at 256 grid points can be achieved with only 64 grid point by employing the adaptive grid (2.5). It must be noted that as can be seen from Table 6, a higher resolution J does not always guarantee a numerical result of higher accuracy. This is the case because the matrices involved get closer to being singular matrices as the resolution increases and solving a linear system with a near-singular matrix introduces inaccuracies.

Table 7: CPU times (in seconds) in case of numerical solutions of the Burgers' equation for cases in Table 2

J	$\nu = \frac{1}{100\pi}$				$\nu = \frac{1}{110\pi}$				$\nu = \frac{1}{120\pi}$			
	Uniform		Nonuniform		Uniform		Nonuniform		Uniform		Nonuniform	
	Δu	Time	Δu	Time	Δu	Time	Δu	Time	Δu	Time	Δu	Time
3	—	1.584	0.004674	0.0299	—	1.518	0.0066496	0.0296	—	1.540	0.005067	0.0351
4	—	5.209	$1.10 \cdot 10^{-4}$	0.217	—	5.360	$1.16 \cdot 10^{-4}$	0.231	—	5.301	$1.31 \cdot 10^{-4}$	0.369
5	—	25.78	$7.03 \cdot 10^{-6}$	1.347	—	23.95	$7.32 \cdot 10^{-6}$	1.458	—	26.31	$7.97 \cdot 10^{-6}$	1.668
6	0.0418	4.736	$5.10 \cdot 10^{-6}$	18.26	0.0875	5.430	$5.19 \cdot 10^{-6}$	13.64	0.202	4.679	$3.88 \cdot 10^{-6}$	17.31
7	$6.84 \cdot 10^{-4}$	93.09	$4.06 \cdot 10^{-6}$	95.08	0.00103	56.20	$4.89 \cdot 10^{-6}$	103.6	0.00161	97.12	$5.99 \cdot 10^{-6}$	109.5

Table 8: CPU times (in seconds) in case of numerical solutions of the KdV, sine-Gordon and mKdV equations for cases in Tables 4–6

J	KdV				sine-Gordon				mKdV			
	Uniform		Adaptive		Uniform		Adaptive		Uniform		Adaptive	
	Δu	Time	Δu	Time	Δu	Time	Δu	Time	Δu	Time	Δu	Time
4	—	—	$6.17 \cdot 10^{-4}$	9.410	1.1898	0.687	0.0332	5.6633	—	—	0.009246	17.14
5	0.01123	6.230	$1.57 \cdot 10^{-4}$	48.78	0.4857	2.895	0.00186	10.20	0.0720	9.682	$1.86 \cdot 10^{-4}$	64.42
6	0.002541	37.84	$1.51 \cdot 10^{-4}$	142.3	0.1039	18.99	$1.03 \cdot 10^{-4}$	13.42	0.0118	87.32	$6.1 \cdot 10^{-5}$	464.8
7	$1.704 \cdot 10^{-4}$	566.2	$1.23 \cdot 10^{-4}$	15478	0.01377	55.74	$1.14 \cdot 10^{-5}$	234.6	$8.49 \cdot 10^{-4}$	470.2	$7.84 \cdot 10^{-4}$	19201

It is clear that the usage of the nonuniform as well as the adaptive grid will also have an impact on the computational time. The computational times of the nonuniform grid approach is compared to the uniform grid approach in case of the Burgers' equation in Table 7. In Table 7 for $J = 8$ only the uniform grid approach is considered since a nonuniform approach was not observed to give a better result. Similar comparison is made for the other model equations in Table 8. Tables 7–8 show that a result of similar or better accuracy is able to be obtained with less CPU time using the adaptive grid approach when compared to the uniform grid approach.

An example of how the grid adapts to the moving wave can be seen in Figure 3. The figure shows that as the wave moves, the grid adapts to its position.

7 Conclusions

A nonuniform grid approach was developed and used alongside the HOHWM in order to account for abrupt changes within the solution. Firstly, two static nonuniform grids were introduced. For either of those grids, a prior knowledge of the shape of the solution is required in order to show significant improvement in accuracy. However, in a lot of cases it is impossible to know the shape of the solution before the start of the calculations. Thus, an adaptive nonuniform grid was proposed. It changes the grid adaptively so that the areas with the most abrupt changes always have the most grid points.

The numerical results (Tables 2–3) showed that in case of the Burgers' equation a significant gain in accuracy can be obtained by the use of a static nonuniform grid when compared to the uniform grid HOHWM. In fact, the same level of accuracy was obtained with the nonuniform grid given 8–16 times fewer grid points.

The adaptive grid (Tables 4–6) also showed a significant gain in accuracy when compared to both the uniform grid approach as well as the static nonuniform grid approach. The same level of accuracy was obtained using 8 times fewer grid points than were needed for the uniform grid approach.

The most computationally expensive part of the numerical calculation is solving the linear system of equations. Therefore, the ability to obtain results with the same accuracy with considerably fewer grid points is quite an advantage. Instead of solving a 256×256 linear system one can solve a 32×32 linear system.

The use of a nonuniform or an adaptive grid alongside the HOHWM have shown to give significant advantages. However, further studies need to be carried out in order to find an optimal way of obtaining the necessary parameters for the adaptive grid. Herein constant boundary conditions were utilized. However, time dependent boundary conditions can be handled similarly to cases where differential equations include time dependent function as coefficients or right-hand side terms (similarly to handling of graded materials in [64]). This is a promising subject for future studies.

Acknowledgements

This research was supported by the Estonian Research Council grants IUT 33-24 and Estonian Centre of Excellence in Zero Energy and Resource Efficient Smart Buildings and Districts, ZEBE, TK146 funded by the European Regional Development Fund (grant 2014-2020.4.01.15-0016).

References

- [1]M. J. Ablowitz and H. Segur. *Solitons and the inverse scattering transform*. SIAM, 1981. <http://dx.doi.org/10.1137/1.9781611970883>.
- [2]E. N. Aksan. A numerical solution of Burgers equation by finite element method constructed on the method of discretization in time. *Appl. Math. Comput.*, **170**(2):895–904, 2005. <http://dx.doi.org/10.1016/j.amc.2004.12.027>.
- [3]S. Amat and M. Moncayo. Non-uniform multiresolution analysis with supercompact multiwavelets. *J. Comput. Appl. Math.*, **235**(1):334–340, 2010. <http://dx.doi.org/10.1016/j.cam.2010.05.013>.
- [4]I. Aziz, A. S. Al-Fhaid and A. S. Al-Fhaid. An improved method based on Haar wavelets for numerical solution of nonlinear integral and integro-differential equations of first and higher orders. *J. Comput. Appl. Math.*, **260**:449–469, 2014. <http://dx.doi.org/10.1016/j.cam.2013.10.024>.
- [5]I. Aziz and Siraj-ul-Islam. New algorithms for the numerical solution of nonlinear Fredholm and Volterra integral equations using Haar wavelets. *J. Comput. Appl. Math.*, **239**:333–345, 2013. <http://dx.doi.org/10.1016/j.cam.2012.08.031>.
- [6]I. Aziz, Siraj-ul-Islam and F. Khan. A new method based on Haar wavelet for the numerical solution of two-dimensional nonlinear integral equations. *J. Comput. Appl. Math.*, **272**:70–80, 2014. <http://dx.doi.org/10.1016/j.cam.2014.04.027>.
- [7]E. Babolian and A. Shamsavaran. Numerical solution of nonlinear Fredholm integral equations of the second kind using Haar wavelets. *J. Comput. Appl. Math.*, **225**(1):87–95, 2009. <http://dx.doi.org/10.1016/j.cam.2008.07.003>.
- [8]C. Basdevant, M. Deville, P. Haldenwang, J. M. Lacroix, J. Ouazzani, R. Peyret, P. Orlandi and A. T. Patera. Spectral and finite difference solutions of the Burgers equation. *Comput. & Fluids*, **14**(1):23–41, 1986. [http://dx.doi.org/10.1016/0045-7930\(86\)90036-8](http://dx.doi.org/10.1016/0045-7930(86)90036-8).
- [9]F. Bashforth and J. C. Adams. *An attempt to test the theories of capillary action: by comparing the theoretical and measured forms of drops of fluid*. Cambridge University Press, 1883.
- [10]E. R. Benton and G. W. Platzman. A table of solutions of the one-dimensional Burgers equation. *Quart. Appl. Math.*, **30**(2):195–212, 1972. <http://dx.doi.org/10.1090/qam/306736>.
- [11]M. J. Berger. Adaptive mesh refinement for hyperbolic partial differential equations. *J. Comput. Phys.*, **53**:484–512, 1982. [http://dx.doi.org/10.1016/0021-9991\(84\)90073-1](http://dx.doi.org/10.1016/0021-9991(84)90073-1).
- [12]S. Bertoluzza. An adaptive collocation method based on interpolating wavelets. In W. Dahmen, A. J. Kurdila and P. Oswald(Eds.), *Wavelet Analysis and Its Applications*, volume 6, pp. 109–135. Elsevier, 1997. [http://dx.doi.org/10.1016/s1874-608x\(97\)80005-2](http://dx.doi.org/10.1016/s1874-608x(97)80005-2).

- [13]G. Beylkin and J. M. Keiser. An adaptive pseudo-wavelet approach for solving nonlinear partial differential equations. In W. Dahmen, A. J. Kurdila and P. Oswald(Eds.), *Wavelet Analysis and Its Applications*, volume 6, pp. 137–197. Elsevier, 1997. [http://dx.doi.org/10.1016/s1874-608x\(97\)80006-4](http://dx.doi.org/10.1016/s1874-608x(97)80006-4).
- [14]E. Bour. *Théorie de la déformation des surfaces*. 1862. Available from Internet: <https://books.google.ee/books?id=HK4qvwEACAAJ>.
- [15]P. Bowcock, E. Corrigan and C. Zambon. Some aspects of jump-defects in the quantum sine-Gordon model. *J. High Energy Phys.*, **2005**(08):023, 2005. <http://dx.doi.org/10.1088/1126-6708/2005/08/023>.
- [16]C. J. Budd, W. Huang and R. D. Russell. Adaptivity with moving grids. *Acta Numerica*, **18**:111–241, 2009. <http://dx.doi.org/10.1017/s0962492906400015>.
- [17]F. Bulut, Ö. Oruç and A. Esen. Numerical solutions of fractional system of partial differential equations by Haar wavelets. *Comput. Model. Eng. Sci.*, **108**(4):263–284, 2015.
- [18]J. M. Burgers. A mathematical model illustrating the theory of turbulence. In R. v. Mises and T. v. Kármán(Eds.), *Advances in Applied Mechanics*, volume 1, pp. 171–199. Academic Press, 1948. [http://dx.doi.org/10.1016/S0065-2156\(08\)70100-5](http://dx.doi.org/10.1016/S0065-2156(08)70100-5).
- [19]J. M. Burgers. Statistical problems connected with the solution of a nonlinear partial differential equation. In W. F. Ames(Ed.), *Nonlinear Problems of Engineering*, pp. 123–137. Academic Press, 1964. <http://dx.doi.org/10.1016/B978-1-4832-0078-1.50015-8>.
- [20]L. M. S. Castro, A. J. M. Ferreira, S. Bertoluzza, R. C. Batra and J. N. Reddy. A wavelet collocation method for the static analysis of sandwich plates using a layerwise theory. *Composite Structures*, **92**(8):1786–1792, 2010. <http://dx.doi.org/10.1016/j.compstruct.2010.01.021>.
- [21]C. Cattani. Haar wavelet-based technique for sharp jumps classification. *Math. Comput. Modelling*, **39**(2-3):255–278, 2004. [http://dx.doi.org/10.1016/s0895-7177\(04\)90010-6](http://dx.doi.org/10.1016/s0895-7177(04)90010-6).
- [22]C. Cattani. Haar wavelets based technique in evolution problems. *Proc. Estonian Acad. Sci.*, **53**(1):45–63, 2004.
- [23]C. Cattani. On the existence of wavelet symmetries in archaea DNA. *Comput. Math. Methods Med.*, **2012**, 2012. <http://dx.doi.org/10.1155/2012/673934>.
- [24]C. Cattani and A. Kudreyko. Harmonic wavelet method towards solution of the Fredholm type integral equations of the second kind. *Appl. Math. Comput.*, **215**(12):4164–4171, 2010. <http://dx.doi.org/10.1016/j.amc.2009.12.037>.
- [25]C. Cattani and Y. Y. Rushchitskii. Cubically nonlinear versus quadratically nonlinear elastic waves: Main wave effects. *Internat. Appl. Mech.*, **39**(12):1361–1399, 2003. <http://dx.doi.org/10.1023/b:inam.0000020823.49759.c9>.
- [26]C. Cattani, J. J. Rushchitsky and S. V. Sinchilo. Physical constants for one type of nonlinearly elastic fibrous micro-and nanocomposites with hard and soft nonlinearities. *Internat. Appl. Mech.*, **41**(12):1368–1377, 2005. <http://dx.doi.org/10.1007/s10778-006-0044-9>.
- [27]C. F. Chen and C. H. Hsiao. Haar wavelet method for solving lumped and distributed-parameter systems. *IEE Proc. Control Theory Appl.*, **144**(1):87–94, 1997. <http://dx.doi.org/10.1049/ip-cta:19970702>.

- [28]J. D. Cole. On a quasi-linear parabolic equation occurring in aerodynamics. *Quart. Appl. Math.*, **9**(3):225–236, 1951. <http://dx.doi.org/10.1090/qam/42889>.
- [29]C. F. Curtiss and J. O. Hirschfelder. Integration of stiff equations. *Proc. Natl. Acad. Sci. USA*, **38**(3):235, 1952. <http://dx.doi.org/10.1073/pnas.38.3.235>.
- [30]P. G. Drazin and R. S. Johnson. *Solitons: an introduction*. Cambridge University Press, 1989. <http://dx.doi.org/10.1017/CBO9781139172059>.
- [31]F. Dubeau, S. Elmejdani and R. Ksantini. Non-uniform Haar wavelets. *Appl. Math. Comput.*, **159**(3):675–693, 2004. <http://dx.doi.org/10.1016/j.amc.2003.09.021>.
- [32]P. R. Eiseman. Adaptive grid generation. *Comput. Methods Appl. Mech. Engrg.*, **64**(1-3):321–376, 1987. [http://dx.doi.org/10.1016/0045-7825\(87\)90046-6](http://dx.doi.org/10.1016/0045-7825(87)90046-6).
- [33]Fazal-i-Haq, Siraj-ul-Islam and I. Aziz. Numerical solution of singularly perturbed two-point BVPs using nonuniform Haar wavelets. *Int. J. Comput. Methods Eng. Sci. Mech.*, **12**(4):168–175, 2011. <http://dx.doi.org/10.1080/15502287.2011.580828>.
- [34]F. C. Frank and J. H. van der Merwe. One-dimensional dislocations. I. Static theory. *Proc. R. Soc. Lond. Ser. A Math. Phys. Eng. Sci.*, **198**(1053):205–216, 1949. <http://dx.doi.org/10.1098/rspa.1949.0095>.
- [35]J. Frenkel and T. Kontorova. On the theory of plastic deformation and twinning. *Izv. Akad. Nauk, Ser. Fiz.*, **1**:137–149, 1939.
- [36]B. Fryxell, K. Olson, P. Ricker, F. X. Timmes, M. Zingale, D. Q. Lamb, P. MacNeice, R. Rosner, J. W. Truran and H. Tufo. Flash: An adaptive mesh hydrodynamics code for modeling astrophysical thermonuclear flashes. *The Astrophysical Journal Supplement Series*, **131**(1):273–334, 2000. <http://dx.doi.org/10.1086/317361>.
- [37]C. W. Gear. *Numerical initial value problems in ordinary differential equations*. Prentice Hall PTR, 1971.
- [38]M. F. Hamilton and D. T. Blackstock(Eds.). *Nonlinear acoustics*. Academic Press, San Diego, 1998.
- [39]G. Hariharan, K. Kannan and K. R. Sharma. Haar wavelet method for solving Fishers equation. *Appl. Math. Comput.*, **211**(2):284–292, 2009. ISSN 0096-3003. <http://dx.doi.org/10.1016/j.amc.2008.12.089>.
- [40]H. Hein and L. Feklistova. Computationally efficient delamination detection in composite beams using Haar wavelets. *Mechanical Systems and Signal Processing*, **25**(6):2257–2270, 2011. <http://dx.doi.org/10.1016/j.ymsp.2011.02.003>.
- [41]A. C. Hindmarsh. ODEPACK, a systematized collection of ODE solvers. *Scientific computing*, pp. 55–64, 1983.
- [42]R. Hirota. Exact solution of the modified Korteweg–de Vries equation for multiple collisions of solitons. *Journal of the Physical Society of Japan*, **33**(5):1456–1458, 1972. <http://dx.doi.org/10.1143/jpsj.33.1456>.
- [43]S. K. Jena and S. Chakraverty. Dynamic behavior of an electromagnetic nanobeam using the Haar wavelet method and the higher-order Haar wavelet method. *Eur. Phys. J. Plus*, **134**(10):538, 2019. <http://dx.doi.org/10.1140/epjp/i2019-12874-8>.
- [44]S. K. Jena, S. Chakraverty and M. Malikan. Implementation of Haar wavelet, higher order Haar wavelet, and differential quadrature methods on buckling response of strain gradient nonlocal beam embedded in an elastic medium. *Engineering with Computers*, pp. 1–14, 2019. <http://dx.doi.org/10.1007/s00366-019-00883-1>.

- [45]G. Jin, X. Xie and Z. Liu. The Haar wavelet method for free vibration analysis of functionally graded cylindrical shells based on the shear deformation theory. *Composite Structures*, **108**:435–448, 2014. <http://dx.doi.org/10.1016/j.compstruct.2013.09.044>.
- [46]J. E. Kim, G.-W. Jang and Y. Y. Kim. Adaptive multiscale wavelet-Galerkin analysis for plane elasticity problems and its applications to multiscale topology design optimization. *Internat. J. Solids Structures*, **40**(23):6473–6496, 2003. [http://dx.doi.org/10.1016/s0020-7683\(03\)00417-7](http://dx.doi.org/10.1016/s0020-7683(03)00417-7).
- [47]M. Kirs, M. Eerme, D. Bassir and E. Tungel. Application of HOHWM for vibration analysis of nanobeams. *Key Eng. Mater.*, **799**:230–235, 2019. <http://dx.doi.org/10.4028/www.scientific.net/kem.799.230>.
- [48]A. V. Kravtsov, A. A. Klypin and A. M. Khokhlov. Adaptive refinement tree: a new high-resolution N-body code for cosmological simulations. *The Astrophysical Journal Supplement Series*, **111**(1):73, 1997. <http://dx.doi.org/10.1086/313015>.
- [49]M. Kumar and S. Pandit. Wavelet transform and wavelet based numerical methods: an introduction. *Int. J. Nonlinear Sci.*, **13**(3):325–345, 2012.
- [50]S. Kutluay, A. R. Bahadır and A. Özdeş. Numerical solution of one-dimensional Burgers equation: explicit and exact-explicit finite difference methods. *J. Comput. Appl. Math.*, **103**(2):251–261, 1999. [http://dx.doi.org/10.1016/s0377-0427\(98\)00261-1](http://dx.doi.org/10.1016/s0377-0427(98)00261-1).
- [51]P. A. Lagerstrom, J. D. Cole and L. Trilling. Problems in the theory of viscous compressible fluids. Guggenheim Aeronautical Laboratory, unnumbered report, California Institute of Technology, 1949.
- [52]G. L. Lamb. *Elements of soliton theory*. Wiley-Interscience, 1980. <http://dx.doi.org/10.1137/1025024>.
- [53]Ü. Lepik. Haar wavelet method for nonlinear integro-differential equations. *Appl. Math. Comput.*, **176**(1):324–333, 2006. <http://dx.doi.org/10.1016/j.amc.2005.09.021>.
- [54]Ü. Lepik. Application of the Haar wavelet transform to solving integral and differential equations. *Proc. Estonian Acad. Sci.*, **56**(1):28–46, 2007.
- [55]Ü. Lepik. Numerical solution of evolution equations by the Haar wavelet method. *Appl. Math. Comput.*, **185**(1):695–704, 2007. <http://dx.doi.org/10.1016/j.amc.2006.07.077>.
- [56]Ü. Lepik. Solving integral and differential equations by the aid of non-uniform Haar wavelets. *Appl. Math. Comput.*, **198**(1):326–332, 2008. <http://dx.doi.org/10.1016/j.amc.2007.08.036>.
- [57]Ü. Lepik. Haar wavelet method for solving stiff differential equations. *Math. Model. Anal.*, **14**(4):467–481, 2009. <http://dx.doi.org/10.3846/1392-6292.2009.14.467-481>.
- [58]Ü. Lepik. Solving fractional integral equations by the Haar wavelet method. *Appl. Math. Comput.*, **214**(2):468–478, 2009. <http://dx.doi.org/j.amc.2009.04.015>.
- [59]Ü. Lepik. Solving PDEs with the aid of two-dimensional Haar wavelets. *Comput. Math. Appl.*, **61**(7):1873–1879, 2011. <http://dx.doi.org/10.1016/j.camwa.2011.02.016>.
- [60]Ü. Lepik and H. Hein. *Haar wavelets: with applications*. Springer, New York, 2014. <http://dx.doi.org/10.1007/978-3-319-04295-4>.

- [61] J. Majak, M. Pohlak and M. Eerme. Application of the Haar wavelet-based discretization technique to problems of orthotropic plates and shells. *Mech. Compos. Mater.*, **45**(6):631–642, 2009.
- [62] J. Majak, M. Pohlak, M. Eerme and T. Lepikult. Weak formulation based Haar wavelet method for solving differential equations. *Appl. Math. Comput.*, **211**(2):488–494, 2009. ISSN 0096-3003. <http://dx.doi.org/10.1016/j.amc.2009.01.089>.
- [63] J. Majak, M. Pohlak, M. Eerme and B. Shvartsman. Solving ordinary differential equations with higher order Haar wavelet method. *AIP Conference Proceedings*, **2116**(1):330002, 2019. <http://dx.doi.org/10.1063/1.5114340>.
- [64] J. Majak, M. Pohlak, K. Karjust, M. Eerme, J. Kurnitski and B. S. Shvartsman. New higher order Haar wavelet method: Application to FGM structures. *Composite Structures*, **201**:72–78, 2018. ISSN 0263-8223.
- [65] J. Majak, B. Shvartsman, M. Pohlak, K. Karjust, M. Eerme and E. Tungal. Solution of fractional order differential equation by the Haar wavelet method. Numerical convergence analysis for most commonly used approach. *AIP Conference Proceedings*, **1738**(1):480110, 2016. <http://dx.doi.org/10.1063/1.4952346>.
- [66] M. B. Mineev and V. V. Shmidt. Radiation from a vortex in a long Josephson junction placed in an alternating electromagnetic field. *Sov. Phys. JETP*, **52**(453):33, 1980.
- [67] T. Musha and H. Higuchi. Traffic current fluctuation and the Burgers equation. *Jpn. J. Appl. Phys.*, **17**(5):811–816, 1978. <http://dx.doi.org/10.1143/jjap.17.811>.
- [68] A. C. Newell. *Solitons in mathematics and physics*. SIAM, 1985. <http://dx.doi.org/10.1137/1.9781611970227>.
- [69] Ö. Oruç. A non-uniform Haar wavelet method for numerically solving two-dimensional convection-dominated equations and two-dimensional near singular elliptic equations. *Comput. Math. Appl.*, **77**(7):1799–1820, 2019. <http://dx.doi.org/10.1016/j.camwa.2018.11.018>.
- [70] Ö. Oruç, F. Bulut and A. Esen. A Haar wavelet-finite difference hybrid method for the numerical solution of the modified Burgers equation. *J. Math. Chem.*, **53**:1592–1607, 2015. <http://dx.doi.org/10.1007/s10910-015-0507-5>.
- [71] Ö. Oruç, F. Bulut and A. Esen. Numerical solution of the KdV equation by Haar wavelet method. *Pramana – J. Phys.*, **87**:94, 2016. <http://dx.doi.org/10.1007/s12043-016-1286-7>.
- [72] Ö. Oruç, F. Bulut and A. Esen. Numerical solutions of regularized long wave equation by Haar wavelet method. *Mediterr. J. Math.*, **13**:3235–3253, 2016. <http://dx.doi.org/10.1007/s00009-016-0682-z>.
- [73] Ö. Oruç, F. Bulut and A. Esen. A numerical treatment based on Haar wavelets for coupled KdV equation. *Int. J. Optim. Control*, **7**(2):195–204, 2016. <http://dx.doi.org/10.1007/s12043-016-1286-7>.
- [74] Ö. Oruç, A. Esen and F. Bulut. A Haar wavelet approximation for two-dimensional time fractional reaction–subdiffusion equation. *Engineering with Computers*, **35**:75–86, 2019. <http://dx.doi.org/10.1007/s00366-018-0584-8>.
- [75] L. Petzold. Automatic selection of methods for solving stiff and nonstiff systems of ordinary differential equations. *SIAM J. Sci. Stat. Comput.*, **4**(1):136–148, 1983. <http://dx.doi.org/10.1137/0904010>.

- [76]M. M. Rai and D. A. Anderson. Application of adaptive grids to fluid-flow problems with asymptotic solutions. *AIAA Journal*, **20**(4):496–502, 1982. <http://dx.doi.org/10.2514/3.51100>.
- [77]M. Ratas and A. Salupere. Application of higher order Haar wavelet method for solving nonlinear evolution equations. *Math. Model. Anal.*, **25**(2):271–288, 2020. <http://dx.doi.org/10.3846/mma.2020.11112>.
- [78]J. J. Rushchitsky, C. Cattani and E. V. Terletskaia. Wavelet analysis of the evolution of a solitary wave in a composite material. *Internat. Appl. Mech.*, **40**(3):311–318, 2004. <http://dx.doi.org/10.1023/b:inam.0000031914.84082.d2>.
- [79]U. Saeed and M. ur Rehman. Haar wavelet–quasilinearization technique for fractional nonlinear differential equations. *Appl. Math. Comput.*, **220**:630–648, 2013. <http://dx.doi.org/10.1016/j.amc.2013.07.018>.
- [80]M. Salerno. Discrete model for DNA-promoter dynamics. *Phys. Rev. A*, **44**(8):5292, 1991. <http://dx.doi.org/10.1103/physreva.44.5292>.
- [81]A. C. Scott, F. Y. F. Chu and D. W. McLaughlin. The soliton: A new concept in applied science. *Proceedings of the IEEE*, **61**(10):1443–1483, 1973. <http://dx.doi.org/10.1109/proc.1973.9296>.
- [82]R. Teyssier. Cosmological hydrodynamics with adaptive mesh refinement—a new high resolution code called ramses. *Astronomy & Astrophysics*, **385**(1):337–364, 2002. <http://dx.doi.org/10.1051/0004-6361:20011817>.
- [83]H. Triki, T. R. Taha and A.-M. Wazwaz. Solitary wave solutions for a generalized KdV–mKdV equation with variable coefficients. *Math. Comput. Simulation*, **80**(9):1867–1873, 2010. <http://dx.doi.org/10.1016/j.matcom.2010.02.001>.
- [84]F. Vazza, G. Brunetti, A. Kritsuk, R. Wagner, C. Gheller and M. Norman. Turbulent motions and shocks waves in galaxy clusters simulated with adaptive mesh refinement. *Astronomy & Astrophysics*, **504**(1):33–43, 2009. <http://dx.doi.org/10.1051/0004-6361/200912535>.
- [85]P. Virtanen, R. Gommers, T. E. Oliphant, M. Haberland, T. Reddy, D. Cournapeau, E. Burovski, P. Peterson, W. Weckesser, J. Bright et al. Scipy 1.0: fundamental algorithms for scientific computing in python. *Nature methods*, **17**(3):261–272, 2020. <http://dx.doi.org/10.1038/s41592-019-0686-2>.
- [86]M. Wang, X. Li and J. Zhang. The $\left(\frac{G'}{G}\right)$ -expansion method and travelling wave solutions of nonlinear evolution equations in mathematical physics. *Physics Letters A*, **372**(4):417–423, 2008. <http://dx.doi.org/10.1016/j.physleta.2007.07.051>.
- [87]S. Wang, Y. Li, Y. Shao, C. Cattani, Y. Zhang and S. Du. Detection of dendritic spines using wavelet packet entropy and fuzzy support vector machine. *NS Neurol. Disord. Drug Targets*, **16**(2):116–121, 2017. <http://dx.doi.org/10.2174/1871527315666161111123638>.
- [88]X. Xiang, J. Guoyong, L. Wanyou and L. Zhigang. A numerical solution for vibration analysis of composite laminated conical, cylindrical shell and annular plate structures. *Composite Structures*, **111**:20–30, 2014. <http://dx.doi.org/10.1016/j.compstruct.2013.12.019>.
- [89]X. Xie, G. Jin and Z. Liu. Free vibration analysis of cylindrical shells using the Haar wavelet method. *Intern. J. Mech. Sci.*, **77**:47–56, 2013. <http://dx.doi.org/10.1016/j.ijmecsci.2013.09.025>.

Appendix 4

IV

M. Ratas. Application of Haar wavelet method for solving nonlinear evolution equations. *AIP Conference Proceedings*, 2116(1):330004, 2019

Application of Haar wavelet method for solving nonlinear evolution equations

Cite as: AIP Conference Proceedings **2116**, 330004 (2019); <https://doi.org/10.1063/1.5114342>
Published Online: 24 July 2019

Mart Ratas



View Online



Export Citation

ARTICLES YOU MAY BE INTERESTED IN

[Evaluation of Haar wavelet method in engineering applications](#)

AIP Conference Proceedings **2116**, 330003 (2019); <https://doi.org/10.1063/1.5114341>

[Solving ordinary differential equations with higher order Haar wavelet method](#)

AIP Conference Proceedings **2116**, 330002 (2019); <https://doi.org/10.1063/1.5114340>

[Numerical solution of stiff ODEs using non-uniform Haar wavelets](#)

AIP Conference Proceedings **2116**, 330008 (2019); <https://doi.org/10.1063/1.5114346>

Lock-in Amplifiers
up to 600 MHz



Application of Haar Wavelet Method for Solving Nonlinear Evolution Equations

Mart Ratas^{1,a)}

¹Tallinn University of Technology, Department of Cybernetics, Laboratory of Solid Mechanics, Estonia

^{a)}Corresponding author: mart.ratas@ttu.ee

Abstract. The Haar wavelet method (HWM) is adapted for solving nonlinear evolution equations. The Burgers equation is considered as a model equation here. The 2D wavelet expansion is employed. The aim of the study is to validate HWM in the case of complex problems (solution include steep slopes). The convergence in regard to mesh has been observed in direction of both axes. The numerical results obtained are found to be in good agreement with analytical solution.

INTRODUCTION

Wavelet methods have been used to solve partial differential equations (PDE-s) since the 1990s [1, 2]. Haar wavelets, as the simplest of all wavelets, deserve attention at this point. While the piecewise constant nature of Haar wavelets means their derivatives do not exist, they can be analytically integrated arbitrarily many times [3, 4]. Thus, they are ideal for integral equations [5]. In case of differential equations, one can expand into the Haar series not the function itself but rather its highest space derivative appearing in the equation [3, 6–11]. By applying various integration algorithms, the solution of the differential equation and the derivatives can be determined and inserted in the differential equation [12–14]. As result a system of algebraic equations is obtained [4, 6, 7]. The wavelet coefficients can be determined as a solution of that algebraic system. Finally, the solution is obtained by substitution the wavelet coefficients in wavelet expansion. In case of evolution equations, the time derivative is often found using some finite difference type approximations [15–18]. Herein, the 2D Haar wavelet expansion is employed.

HAAR WAVELET METHOD APPROACH IN CASE OF BURGERS EQUATION

In the current study the nonlinear Burgers equation is considered in the following form

$$u_t + uu_x - \nu u_{xx} = 0 \quad (1)$$

in the domain $x \in [a, b]$, $t \in [0, t_f]$. The number of grid points on either axis (N_x and N_t) are taken as a power of two and the collocation points used are $x_i = (i + 1/2) \frac{b-a}{N_x} + a$ and $t_j = (j + 1/2) \frac{t_f}{N_t}$. Note, that the approach discussed, can be applied in similar manner for a wide class of PDE-s with the same order of highest derivatives.

According to the approach introduced by Chen and Hsiao the highest order derivative in the differential equation is expanded into wavelets [3]. In the case of the PDE considered one obtains

$$u_{xxt}(x, t) = H_x^T A H_t, \quad (2)$$

where A is the matrix of wavelet coefficients, H_x and H_t are the Haar wavelet matrices for x and t , respectively, as described in [3]. The dimensions of the two matrices depend on the number of grid points on either axis.

After integrating Equation (2) multiple times one arrives at

$$u(x, t) = P_{x2}^T A P_{t1} + \phi(x) + x\psi_1(t) + \psi_2(t), \quad (3)$$

where P_{xm} is the n th integral of the H_x and P_m is the n th integral of H_t denoted as $P^n H$ for either axis in [3].

Considering the following initial and boundary conditions

$$u(x, 0) = u_0(x), \quad u(a, t) = u_a(t), \quad u(b, t) = u_b(t), \quad (4)$$

one obtains the unknown functions $\phi(x)$, $\psi_1(t)$ and $\psi_2(t)$ as

$$\begin{aligned} \phi(x) &= u_0(x) - x\psi_1(0) - \psi_2(0), \\ \psi_1(t) &= \frac{u_b(t) - u_a(t) - P_{x2}^T(b)AP_{t1} - \phi[b] + \phi[a]}{b - a}, \\ \psi_2(t) &= \frac{bu_a(t) - au_b(t) + aP_{x2}^T(b)P_{t1} + a\phi[b] - b\phi[a]}{b - a}. \end{aligned} \quad (5)$$

where $P_{x2}^T(b)$ is the second integral P_{x2} at $x = b$.

Substituting functions (5) into Equation (3) one can arrive at

$$\begin{aligned} u(x, t) &= R_2AP_{t1} + S_2(x, t), \\ R_2 &= P_{x2}^T - \frac{x - a}{b - a}P_{x2}^T(b), \\ S_2(x, t) &= \frac{(b - x)(u_a(t) - u_a(0)) + (x - a)(u_b(t) - u_b(0))}{b - a} + u_0(x), \end{aligned} \quad (6)$$

where R_2 and S_2 and their derivatives are quantities that do not change over iteration and can therefore be calculated beforehand. Equation (6) can be differentiated to find u_t , u_x and u_{xx} as required in Equation (1).

DISCRETIZATION

The nonlinear Burgers equation (1) can be quasilinearised as

$$\dot{u}_{r+1} + (u_{r+1}u'_r + u_r u'_{r+1}) - \nu u''_{r+1} = u_r u'_r, \quad (7)$$

where r is the iteration step. Derivatives with respect to time have been denoted as \dot{u} while space derivatives have been denoted as u' .

The function u_{r+1} and its derivatives (see Equation (6)) can be inserted into Equation (7) and a discrete equation of the space-time grid can be derived as

$$\begin{aligned} \sum_{k=0}^{N_x-1} \sum_{l=0}^{N_t-1} \left((R_2)_{ik} (H_t)_{lj} - \nu (H_x^T)_{ik} (P_{t1})_{lj} + c \left((u'_r)_{ij} (R_2)_{ik} + (u_r)_{ij} (R'_2)_{ik} \right) (P_{t1})_{lj} \right) (A_{r+1})_{kl} = \\ = c (u_r)_{ij} (u'_r)_{ij} - (u'_r)_{ij} (S_2)_{ij} - (S_{2,t})_{ij} - (u_r)_{ij} (S_{2,x})_{ij} + \nu (u''_r)_i, \end{aligned} \quad (8)$$

$$\begin{aligned} i &= 0, \dots, N_x - 1, \\ j &= 0, \dots, N_t - 1, \end{aligned}$$

where the derivatives R'_2 , $S_{2,t}$, $S_{2,x}$ and $S_{2,xx}$ can be calculated easily from Equation (6) and it is easy to see that $S_{2,xx} = u''_0(x)$ and $R'_2 = \dot{H}_x^T$ (which are already used in the above equation).

The coefficients of $(A_{r+1})_{kl} \forall i, \forall j$ in Equation (8) form the matrix T of size $(N_x N_t \times N_x N_t)$. The right hand side of Equation (8) forms a vector f of length $N_x N_t$. The coefficient matrix A_{r+1} can be computed as

$$A_{r+1} = T^{-1}f. \quad (9)$$

After resizing A_{r+1} found in Equation (9) one can calculate $u_{r+1}(x, t)$ and its derivatives using Equation (6).

The steps described above need to be repeated until the difference between two successive u_{r+1} become sufficiently small. The initial (iteration 0) solution can be set equal to the initial condition at all time points.

RESULTS AND DISCUSSION

The Burgers equation (1) was solved in case of various values of the coefficient ν as well as different number of grid points on both axes. The result was compared to the exact solution presented in [19] where applicable. The convergence k_i of the numerical method was presented in accordance to [20, 21].

The convergence of the numerical solutions for $\nu = 0.1$ and $\nu = \frac{1}{10\pi}$ with different number of grid points for either (x and t) axis has been observed (see Table 1). The order of convergence tends to two with respect to both axes.

The maximum deviation from the exact solution for a set of solutions can be seen in Table 2. While the maximum deviation seems to grow as the value of ν diminishes, the results match the exact solution rather well as a whole. It must also be noted that higher number of grid points on the x axis are required for lower values of ν simply due to the nature of the solution at the boundary where there are no grid points.

The numerical solution as well as the exact solution in case of $\nu = \frac{1}{160\pi}$ on a 256×16 grid are shown in Figure 1. In case of small values of ν such as in this case, the solution creates a shockwave, after which numerical evaluation becomes impossible. However, the method has clearly coped with quite a steep slope at the boundary.

TABLE 1. Convergence in case of $\nu = 0.1$ and $\nu = \frac{1}{10\pi}$

N_x	N_t	Position	k_i		N_t	N_x	Position	k_i	
			$\nu = 0.1$	$\nu = \frac{1}{10\pi}$				$\nu = 0.1$	$\nu = \frac{1}{10\pi}$
4	16	u(0.5, 0.5)			4	16	u(0.5, 0.5)		
8	16	u(0.5, 0.5)			8	16	u(0.5, 0.5)		
16	16	u(0.5, 0.5)	2.5155	3.9938	16	16	u(0.5, 0.5)	2.5914	2.2742
32	16	u(0.5, 0.5)	2.1310	2.4626	32	16	u(0.5, 0.5)	2.0601	2.0625
64	16	u(0.5, 0.5)	2.0328	2.0394	64	16	u(0.5, 0.5)	2.0130	2.0154
128	16	u(0.5, 0.5)	2.0082	2.0103	128	16	u(0.5, 0.5)	2.0031	2.0038
256	16	u(0.5, 0.5)	2.0021	2.0026	256	16	u(0.5, 0.5)	2.0008	2.0010
512	16	u(0.5, 0.5)	2.0005	2.0006	512	16	u(0.5, 0.5)	2.0002	2.0002

TABLE 2. Maximum deviation from the exact solution on a 16×16 grid for $\nu = 0.1$, $\nu = \frac{1}{5\pi}$ and $\nu = \frac{1}{10\pi}$; on a 256×16 grid for $\nu = \frac{1}{100\pi}$ and $\nu = \frac{1}{160\pi}$

$\nu = 0.1$	$\nu = \frac{1}{5\pi}$	$\nu = \frac{1}{10\pi}$	$\nu = \frac{1}{100\pi}$	$\nu = \frac{1}{160\pi}$
0.00168	0.00359	0.01874	0.00612	0.02332

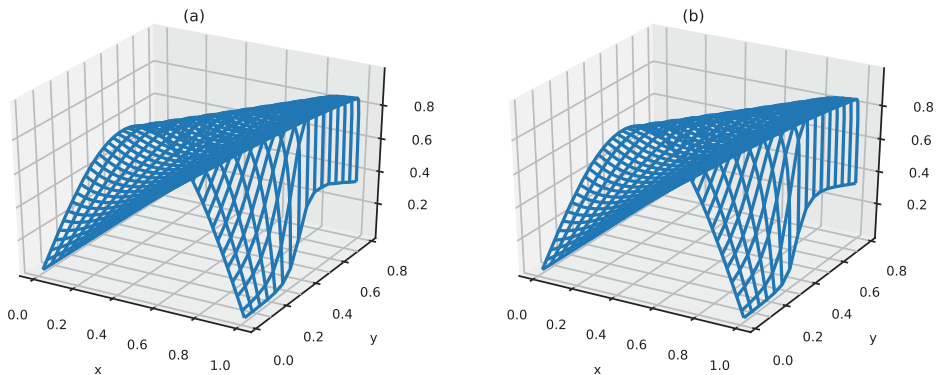


FIGURE 1. The calculated solution (a) and exact solution (b) in case of $\nu = \frac{1}{160\pi}$ on a 256×16 grid.

CONCLUSION

The 2D HWM was adapted for solution of the nonlinear Burgers equation. The solution was shown to be viable to cover relatively steep sloped solutions. The equations with solitary wave (or even soliton) solutions described in [22, 23] could be a next step for the method. The numerical rate of convergence computed has been found in good agreement with convergence theorem given in [21]. Furthermore, the method was demonstrated to work for relatively small grids as well as for near shock-wave like solutions. In future study, the accuracy of the solution is planned to improve by applying higher order Haar wavelet method introduced in [24].

ACKNOWLEDGMENTS

The author would like to thank his supervisor professor Andrus Salupere for important insights and editorial advice. This research was supported by the Estonian Research Council (IUT 33-24) as well as the European Regional Development Fund via Archimedes Foundation through the Dora Pluss scholarship program.

REFERENCES

- [1] S. Bertoluzza, in *Wavelet Analysis and Its Applications*, Vol. 6 (Elsevier, 1997), pp. 109–135.
- [2] G. Beylkin and J. M. Keiser, in *Wavelet Analysis and Its Applications*, Vol. 6 (Elsevier, 1997), pp. 137–197.
- [3] C. Chen and C. Hsiao, *IEEE Proc. Control Theory Appl.* **144**, 87–94 (1997).
- [4] Ü. Lepik and H. Hein, *Haar wavelets: with applications* (Springer Science & Business Media, 2014).
- [5] I. Aziz *et al.*, *Journal of Computational and Applied Mathematics* **239**, 333–345 (2013).
- [6] Ü. Lepik, *Math. Comput. Simulation* **68**, 127 – 143 (2005).
- [7] J. Majak, M. Pohlak, and M. Eerme, *Mechanics of Composite Materials* **45**, 631–642 (2009).
- [8] Ü. Lepik, *Appl. Math. Comput.* **185**, 695–704 (2007).
- [9] I. Aziz, B. Šarler, *et al.*, *Mathematical and Computer Modelling* **52**, 1577–1590 (2010).
- [10] H. Hein and L. Feklistova, *Engineering Structures* **33**, 3696–3701 (2011).
- [11] G. Hariharan and K. Kannan, *Applied Mathematical Modelling* **38**, 799 – 813 (2014).
- [12] Ü. Lepik, *Comput. Math. Appl.* **61**, 1873–1879 (2011).
- [13] M. Kirs, M. Mikola, A. Haavajõe, E. Õunapuu, B. Shvartsman, and J. Majak, *Waves, Wavelets and Fractals* **2**, 20–28 (2016).
- [14] J. Majak, B. Shvartsman, M. Pohlak, K. Karjust, M. Eerme, and E. Tungel, *AIP Conference Proceedings* **1738**, p. 480110 (2016), <https://aip.scitation.org/doi/pdf/10.1063/1.4952346>.
- [15] U. Andersson, B. Engquist, G. Ledfelt, and O. Runborg, *Appl. Comput. Harmon. Anal.* **7**, 151–164 (1999).
- [16] C. Cattani, *Proceedings of the Estonian Academy of Sciences. Physics, Mathematics*, **5301** (2004).
- [17] J. Majak, M. Pohlak, M. Eerme, and T. Lepikult, *Appl. Math. Comput.* **211**, 488 – 494 (2009).
- [18] G. Hariharan, K. Kannan, and K. Sharma, *Appl. Math. Comput.* **211**, 284 – 292 (2009).
- [19] J. D. Cole, *Quart. Appl. Math.* **9**, 225–236 (1951).
- [20] J. Majak, B. Shvartsman, M. Kirs, M. Pohlak, and H. Herranen, *Composite Structures* **126**, 227 – 232 (2015).
- [21] J. Majak, B. Shvartsman, K. Karjust, M. Mikola, A. Haavaje, and M. Pohlak, *Composites Part B: Engineering* **80**, 321 – 327 (2015).
- [22] A. Salupere, in *Applied Wave Mathematics: Selected Topics in Solids, Fluids, and Mathematical Methods*, edited by E. Quak and T. Soomere (Springer, Berlin, 2009), pp. 301–333.
- [23] A. Salupere, G. A. Maugin, J. Engelbrecht, and J. Kalda, *Wave Motion* **23**, 49–66 (1996).
- [24] J. Majak, M. Pohlak, K. Karjust, M. Eerme, J. Kurnitski, and B. Shvartsman, *Composite Structures* **201**, 72 – 78 (2018).

Appendix 5

V

M. Ratas, S. K. Jena, and S. Chakraverty. Application of Haar wavelet based methods for solving wave propagation problems. *AIP Conference Proceedings*, 2293(1):230002, 2020

Application of Haar Wavelet based methods for solving wave propagation problems

M. Ratas^{1,a)}, S. K. Jena^{2,b)} and S. Chakraverty^{2,c)}

¹Tallinn University of Technology, Department of Cybernetics, Laboratory of Solid Mechanics
²Department of Mathematics, National Institute of Technology Rourkela, Odisha-769008, India

a)Corresponding author: mart.ratas@ttu.ee
b)sjena430@gmail.com
c)sne_chak@yahoo.com

Abstract. The Haar wavelet method (HWM) is adapted for solving 2D nonlinear wave propagation problems. The 2D Burgers equation is considered as a model equation here. The 2D wavelet expansion is employed for the spatial derivatives and standard ordinary differential equation solvers are used for the temporal derivative. The aim of the study is to validate HWM in multi-dimensional case. The numerical results obtained are found to be in good agreement with analytical solution.

INTRODUCTION

Wavelet methods have been used to solve partial differential equations (PDE-s) since the 1990s [1, 2]. Haar wavelets, as the simplest of all wavelets, deserve attention at this point. While the piecewise constant nature of Haar wavelets means that their derivatives do not exist, they can be analytically integrated arbitrarily many times [3, 4]. Thus, they are ideal for integral equations [5]. In case of differential equations, one can expand into the Haar series not the function itself but rather its highest space derivative appearing in the equation [3, 6–11]. By applying various integration algorithms, the solution of the differential equation and the derivatives can be determined and inserted into the differential equation [12–14]. As a result a system of algebraic equations is obtained [4, 6, 7]. The wavelet coefficients can be determined as a solution of that algebraic system. Finally, the solution is obtained by substitution the wavelet coefficients into the wavelet expansion. In case of wave propagation problems, the time derivative is often found using some finite difference type approximations [15–18]. The same approach is used here.

HAAR WAVELET METHOD IN CASE OF 2D BURGERS EQUATION

The following system of partial differential equations is considered the 2D Burgers equations [19–23]:

$$u_t + uu_x + vu_y = \frac{1}{R} (u_{xx} + u_{yy}), \quad v_t + uv_x + vv_y = \frac{1}{R} (v_{xx} + v_{yy}), \quad (1)$$

where R is the Reynolds number, u and v represent velocities in the x and y coordinates, respectively [19]. The Burgers equations are subject to the initial and boundary conditions

$$\begin{aligned} u(x, y, 0) = u_0(x, y), \quad u(a, y, t) = f_0^u(y, t), \quad u(x, c, t) = g_0^u(x, t), \quad v(a, y, t) = f_0^v(y, t), \quad v(x, c, t) = g_0^v(x, t), \\ v(x, y, 0) = v_0(x, y), \quad u(b, y, t) = f_1^u(y, t), \quad u(x, d, t) = g_1^u(x, t), \quad v(b, y, t) = f_1^v(y, t), \quad v(x, d, t) = g_1^v(x, t), \end{aligned} \quad (2)$$

where $x \in [a, b]$ and $y \in [c, d]$.

There exists an exact solution for the 2D Burgers equation [24]

$$u_e(x, y, t) = \frac{3}{4} - \frac{1}{4 \{1 + \exp [(-4x + 4y - t)R/32]\}}, \quad v_e(x, y, t) = \frac{3}{4} + \frac{1}{4 \{1 + \exp [(-4x + 4y - t)R/32]\}}. \quad (3)$$

In order to validate the numerical method, the initial and boundary conditions (2) are obtained from the above exact solution.

In order to numerically solve the 2D Burgers equations, u_{xx} , u_{yy} , v_{xx} and v_{yy} were expanded into the Haar wavelet series as per [25]

$$\frac{\partial^2 u(x,y)}{\partial x^2} = A_x^u \cdot H_x, \quad \frac{\partial^2 u(x,y)}{\partial y^2} = H_y^T \cdot A_y^u, \quad \frac{\partial^2 v(x,y)}{\partial x^2} = A_x^v \cdot H_x, \quad \frac{\partial^2 v(x,y)}{\partial y^2} = H_y^T \cdot A_y^v. \quad (4)$$

In (4) H_x and H_y are the Haar wavelet matrices for the x and y axis, respectively, and A_x^u , A_y^u , A_x^v , A_y^v are the Haar wavelet coefficients. After integrating, one arrives at

$$u(x,y) = A_x^u \cdot R_{x2} + S_{x2}^u, \quad u(x,y) = R_{y2} \cdot A_y^u + S_{y2}^u, \quad v(x,y) = A_x^v \cdot R_{x2} + S_{x2}^v, \quad v(x,y) = R_{y2} \cdot A_y^v + S_{y2}^v, \quad (5)$$

where

$$\begin{aligned} R_{x2} &= P_{x2} - P_{x2}(1)x, & R_{y2} &= P_{y2}^T - yP_{y2}^T(1), \\ S_{x2}^u &= (f_1^u(y,t) - f_0^u(y,t)) \cdot x + f_0^u(y,t), & S_{y2}^u &= y \cdot (g_1^u(x,t) - g_0^u(x,t)) + g_0^u(x,t), \\ S_{x2}^v &= (f_1^v(y,t) - f_0^v(y,t)) \cdot x + f_0^v(y,t), & S_{y2}^v &= y \cdot (g_1^v(x,t) - g_0^v(x,t)) + g_0^v(x,t), \end{aligned} \quad (6)$$

where P_{x2} and P_{y2} are the second Haar wavelet integration matrices. The unknown functions defined as the initial and boundary conditions in (2) are obtained from the exact solution as

$$\begin{aligned} f_0^u(y,t) &= u_e(a,y,t), & f_1^u(y,t) &= u_e(b,y,t), & f_0^v(y,t) &= v_e(a,y,t), & f_1^v(y,t) &= v_e(b,y,t), \\ g_0^u(y,t) &= u_e(x,c,t), & g_1^u(y,t) &= u_e(x,d,t), & g_0^v(y,t) &= v_e(x,c,t), & g_1^v(y,t) &= v_e(x,d,t). \end{aligned} \quad (7)$$

Since the two equations for u in (5) need to represent the same result, equating them will yield a relation between A_x^u and A_y^u . Similarly, we can arrive at the relation between A_x^v and A_y^v . These relations can be shown as

$$A_x^u = R_{y2}^{-1} \cdot (A_x^u \cdot R_{x2} + S_{x2}^u - S_{y2}^u), \quad A_y^v = R_{y2}^{-1} \cdot (A_x^v \cdot R_{x2} + S_{x2}^v - S_{y2}^v). \quad (8)$$

Given (8) and (5) one can find the needed derivatives of $u(x,y)$ and $v(x,y)$ as

$$\begin{aligned} u &= A \cdot R_{x2} + S_{x2}^u, & v &= A \cdot R_{x2} + S_{x2}^v, \\ u_x &= A_x^u \cdot R_{x1} + S_{x1}^u, & v_x &= A_x^v \cdot R_{x1} + S_{x1}^v, \\ u_{xx} &= A_x^u \cdot H_x, & v_{xx} &= A_x^v \cdot H_x, \\ u_y &= R_{y1} \cdot R_{y2}^{-1} \cdot (A_x^u \cdot R_{x2} + S_{x2}^u - S_{y2}^u) + S_{y1}^u, & v_y &= R_{y1} \cdot R_{y2}^{-1} \cdot (A_x^v \cdot R_{x2} + S_{x2}^v - S_{y2}^v) + S_{y1}^v, \\ u_{yy} &= H_y^T \cdot R_{y2}^{-1} \cdot (A_x^u \cdot R_{x2} + S_{x2}^u - S_{y2}^u), & v_{yy} &= H_y^T \cdot R_{y2}^{-1} \cdot (A_x^v \cdot R_{x2} + S_{x2}^v - S_{y2}^v), \end{aligned} \quad (9)$$

where $R_{x1} = \frac{\partial R_{x2}}{\partial x}$, $R_{y1} = \frac{\partial R_{y2}}{\partial y}$ and similarly $S_{x1}^u = \frac{\partial S_{x2}^u}{\partial x}$, $S_{y1}^u = \frac{\partial S_{y2}^u}{\partial y}$ as well as $S_{x1}^v = \frac{\partial S_{x2}^v}{\partial x}$ and $S_{y1}^v = \frac{\partial S_{y2}^v}{\partial y}$. In order to use ordinary differential equation (ODE) solvers, one needs both equations in the form $u_t = f(u, u_x, u_{xx}, u_y, u_{yy})$. From Eq. (1) one obtains

$$u_t = \frac{1}{R} (u_{xx} + u_{yy}) - (uu_x + vu_y), \quad v_t = \frac{1}{R} (v_{xx} + v_{yy}) - (uv_x + vv_y). \quad (10)$$

Thus substituting (9) into (10) at each time moment, one can calculate the temporal derivative and thus use ODE solvers so solve the system of PDEs.

RESULTS AND DISCUSSION

The 2D Burgers Eqs. (1) was solved at different resolutions and different Reynolds number values. The number of grid points on a given axis is given as $N = 2^{J+1}$, where J denotes the resolution. The resolution values of $J = 2, \dots, 6$ were considered. In the current study the resolution is kept the same on both axes. Reynolds number values $R = 220, 260, 300, 340$ were considered. Calculations were carried out within the domain $x \in [0, 1]$, $y \in [0, 1]$, $t \in [0, 1]$.

The numerical results' deviation from the exact solution (3) is shown in Table 1. The results clearly show that the numerical results for both u as well as v are in good agreement with the exact solution. It also evident that accuracy increases as the resolution J increases as would be expected. It is clear that the accuracy of the numerical solution diminishes with increase of Reynolds number R , especially at low resolutions. This can be attributed to the steepening nature of the exact solution as R increases. The slope at $R = 340$ can be seen in Figure 1. Given the exact solution (3), one can see that since $v_e(x, y, t) = \frac{3}{2} - u_e(x, y, t)$, the slope of v is as steep as that of u .

The computation time for results presented in Table 1 are shown in Table 2. The computational time stays relatively low for $J < 6$ but rises significantly at $J = 6$. The number of grid points at $J = 6$ is 128 on both axes and thus a system of 128 linear equations are solved at each time moment. Some of the additional time comes from the limited amount of logical cores available in the computer the computations were run on (*MATLAB's mdivide* is multithreaded [26]).

The ability to solve equations with steep slopes makes this method a promising addition to existing pseudospectral methods in areas such as solitary waves and solitons [27, 28]. With the increased accuracy provided by the recently developed Higher Order Haar Wavelet Method in [29], Haar wavelets could prove an exciting new tool within this area.

TABLE 1. Maximal deviation from exact solution (3) at different resolutions and Reynolds numbers for u and v

J	$R = 220$		$R = 260$		$R = 300$		$R = 340$	
	max err. u	max err. v						
2	0.0345186	0.0420620	0.0614871	0.0684815	0.1153377	0.1193631	0.2178892	0.2274026
3	0.0065951	0.0089431	0.0102949	0.0134474	0.0153208	0.0185581	0.0230894	0.0253803
4	0.0018286	0.0015675	0.0026377	0.0025030	0.0035963	0.0036502	0.0046713	0.0052699
5	0.0006597	0.0006814	0.0007456	0.0007940	0.0009196	0.0009025	0.0010940	0.0010823
6	0.0005707	0.0005707	0.0005952	0.000595	0.0005832	0.0005974	0.0005858	0.0006499

TABLE 2. Calculation time for numerical results presented in Table 1

	$J = 2$	$J = 3$	$J = 4$	$J = 5$	$J = 6$
$R = 220$	0.0468	0.0856	0.1573	0.7622	10.3037
$R = 260$	0.0471	0.0705	0.1370	0.5511	8.1181
$R = 300$	0.0424	0.0657	0.1340	0.6494	7.2962
$R = 340$	0.0362	0.0636	0.1218	0.4498	5.9679

CONCLUSION

The HWM was adapted for solving the 2D Burgers equation. The numerical solutions for both u and v were shown to be in good agreement with the exact solution, even at relatively steep slopes. Thus the HWM was shown to be adequate for solving the 2D wave propagation problem. Use of the higher order Haar wavelet method introduced in [29] is the next planned step in order to further increase the accuracy of the numerical solution.

ACKNOWLEDGMENTS

The author would like to thank his supervisor professor Andrus Salupere for important insights and editorial advice. This research was supported by the Estonian Research Council (IUT 33-24) as well as the European Regional Development Fund via Archmiedes Foundation through the Dora Pluss program.

REFERENCES

- [1] S. Bertoluzza, in *Wavelet Analysis and Its Applications*, Vol. 6 (Elsevier, 1997), pp. 109–135.
- [2] G. Beylkin and J. M. Keiser, in *Wavelet Analysis and Its Applications*, Vol. 6 (Elsevier, 1997), pp. 137–197.
- [3] C. Chen and C. Hsiao, *IEE Proc. Control Theory Appl.* **144**, 87–94 (1997).

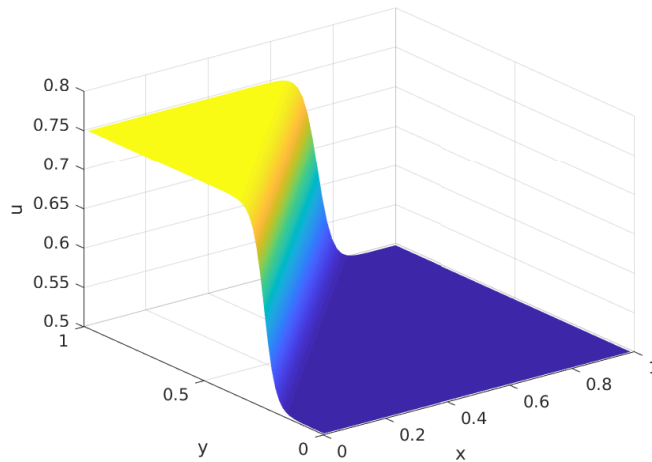


FIGURE 1. Calculated u in case of $R = 340$ and $J = 5$ at $t = 1$

- [4] Ü. Lepik and H. Hein, *Haar wavelets: with applications* (Springer Science & Business Media, 2014).
- [5] I. Aziz *et al.*, *Journal of Computational and Applied Mathematics* **239**, 333–345 (2013).
- [6] Ü. Lepik, *Math. Comput. Simulation* **68**, 127 – 143 (2005).
- [7] J. Majak, M. Pohlak, and M. Eerme, *Mechanics of Composite Materials* **45**, 631–642 (2009).
- [8] Ü. Lepik, *Appl. Math. Comput.* **185**, 695–704 (2007).
- [9] I. Aziz, B. Šarler, *et al.*, *Mathematical and Computer Modelling* **52**, 1577–1590 (2010).
- [10] H. Hein and L. Feklistova, *Engineering Structures* **33**, 3696–3701 (2011).
- [11] G. Hariharan and K. Kannan, *Applied Mathematical Modelling* **38**, 799 – 813 (2014).
- [12] Ü. Lepik, *Comput. Math. Appl.* **61**, 1873–1879 (2011).
- [13] M. Kirs, M. Mikola, A. Haavajõe, E. Öunapuu, B. Shvartsman, and J. Majak, *Waves, Wavelets and Fractals* **2**, 20–28 (2016).
- [14] J. Majak, B. Shvartsman, M. Pohlak, K. Karjust, M. Eerme, and E. Tungel, *AIP Conference Proceedings* **1738**, p. 480110 (2016), <https://aip.scitation.org/doi/pdf/10.1063/1.4952346>.
- [15] U. Andersson, B. Engquist, G. Ledfelt, and O. Runborg, *Appl. Comput. Harmon. Anal.* **7**, 151–164 (1999).
- [16] C. Cattani, *Proceedings of the Estonian Academy of Sciences. Physics, Mathematics*, **5301** (2004).
- [17] J. Majak, M. Pohlak, M. Eerme, and T. Lepikult, *Appl. Math. Comput.* **211**, 488 – 494 (2009).
- [18] G. Hariharan, K. Kannan, and K. Sharma, *Appl. Math. Comput.* **211**, 284 – 292 (2009).
- [19] A. J. Chorin, *Mathematics of computation* **23**, 341–353 (1969).
- [20] P. Jain and D. Holla, *International Journal of Non-Linear Mechanics* **13**, 213 – 222 (1978).
- [21] A. Bahadir, *Applied Mathematics and Computation* **137**, 131 – 137 (2003).
- [22] J. Biazar and H. Aminikhah, *Mathematical and Computer Modelling* **49**, 1394 – 1400 (2009).
- [23] H. Zhu, H. Shu, and M. Ding, *Computers & Mathematics with Applications* **60**, 840 – 848 (2010).
- [24] C. A. Fletcher, *International Journal for Numerical Methods in Fluids* **3**, 213–216 (1983).
- [25] I. Aziz, B. Šarler, *et al.*, *Applied Mathematical Modelling* **37**, 676–694 (2013).
- [26] MathWorks, “Run MATLAB on multicore and multiprocessor machines,” (2008).
- [27] A. Salupere, in *Applied Wave Mathematics: Selected Topics in Solids, Fluids, and Mathematical Methods*, edited by E. Quak and T. Soomere (Springer, Berlin, 2009), pp. 301–333.
- [28] J. Engelbrecht and A. Salupere, *Chaos* **15**, p. 015114 (2005).
- [29] J. Majak, M. Pohlak, K. Karjust, M. Eerme, J. Kurnitski, and B. Shvartsman, *Composite Structures* **201**, 72 – 78 (2018).

Curriculum Vitae

1. Personal data

Name	Mart Ratas
Date and place of birth	4 September 1990 Tartu, Estonia
Nationality	Estonian

2. Contact information

Address	Tallinn University of Technology, School of Science, Department of Cybernetics, Akadaemia tee 21B, 12618 Tallinn, Estonia
Phone	+372 620 4227
E-mail	mart.ratas@taltech.ee

3. Education

2016–...	Tallinn University of Technology, School of Science, Physical Sciences, PhD studies
2014–2016	Tallinn University of Technology, Institute of Cybernetics, Engineering Physics, MSc <i>cum laude</i>
2010–2014	Tallinn University of Technology, Institute of Cybernetics, Engineering Physics, BSc <i>cum laude</i>
2007–2010	Tallinn Secondary School of Science High School

4. Language competence

Estonian	native
English	fluent
Russian	beginner

5. Professional employment

2016– ...	Tallinn University of Technology, Department of Cybernetics, Early Stage Researcher
2016–2016	Tallinn University of Technology, Institute of Cybernetics, Engineer
2014–2016	Tallinn University of Technology, Centre for Biorobotics, Engineer

6. Voluntary work

2012–...	The Academic Male Choir of Tallinn University of Technology, board member
2019–...	The cultural centre of Tallinn University of Technology, board member

7. Computer skills

- Operating systems: Windows, Linux
- Document preparation: Office, LibreOffice
- Programming languages: Python, java
- Scientific packages: MATLAB, Wolfram Mathematica

8. Honours and awards

- 2015, The scholarship of the Student Union

9. Defended theses

- 2016, Spectral analysis of two-dimensional solitary waves, MSc, supervisor Prof. Andrus Salupere, Tallinn University of Technology, Institute of Cybernetics
- 2014, Analysis of the formation of solitons in case of the generalised Korteweg–de Vries equation, supervisor Prof. Andrus Salupere, Tallinn University of Technology, Institute of Cybernetics

10. Field of research

- Mathematical and theoretical physics
- Differential equations
- Nonlinear equations
- Numerical methods

11. Scientific work

Papers

1. A. Salupere and M. Ratas. On the application of 2D discrete spectral analysis in case of the KP equation. *Mech. Res. Comm.*, 93:141–147, 2018
2. M. Ratas and A. Salupere. Application of higher order Haar wavelet method for solving nonlinear evolution equations. *Math. Model. Anal.*, 25(2):271–288, 2020
3. M. Ratas, A. Salupere, and J. Majak. Solving nonlinear PDEs using the higher order Haar wavelet method on nonuniform and adaptive grids. *Math. Model. Anal.*, [accepted]
4. M. Ratas. Application of Haar wavelet method for solving nonlinear evolution equations. *AIP Conference Proceedings*, 2116(1):330004, 2019
5. M. Ratas, S. K. Jena, and S. Chakraverty. Application of Haar wavelet based methods for solving wave propagation problems. *AIP Conference Proceedings*, 2293(1):230002, 2020
6. J. Majak, B. Shvartsman, M. Ratas, D. Bassir, M. Pohlak, K. Karjust, and M. Eerme. Higher-order haar wavelet method for vibration analysis of nanobeams. *Materials Today Communications*, 25:101290, 2020
7. S. K. Jena, S. Chakraverty, M. Ratas, and M. Kris. Application of HOHWM in the stability analysis of nonlocal Euler–Bernoulli beam. *AIP Conference Proceedings*

Conference presentations

1. M. Ratas. ‘Application of Haar wavelet method for solving nonlinear evolution equations’, 16th International Conference of Numerical Analysis and Applied Mathematics 2018: 8–12 September 2018, Rhodes, Greece

2. M. Ratas. 'Numerical solution of PDE-s using Haar wavelet based methods', Mathematical Modelling and Analysis: 28–31 May 2019, Tallinn
3. M. Ratas, S. K. Jena, S. Chakraverty. 'Application of Haar Wavelet based methods for solving wave propagation problems', 17th International Conference of Numerical Analysis and Applied Mathematics 2019: 23–28 September 2019, Rhodes, Greece
4. M. Ratas. 'Application of the Adaptive Higher Order Haar Wavelet based methods for solving the sine-Gordonequation', 18th International Conference of Numerical Analysis and Applied Mathematics 2020: 17–23 September 2020, Rhodes, Greece [virtual presentation]

Elulookirjeldus

1. Isikuandmed

Nimi Mart Ratas
Sünniaeg ja -koht 04.09.1990, Tartu, Eesti
Kodakondsus Eesti

2. Kontaktandmed

Address Tallinna Tehnikaülikool, Küberneetika Instituut,
Akadeemia tee 21B, 12618 Tallinn, Estonia
Telefon +372 620 4227
E-post mart.ratas@taltech.ee

3. Haridus

2016–... Tallinna Tehnikaülikool, Loodusteaduskond,
Füüsikalised loodusteadused, doktoriõpe
2014–2016 Tallinna Tehnikaülikool, Küberneetika instituut,
Tehniline füüsika, MSc *cum laude*
2010–2014 Tallinna Tehnikaülikool, Küberneetika instituut,
Tehniline füüsika, BSc *cum laude*
2007–2010 Tallinna Reaalkool,
Keskkharidus

4. Keelteoskus

eesti keel emakeel
inglise keel kõrgtase
vene keel algtase

5. Teenistuskäik

2016– ... Tallinna Tehnikaülikool, Tahkimsehaanika labor, nooremteadur
2016–2016 Tallinna Tehnikaülikool, Tahkimsehaanika labor, insener
2014–2016 Tallinna Tehnikaülikool, Biorobotika keskus, insener

6. Vabatahtlik töö

2012–... Tehnikaülikooli Akadeemiline Meeskoor, juhatuse liige
2019–... Tallinna Tehnikaülikooli Kultuurikeskus, juhatuse liige

7. Arvutioskused

- Operatsioonisüsteemid: Windows, Linux
- Kontoritarkvara: Office, LibreOffice
- Programmeerimiskeeled: Python, Java
- Teadustarkvara paketid: MATLAB, Wolfram Mathematica

8. Autasud

- 2015, Üliõpilasesinduse stipendium

9. Kaitstud lõputööd

- 2016, Kahemõõtmeliste üksiklainete spektraalanalüüs, MSc, juhendaja prof. Andrus Salupere, Tallinna Tehnikaülikool, Küberneetika Instituut
- 2014, Solitonide formeerumise analüüs üldistatud Kortewegi–de Vriesi võrrandi näitel, BSc, juhendaja prof. Andrus Salupere, Tallinna Tehnikaülikool, Küberneetika Instituut

10. Teadustöö põhisuunad

- Matemaatiline ja üldine teoreetiline füüsika
- Diferentsiaalvõrrandid
- Mittelineaarsed võrrandid
- Numbrilised meetodid

11. Teadustegevus

Teadusartiklite, konverentsiteeside ja konverentsiettekannete loetelu on toodud ingliskeelse elulookirjelduse juures.